# Enclosure 2 – PG&E Moss Landing Tower Collapse Direct Cause Analysis

*Failure Analysis Associates*

Exponent®

# Moss Landing Tower Collapse Analysis

Exponent

# Moss Landing Tower Collapse Analysis

Prepared for

[redacted]
Supervising Civil Engineer TLine
Pacific Gas and Electric Company
6111 Bollinger Canyon Road
San Ramon, CA 94583

Prepared by

Brian M. McDonald, Ph.D., P.E.
Ryan Birringer, Senior Associate

Exponent
149 Commonwealth Drive
Menlo Park, CA 94025


December 23, 2015



Doc. no. 1507946.000 - 2517

# Contents

# Limitations

At the request of PG&E, Exponent has conducted an investigation of the October 18, 2015 collapse of the Metcalf-Moss Landing #1 Tower 61/268 (G95 Tower) near Moss Landing, CA. Exponent investigated specific issues relevant to this failure, as requested by the client. The scope of services performed during this investigation may not adequately address the needs of other users of this report, and any re-use of this report or its findings, conclusions, or recommendations presented herein is at the sole risk of the user. The opinions and comments formulated during this assessment are based on observations and information available at the time of the investigation. No guarantee or warranty as to future life or performance of any reviewed condition is expressed or implied.

Exponent has no direct knowledge of, and offers no warranty regarding the condition of concealed construction or subsurface conditions beyond what was exposed during our investigation. Comments regarding concealed construction or subsurface conditions are professional opinions, derived in accordance with current standards of professional practice based on our geologic and engineering experience and judgment.

The findings herein are made to a reasonable degree of engineering certainty based on information available to Exponent as of the date of this report. Exponent may supplement this report to expand or modify our findings based on review of additional information as it becomes available.

# Executive Summary

On October 18, 2015 a lattice tower owned and operated by Pacific Gas and Electric (PG&E) toppled near the Moss Landing Power Plant in Moss Landing, California. PG&E retained Exponent Failure Analysis Associates (Exponent) to investigate the direct cause(s) of the accident, and in particular, to evaluate the tower design and material properties for possible contribution. The subject tower supported two circuits designated as Metcalf-Moss Landing #1 and Metcalf-Moss Landing #2. Both circuits made an approximately 90 degree angle at the tower, resulting in a net overturning load to the southeast. The entire tower toppled in one piece to the southeast after the two northwest steel stub angles, which supported the northwest tower legs, failed at the lowest line of bolt holes.

Exponent's investigation has included:

- visual observations, measurements and photo-documentation of the accident site on the day of the accident;
- collection and storage of key physical evidence;
- review of design documents and summaries of the design and construction process for this tower (provided by PG&E);
- structural analysis of the subject tower under expected loads during construction and at the time of the accident;
- verification of tower design loads and member sizes as they relate to the accident;
- structural analysis of potential forced fit-up loads based on measured misalignment of the stub angles;
- metallurgical analysis of steel specimens recovered from the accident site as well as exemplar material provided by PG&E;
- mechanical properties testing of steel specimens recovered from the accident site as well as exemplar material provided by PG&E;
- finite element-based analysis of local stress conditions around the stub angle bottom bolt holes; and
- linear-elastic fracture mechanics analysis.

Based on the totality of our investigation, Exponent has identified two principal contributors to the tower collapse:

1. Based on measurements made of the foundations after the accident, it appears that the stub angles were not correctly aligned to the tower legs at the time of foundation construction. The stub angles, which are embedded in the concrete foundation and bolt to the tower legs, were installed with insufficient slope to match the tower legs. Because of this, the lowest tower leg members would have needed to be force-fit in the field by pulling their tops inward toward the tower center. This field adjustment would have

overloaded the stub angle, causing cracks at two of the legs (B and D, which exhibited corroded fracture surfaces at the time of collapse, indicating pre-existing cracks) and inducing a detrimental initial stress at the remaining two legs (A and C, which exhibited shiny fracture surfaces at the time of collapse).

2. Based on metallurgical examination and testing of steel specimens of the stub angles recovered from the site, the steel met the mechanical and chemical requirements for ASTM A572 Grade 50 at the time of the specification and purchase. However, the accident fracture surfaces and subsequent testing indicates that this steel is more brittle than desirable for the subject tower application. This brittleness made the stub angles more sensitive to normal and expected damage around the punched bolt holes, and thus more vulnerable to brittle fracture under the stresses induced during construction fit-up. We note that the chemical requirements for A572 Grade 50 steel have been tightened since the time of specification and purchase of the subject stub angles, and that the purchased steel would not meet the new requirements.

Based on our analysis, Exponent offers the following recommendations. We anticipate that these recommendations will be further refined in a supplemental root cause analysis report:

1. Exponent recommends that PG&E interview the crew that erected the tower to determine how the incident stubs came to be misaligned during tower foundation construction, and to implement a process to mitigate the risk of this recurring.
2. Exponent recommends that PG&E consider updating material specifications for lattice tower construction to include minimum toughness requirements.
3. Exponent recommends that PG&E consider sub-punching and reaming any stub angles to be fabricated from recently purchased steel members unless they are shown to meet minimum notch toughness requirements.
4. Exponent recommends that PG&E conduct non-destructive analyses of other recently constructed towers to ensure that the stubs project from the concrete at the proper angle, and visually inspect these towers for local deformation or cracking at stub angle bolt holes. If stubs are found to be installed at an improper angle, additional nondestructive evaluation and/or testing of the stub angles and tower legs should be considered.
5. Exponent recommends that PG&E consider reviewing the instructions to field crews regarding proper actions to take when lattice tower members require forced fit-up, and to expand the instructions or training as required.

# Background

On October 18, 2015, an Exponent Structural Engineer[1] was informed of a lattice tower failure near Moss Landing, California, and was requested to meet with PG&E personnel at the site. The purpose of that site visit was to assist PG&E with determination of the potential causes of the accident, and to help identify key physical evidence to be retained and tested. Upon arrival at the site, Dr. McDonald visually observed the collapse site, including some photo-documentation and measurements of the failed stub angles and foundation layout.

The subject tower is a 124-foot tall, steel lattice, overhead transmission tower of a type designated by PG&E as G95-DE with a 32.5-foot extension. We understand that the subject tower was designed for expected stringing and operational loads by Black and Veatch. The tower supports two circuits (Metcalf-Moss Landing #1 and Metcalf-Moss Landing #2) each composed of three Cardinal ACSS conductors spanning 823 feet to the east, and three bundled (paired) Marigold[2] AAC conductors dropping to the substation to the south. The tower is of bolted steel construction whose basic design is shown on Drawings 403912 (Rev. 8) and 5P17, provided to us by PG&E.

From documents provided by PG&E, we understand that the subject tower was constructed in March and April 2015. The four concrete foundation piers (with embedded / protruding stub angles) were cast on March 19, 2015. Construction of the tower superstructure occurred April 6 through 8, 2015. The tower was constructed piecewise by first erecting a 17.5-foot base extension (lower tower legs, diagonal lacing, and horizontals). Another 15-foot extension was then added by lifting two pre-assembled faces into place by crane and tying them together with lacing and horizontals. After the base was erected, the tower body and cage/arms, which had been pre-assembled on site, were placed atop the base with a crane. The stringing/sagging operations were conducted on September 12, 2015 (Metcalf-Moss Landing #1) and October 10, 2015 (Metcalf-Moss Landing #2).

Figure 1 shows the location of the site, Figure 2 shows an aerial photo taken during tower erection, and Figure 3 and Figure 4 show photos at the site from October 18, 2015 after the tower collapsed.

PG&E retained Exponent to conduct an engineering failure analysis of the direct, technical causes of the failure. We anticipate that this report will become part of a supplemental root cause analysis to be issued subsequently.

---

1 Brian McDonald, Registered Structural Engineer, California, #S4330

2 PG&E Drawing 233101 specifies type "Pigweed" conductors (2300 KCMIL AAC), 2 per phase. However, a document provided to Exponent by PG&E titled "Moss Landing-Metcalf Wire Transfer" states that the bundled conductors were 1113 KCMIL AAC, or type "Marigold", which is consistent with Exponent's measurement of the wire diameter in the field.


Figure 1. Site of the tower collapse at grey and white pin marker (Google Maps)

Figure 2. Overhead photo of subject tower, taken in April 2015 during tower construction. Tower base is visible in photo, identified with yellow arrow. (Google Earth)

Figure 3. Failed tower as seen October 18, 2015, partial panoramic view, generally to the east.

Figure 4. Failed tower as seen October 18, 2015. View to South.

# Structural Analysis

The four foundation stub angles of the subject tower (Tower 61/268) failed through a section containing the bottom four bolt holes (herein referred to as the critical section). As will be discussed in a later section, the fracture surfaces suggest that the initial fractures were due to tensile overload; there were no indications that fatigue or material degradation had weakened the cross sections. The fracture surfaces of two of the four stub angles, B (east leg) and D (west leg), exhibited corrosion on the day of the collapse, indicating that those stubs had fractured sometime earlier; stub angles A (north) and C (south) exhibited shiny fracture surfaces indicating they were created on the day of the collapse.

Exponent has calculated forces at the critical section for two load sets: 1) phased loads on the tower from initial construction up to the time of collapse; and 2) loads due to displacing the tops of the 17.5-ft leg extensions inward to enable fit-up during erection of the tower. The forces calculated in both sets of analyses were compared to the strength of the critical section as determined by code-like nominal capacity equations (described below) and by linear elastic fracture mechanics (described in a later section). The results of these two analysis sets are described in the following sections.

## Expected Loads up to the Time of Failure

Using wind speeds measured at nearby Elkhorn Slough, the wind pressure on the tower and attached conductors at the time of the accident was well below the design wind loads considered in Black & Veatch's analysis, and was determined not to be a major contributor to the collapse. Figure 5 shows the average and maximum wind speeds recorded near the site from the date the conductor stringing was completed to the time of collapse. Figure 6 shows the maximum and average wind speeds near the site the day the tower collapsed. We understand that the tower collapsed at about 7:00 am, at which time the wind loads would have been negligible.

The ambient air temperatures over the period of tower erection (April 6-8, 2015) are shown in Figure 7, and the ambient air temperatures from the date the conductor stringing was completed to the time of collapse are shown in Figure 8. All of these recordings were obtained from a weather station located approximately two miles from the site as shown in Figure 9. While one can conclude that extreme temperature was not a contributor to the collapse, the effect of cool temperatures on the subject steel and the resulting fracture morphology is discussed in a later section.

Exponent evaluated the demands on the Tower 61/268 bolted foundation connections during and after transfer of the Metcalf-Moss Landing #1 and #2 circuits using the commercial finite element analysis software SAP2000. The model was constructed based on drawings of the G95-DE tower, leg extensions, and foundations as provided by PG&E,[3] line profiles and data sheets[4]

[3] PG&E Drawing No. 403912, Bethlehem Pacific Coast Steel Corp. Drawing No. 5P17, and PG&E Drawing Nos. 313438 and 309933, respectively.

[4] PG&E Drawing Nos. 3001405 and 233101, respectively.

for the new installations, and a description of the conductor stringing/sagging procedures from PG&E's Line Department (including the conductor tensions applied during installation). The predominant loads on Tower 61/268 at the time of failure include the horizontal and vertical forces from the attached conductors as well as the tower self-weight.

In Exponent's computer model, the tower body was simplified as a single frame element to transfer loads from the conductor attachments to the tower base; cantilever single-element arms were used to reach the conductor attachment locations. Because the forces in the tower base members and critical sections were each needed, the individual members of the bottom extension of the tower were modeled explicitly. The conductors were modeled with nonlinear elastic catenary elements, rigidly fixed where they attach to the substation bays and to the next tower (61/267). Figure 10 shows the analysis model and location of key components. Figure 11 shows the base extension and identifies the tower legs A, B, C and D. Figure 12 shows the geometry of the bolted connection between the tower leg angle and the foundation stub angle.

The purpose of this analysis is to determine whether the members and connections were sized correctly to carry the anticipated design loads for each phase of construction including the time of collapse. Exponent has checked our results against member forces and reactions reported by Black & Veatch (presumably using the design model representation in PLS-CADD) and found them to be consistent. Precise reproduction of the Black & Veatch leg forces at the critical section was neither intended nor expected.

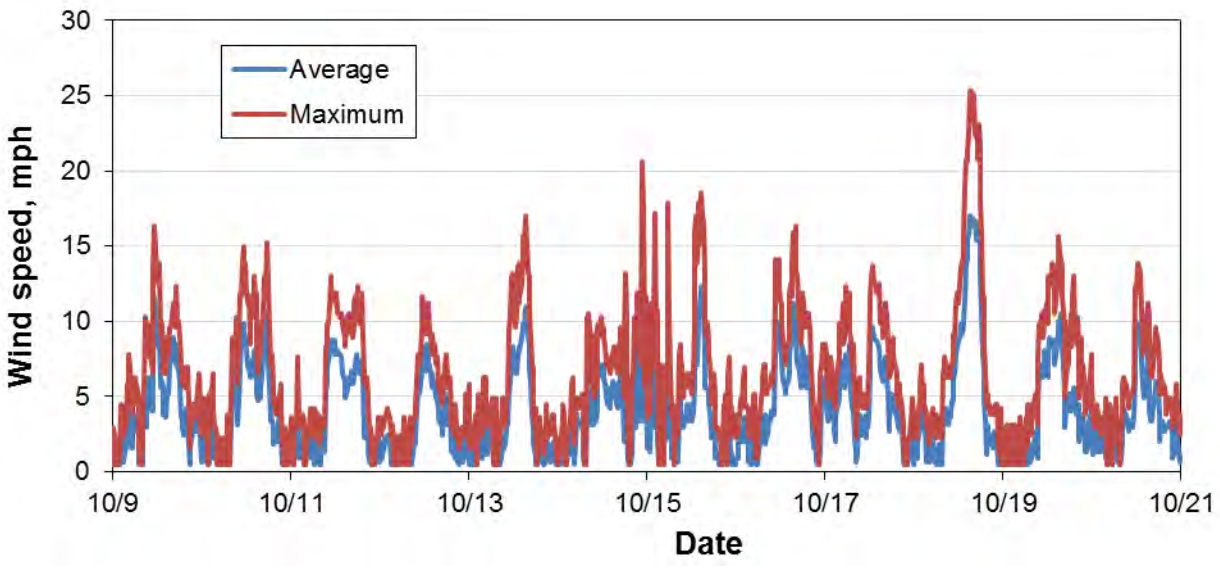


Figure 5. Maximum and average wind speeds recorded at Elkhorn Slough October 9, 2015 to October 21, 2015.[5]

[5] NNDC Climate Data Online, National Environment Satellite, Data, and Information Service, National Oceanic and Atmospheric Association. Climate Data for Elkhorn Slough Reserve Station #99799799999. Accessed: December 15, 2015. http://www7.ncdc.noaa.gov/CDO/cdopoemain.cmd?datasetabbv=DS3505&countryabbv=&georegionabbv=&resolution=40.

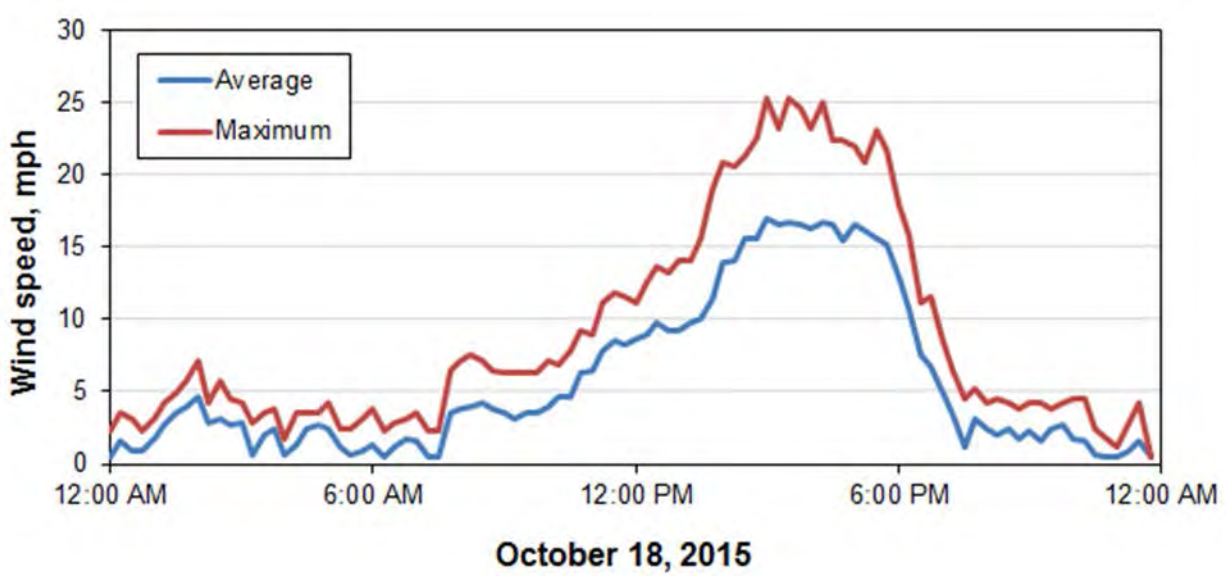


Figure 6. Maximum and average wind speeds recorded at Elkhorn Slough on October 18, 2015.[6]

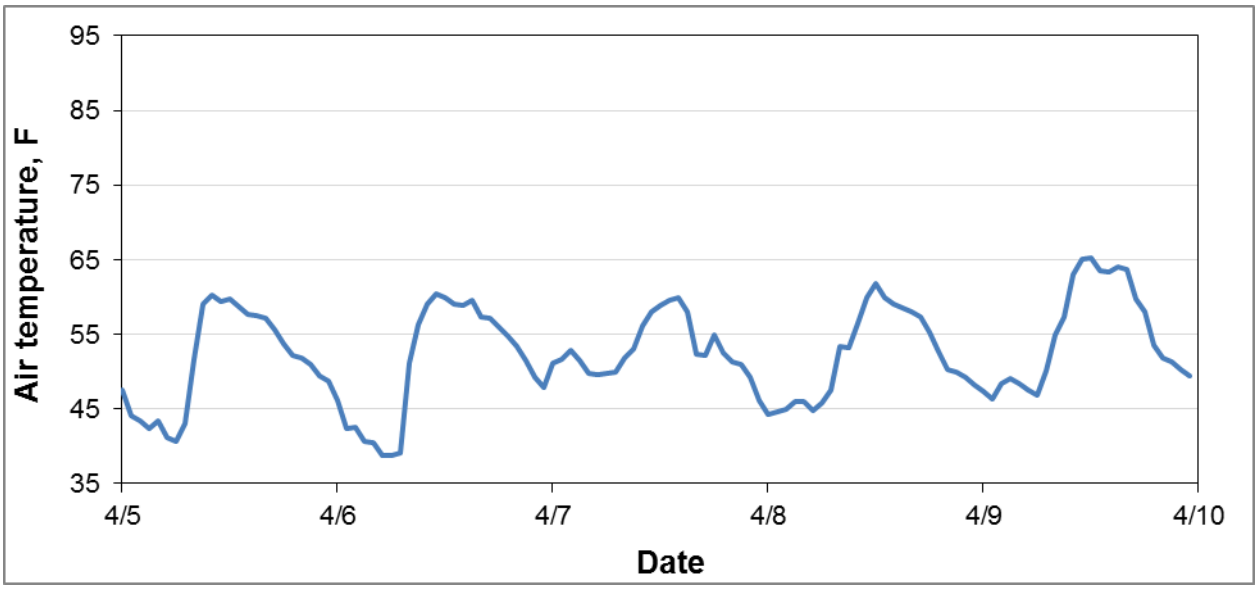


Figure 7. Ambient air temperature at Elkhorn Slough, April 5, 2015 to April 9, 2015.[5]

[6] NOAA National Estuarine Research Reserve System (NERRS). Weather Data for Caspian Weather Station ELKCWMET. System-wide Monitoring Program. Data accessed from the NOAA NERRS Centralized Data Management Office website: http://www.nerrsdata.org/. Accessed: December 15, 2015.

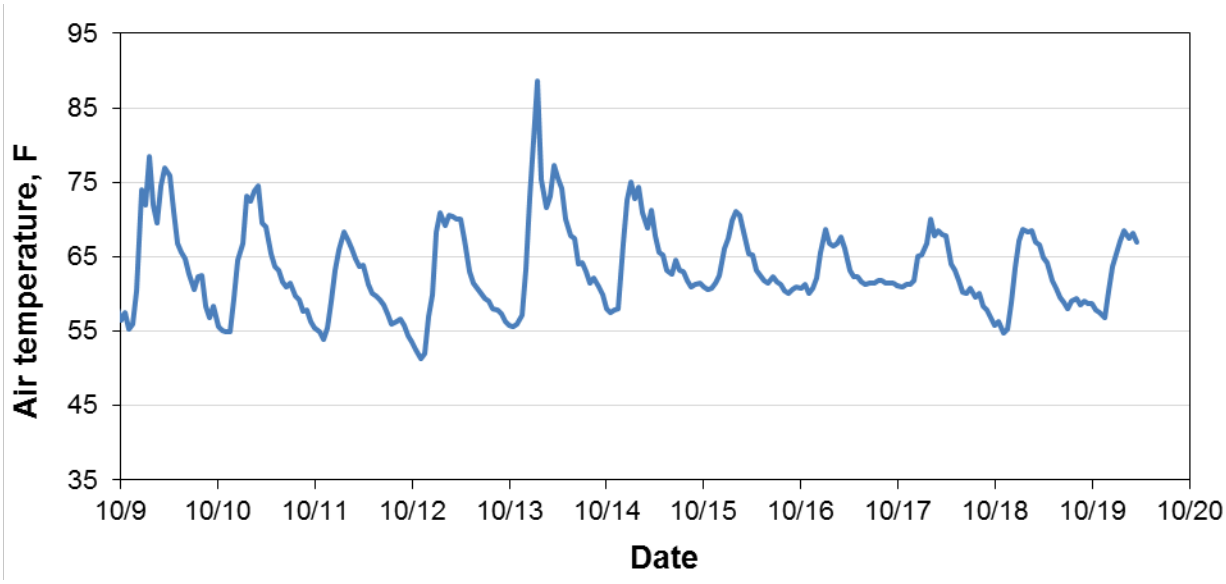


Figure 8. Ambient air temperature at Elkhorn Slough, October 9, 2015 to October 20, 2015.[5]

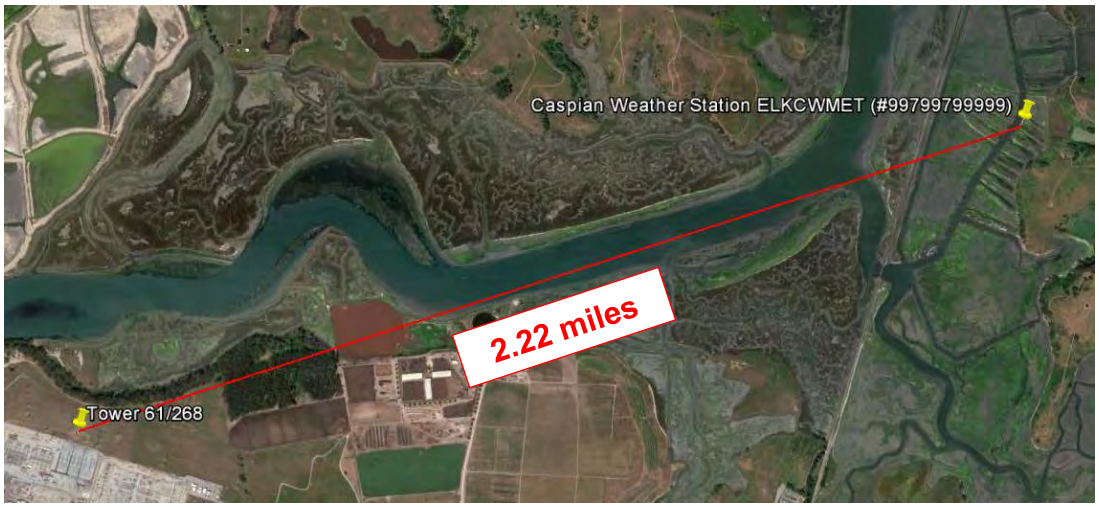


Figure 9. Proximity of Caspian Weather Station to Tower 61/268 (Google).

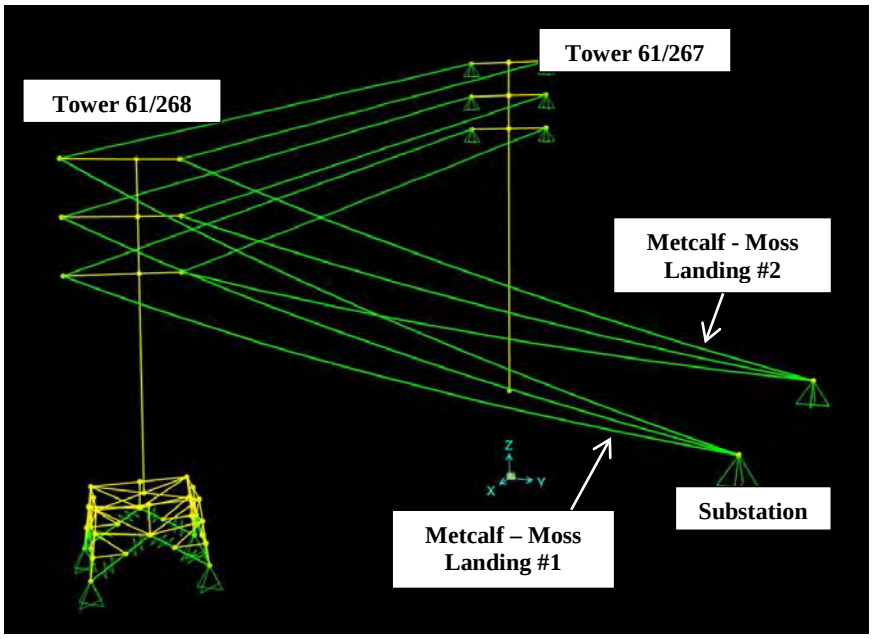


Figure 10. Screenshot of analysis model from SAP2000.

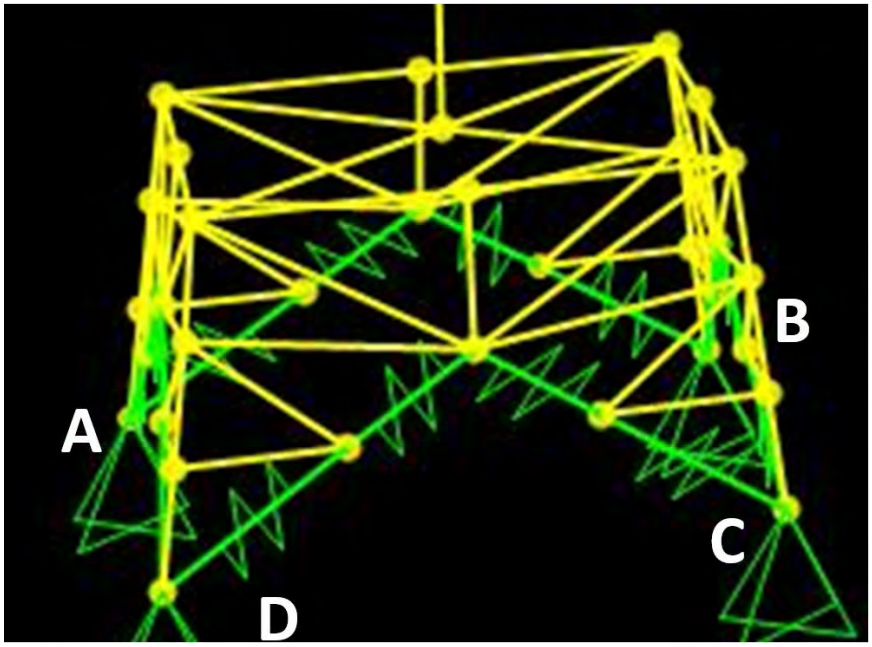


Figure 11. Orientation of tower legs shown in the figure above. This depiction of the model is presented looking Northeast.

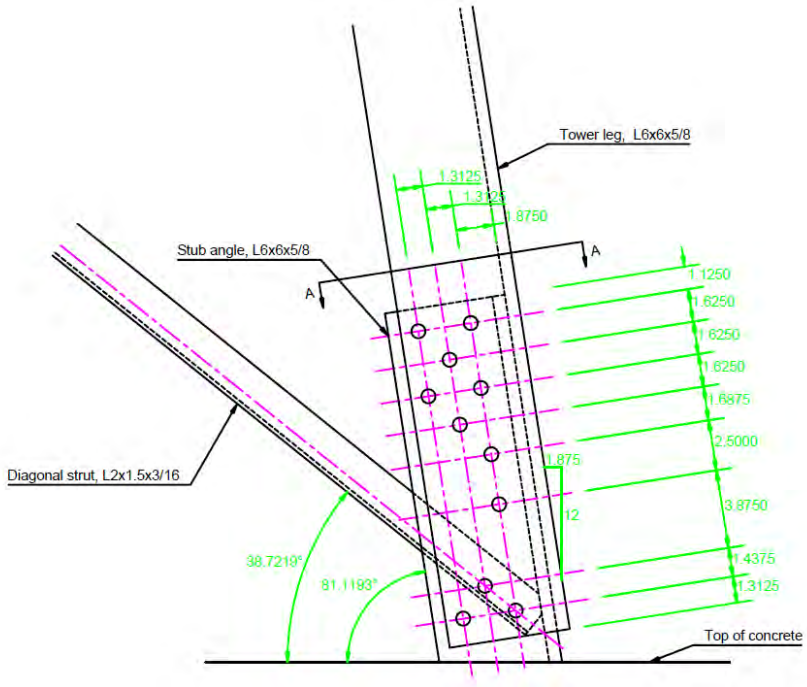


Figure 12. Bolted connection at base of tower 61/268.

Exponent isolated four different construction phases that occurred during the conductor stringing/sagging procedures, resulting in four unique loading cases on the tower at the end of each phase. Phase I consisted of moving, attaching, and tensioning the Metcalf-Moss Landing #1 circuit spanning between Towers 61/267 and 61/268. Phase II consisted of attaching and tensioning the Metcalf-Moss Landing #1 circuit bundles spanning between tower 61/268 and substation Bay 3. Phase III consisted of moving, attaching, and tensioning the Metcalf-Moss Landing #2 circuit spanning between Towers 61/267 and 61/268. Phase IV consisted of attaching and tensioning the Metcalf-Moss Landing #2 circuit spanning between tower 21/268 and substation Bay 4. One additional analysis was performed to evaluate the Phase IV load redistribution assuming the connection at Leg D had already failed.

Figure 13 shows a summary of the axial force demands on each foundation stub angle at the end of each installation phase. The axial force is a combination of the tension or compression load in the tower leg as well as the component of the diagonal strut braces forces (see Figure 12) oriented along the leg axis. (Any compression resistance of the diagonal struts was neglected in the model since the slenderness, KL/r, of those elements exceeds 200.) The axial tension in the stub angles at the critical section was compared to the tensile rupture strength ($R_n$) of 338 kips per the requirements of AISC 360, 13$^{th}$ edition, Section J4.1 (assuming $F_u$ = 65 ksi). As can be seen, the expected tension in the tower stub angles due to construction loads (including the load at the time of failure) remain well below half the expected strength. The nominal compressive strength ($P_n$) of the leg according to AISC Section E5 was calculated to be 170 kips.

In conclusion, the design of the stub angles, and in particular the strength of the critical section, is adequate for the intended loads from construction up to the time of failure.

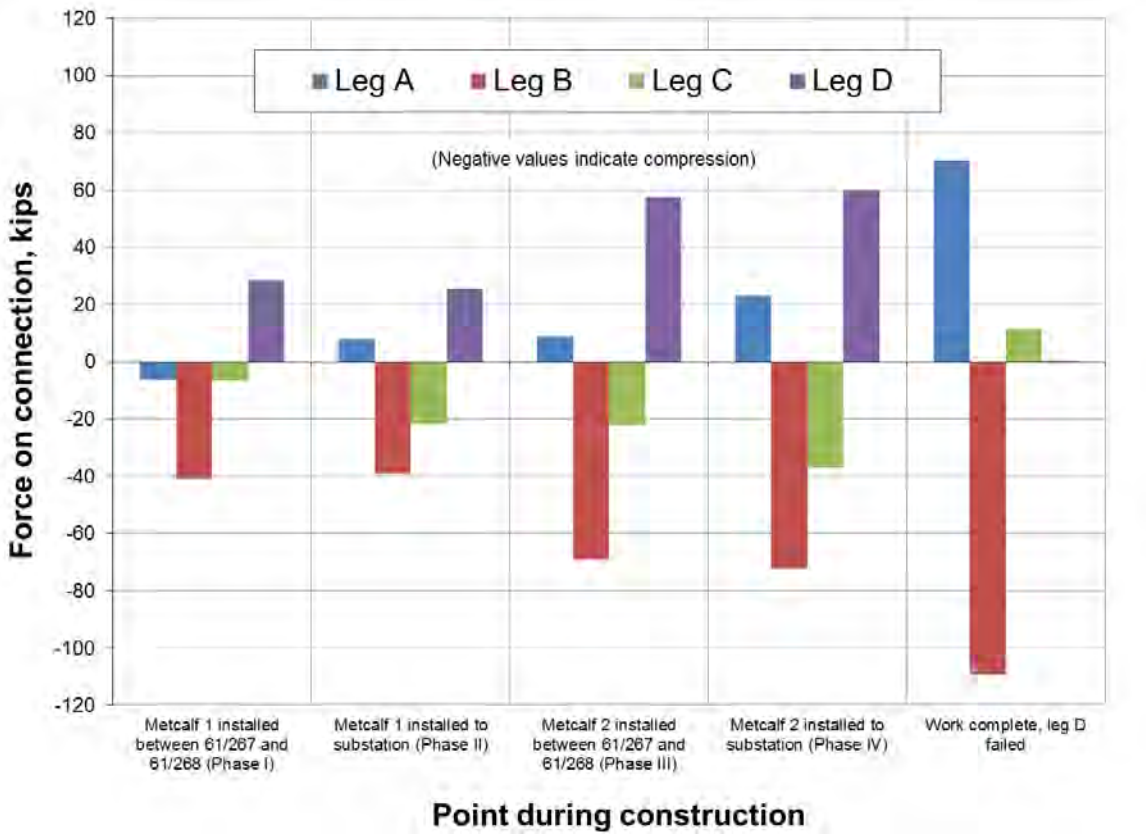


Figure 13. Axial forces on tower stub angle connections.

## Construction Fit-Up Loads

The fracture origins and trajectories, as described in a later section, suggest that failures of stub angles B and D generally initiated first near the outboard knee (heel) of the angles, then progressed toward the inboard toes. This implies that a bending moment was applied to legs B and D at the time that the stub angles of legs B and D had fractured. The orientation of that bending would be consistent with loads applied to the critical section had the tower legs been pulled inward. Inward displacement of the tops of the 17.5-ft tower leg extensions, as might be needed for fit-up during tower erection, was investigated as a possible failure load scenario.

Exponent engineer Will Trono visited the site on December 1, 2015 to observe PG&E's reconstruction of the foundation stub angles as they appeared in their as-built configuration. The objective of this work was to determine if the stubs were angled out-of-plumb according to the original construction drawings. Prior to that visit, portions of each stub angle below the fracture surfaces had been cut and removed as physical evidence for laboratory testing, but the remainder of each stub angle remained embedded in the concrete foundations. PG&E personnel

used C-clamps to splice an identical angle to the remaining stub, and the elevation of the top of the splice was reportedly set using the same survey point that was used during the original construction (Figure 14).

Field measurements were taken using a plumb bob and tape once the splices were set at the proper elevation.[7] Measurements included the batter angle (plumbness) of each stub relative to the vertical plane, as well as the horizontal dimensions between the stubs. According to PG&E's stub setting plan, the horizontal dimension was to be 29-feet – 1/8-inch between the top of the stub heals along the tower face and 41-feet – 3/8-inch between the top of stub heals on the tower diagonal. Field measurements deviated by at most 5/8-inch from these design dimensions.

Stub A was found to be out-of-plumb by one inch per foot toward Stub D. This deviation can be attributed to local damage at the base of the exposed stub (see Figure 15) caused by the ram used to chip the surrounding concrete. The other stubs were out-of-plumb by at most 1/12 inch per foot.

The as-built (as-measured) heel batter of the foundation stub angles were approximately one inch per foot too steep relative to the design drawings, and as such the top of any tower leg bolted to them would have been significantly outboard of its intended position. This outboard offset would be approximately 17 inches, as shown in Figure 16.

The tower's steel members were pre-fabricated with pre-punched holes based on the design dimensions shown on drawings. According to PG&E's erection sequence, lacing of Legs A and B occurred after the four legs were semi-bolted (loosely bolted) to the foundation stubs. Lacing of Legs D and C followed. Finally, these two opposite "frames" were joined by lacing Legs B and C and Legs D and A.

The offsets shown in Figure 16 would cause difficulty in fitting up additional members after installation of the tower legs. Installation of the double angle (2L3.5x3.25x0.25) horizontal stringers (see Figure 16) would require the each leg to be pulled inward by a significant amount, resulting in large bending moments at the critical section of each leg - a load that was unanticipated in the design. PG&E personnel reported that all of the lacing members are first bolted to the central gusset plate, then they are attached to the legs working from the bottom up, with the horizontal stringer connected to the legs last. Therefore, as each lacing connection was made, the top of the leg would displace inward by some amount, and the full 17 inches of offset may not have been apparent when workers made the top stringer-leg connection. (We note that the bolts were reportedly loose during erection of the 17.5-foot extension, and the high fit-up forces at the critical section may not have been fully realized until the bolts were subsequently tightened/cinched.)

[7] PG&E subsequently conducted a field survey of the reconstructed stubs using an electronic survey total station on December 17, 2015. The survey essentially confirmed the earlier measurements showing the misalignment of the stub angles. In all instances, the heel batter angles determined from the survey were within 3/16-inch per foot of the earlier field measurements, and the horizontal dimensions determined from the survey were within ¼-inch of the earlier field measurements.

Exponent evaluated two load cases: Figure 17(a) shows Case I used to determine the loads caused by lacing of Legs A and B and Legs D and C, assuming that the stub angle and tower leg are rigidly attached (fully bolted and tightened). Figure 17(b) shows Case II used to determine the loads caused by lacing of Legs B and C and Legs D and A. The analysis was linear elastic; that is, it did not consider softening due to plastic deformation or other damage. Figure 18 shows the analysis results, with moment at the critical section (bottom row of bolts) on the vertical axis and displacement of the top of the 17.5-foot leg extension on the horizontal axis.

Exponent compared the demands with the expected capacity of the tower leg and the foundation stub based on code equations. The capacity of the L6x6x5/8 both with and without bolt holes was calculated using AISC 360-10 §F10 for single angles under bending loads. Demand-to-capacity ratios were calculated for the tower leg just above the top row of bolts (i.e. point of maximum moment on the gross cross section) and for the foundation stub at the bottom row of bolts (i.e. point of maximum moment on the net cross section).

The results (Table 1) indicate that the expected capacities of both the stub angle critical section and tower leg would be exceeded if the misalignment of the stub angle were to be corrected by forced fit-up during construction. This overstress is consistent with the nature and sequence of critical section fractures discussed below. The overstress is also consistent with the presence of corrosion on fracture surfaces at Stubs B and D, indicating that those fractures occurred well before the day of the tower collapse (i.e., from loads resulting from forced fit-up during tower erection rather than externally applied loads on the towers and conductors at the time of failure).


Figure 14. Measuring the plumb of stub angle on December 1, 2015 (extended to original height using additional angle sections)


Figure 15. Deformation in Stub A

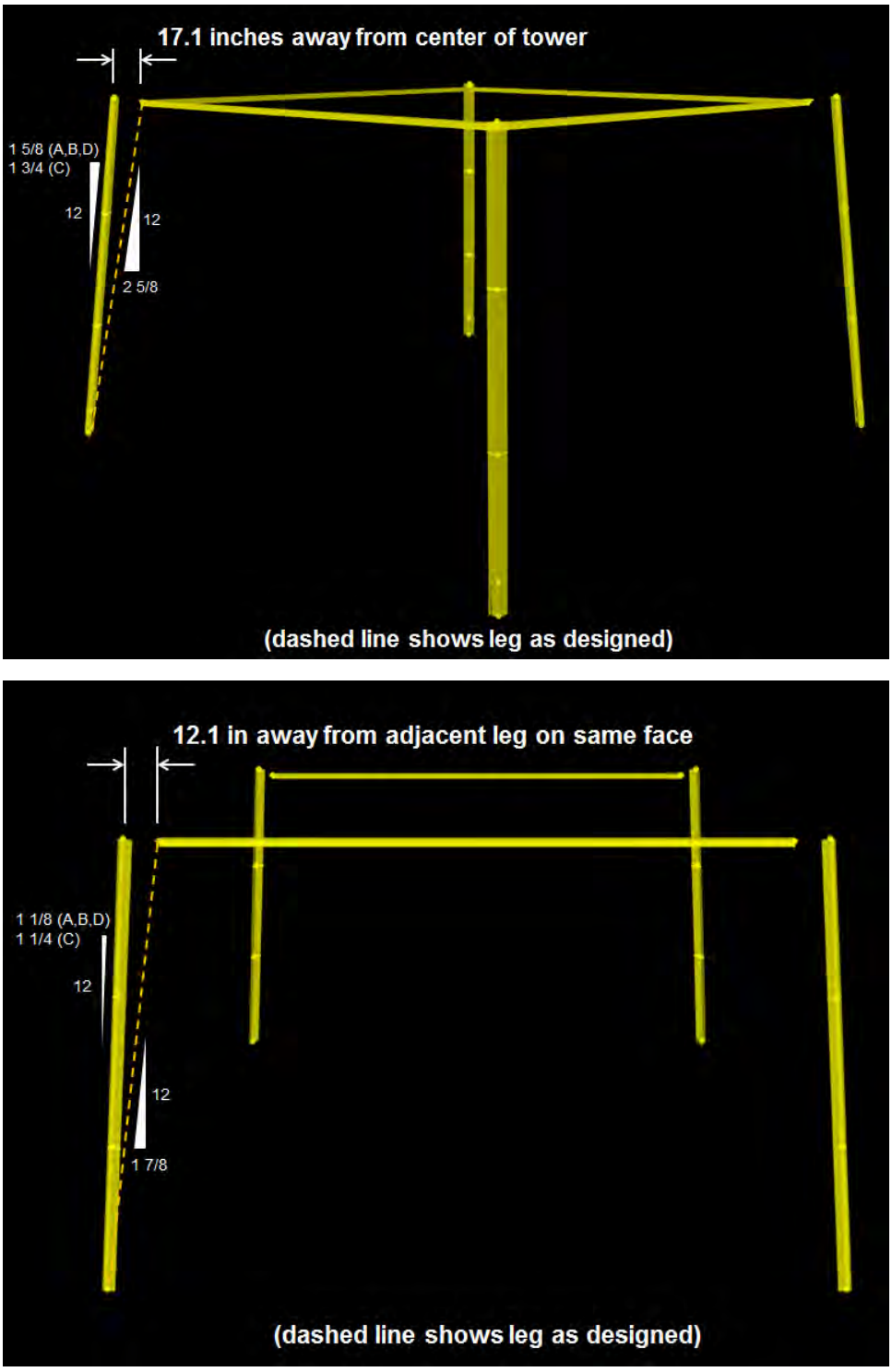


Figure 16. Offsets caused by error in stub heel batter angle.

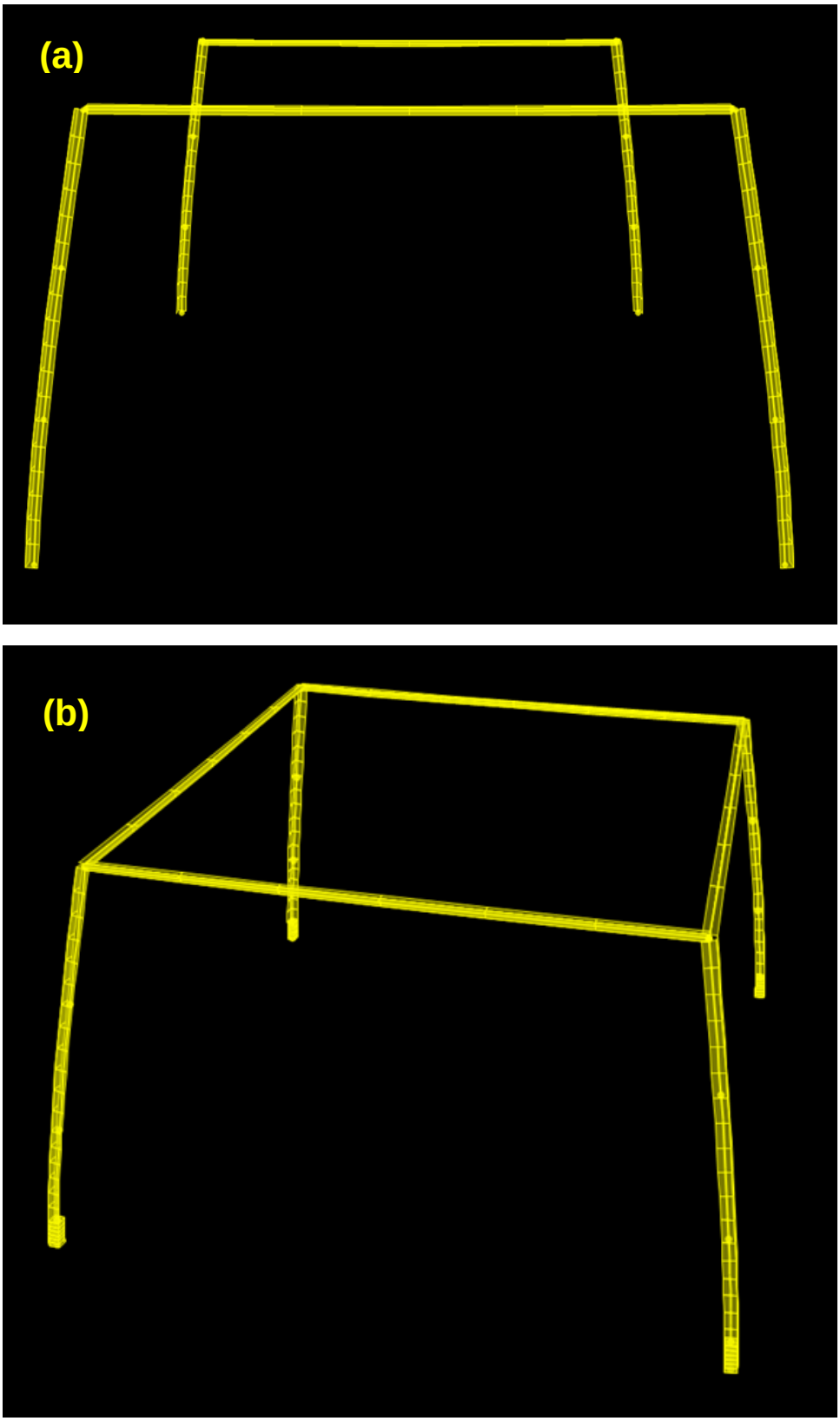


Figure 17. Loading scenarios during tower fit-up. (a) Case I - connection of legs A&B and D&C (b) Case II - connection of legs B&C and D&A

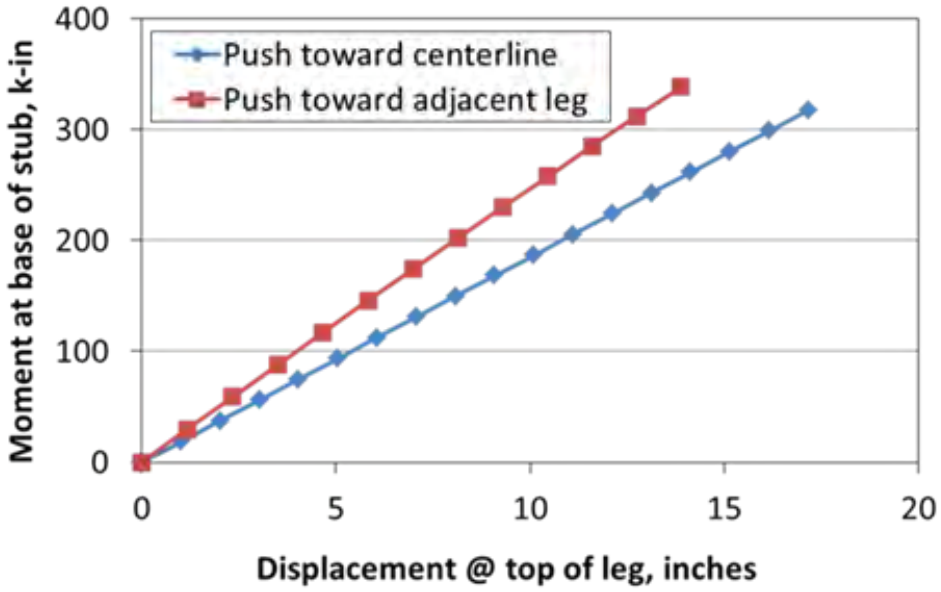


Figure 18. Moment demand at base of stub versus displacement at top of leg.

**Table 1 Demand-to-capacity ratios for tower leg and foundation stub.**

| Load Case | Leg above top row of bolts | Stub at bottom row of bolts |
|---|---|---|
| I. Push to adjacent leg | 0.89 | 1.10 |
| II. Push to tower centerline | 1.17 | 1.38 |

# Metallurgical Analysis

Exponent conducted a metallurgical investigation to help determine why the relatively newly-constructed Tower 61/268 collapsed on October 18, 2015. As described below, our metallurgical analysis included visual, fractographic, and metallographic examination of the fractured components, as well as chemical analysis, hardness testing, tensile and Charpy V-Notch (CVN) testing. Exponent also conducted linear-elastic fracture mechanics-based analyses to assess which service stresses were sufficient to cause the collapse. The following describes our analyses:

## Visual Examination

The four incident stubs, identified as Stub A through D, were cut and unbolted from the accident site and shipped to Exponent's Menlo Park laboratory for analysis. In this report, the bottom of each stub fracture (closest to the concrete pier) will be identified as the base-side, while the fractured portion of each stub that was bolted to the tower will be called the tower-side. An image that shows the base- and tower-sides of each of the fractured stubs (in the as-received condition) is shown in Figure 19. Images of the base-side of each of the broken stubs are shown in Figure 20 through Figure 23. (Note that the stub cutting process created some concrete dust that slightly obscured the base-side fracture surfaces in the as-received condition.) Visual inspection showed that the incident stubs displayed primarily brittle fracture morphology, with little plastic deformation (with the exception of portions of Stubs B and C that displayed plastic deformation associated with final bending as Tower 61/268 fell). Laminar separation along a longitudinal plane was also observed in Stubs B and C (an example is shown in Figure 24). This laminar separation was only observed in ductile, final fracture areas: no evidence of any defect was observed at the delamination locations in Stubs B and C. This laminar separation did not contribute to the collapse of the subject tower and was only caused by large bending strains that occurred at final failure.

Exponent examined the fractured stubs within hours of the collapse; at that time, portions of the Stub B and D fractures exhibited significant corrosion (Figure 19, Figure 21, and Figure 23). Stubs A and C fracture surfaces exhibited no corrosion (Figure 19, Figure 20, and Figure 22), consistent with recent fracture. The extensive corrosion present on Stub B and D fracture surfaces indicates that these fracture areas likely existed for weeks prior to the October 18, 2015 collapse.

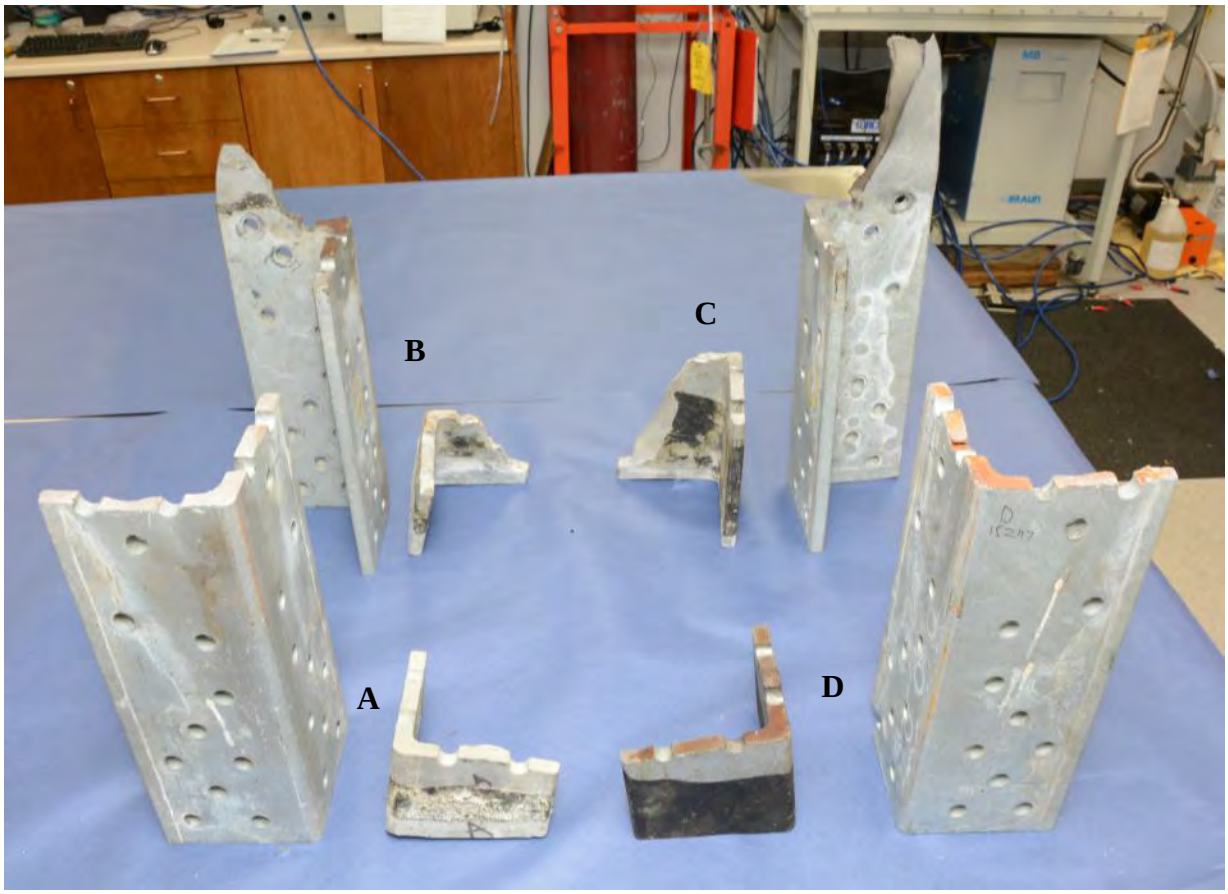


Figure 19. Photograph that shows both halves of each of the fractured incident stubs.


Figure 20. Photograph of the Stub A base fracture during visual examination.


Figure 21. Photograph of the Stub B base fracture during visual examination.

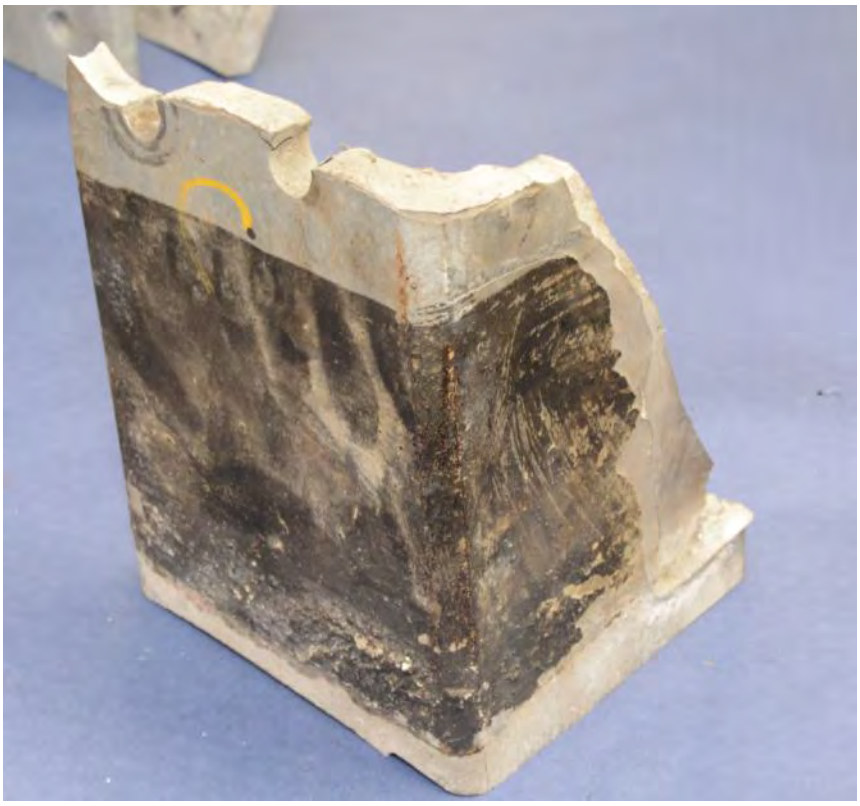

Figure 22. Photograph of the Stub C base fracture during visual examination.


Figure 23. Photograph of the Stub D base fracture during visual examination.

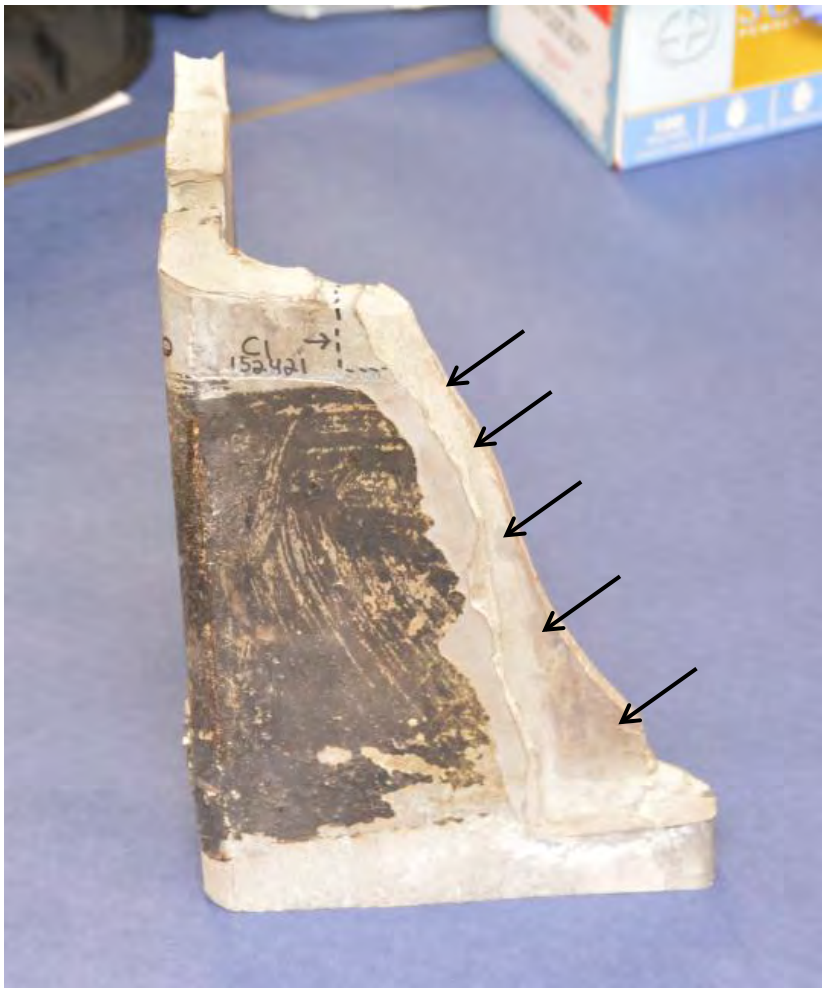

Figure 24. Laminar separation in the ductile overload portion of Stub C, shown by arrows.

# Fractography

## Visual Analysis

Visual analysis was sufficient to determine the fracture origins and direction of crack propagation for each of the four stubs. Chevron marks, as shown in Figure 25, point to the crack origins and indicate the direction of growth. The schematic shown in Figure 26 shows the fracture origins on the base-side of the subject tower stubs (viewed from above), crack propagation directions, and the portions of the fractures that pre-existed the October 18th, 2015 collapse. Each of the fractures initiated at bolt holes. Both Stubs B and D, which each exhibited fractures that pre-existed the collapse, contained two fracture initiation locations, one on each "leg" of the L-shaped cross section (shown in Figure 26). Stubs A and C, which fractured at the time of collapse, each had a single fracture origin. Photographic montages that show the tower-side fracture surfaces of Stubs A and D (the two stubs without large amounts of tearing/bending associated with final fracture) are shown in Figure 27 and Figure 28.

The existence of chevron marks on the fracture surfaces and lack of significant plastic deformation (aside from the plastic-hinge locations on Stubs B and C) indicates that the incident tower fractured primarily in a brittle manner. Brittle fracture occurs on planes perpendicular to the maximum principal (tensile) stress. Thus, examination of the fracture planes, particularly at the fracture origins helps to indicate the direction of the stress that caused the break. As shown in Figure 20 through Figure 23, fracture surfaces were predominantly perpendicular to the stub axis (except for the final plastic-hinge areas in Stubs B and C). Thus, the fractures were caused by tensile forces that generally acted long the length of the stubs.

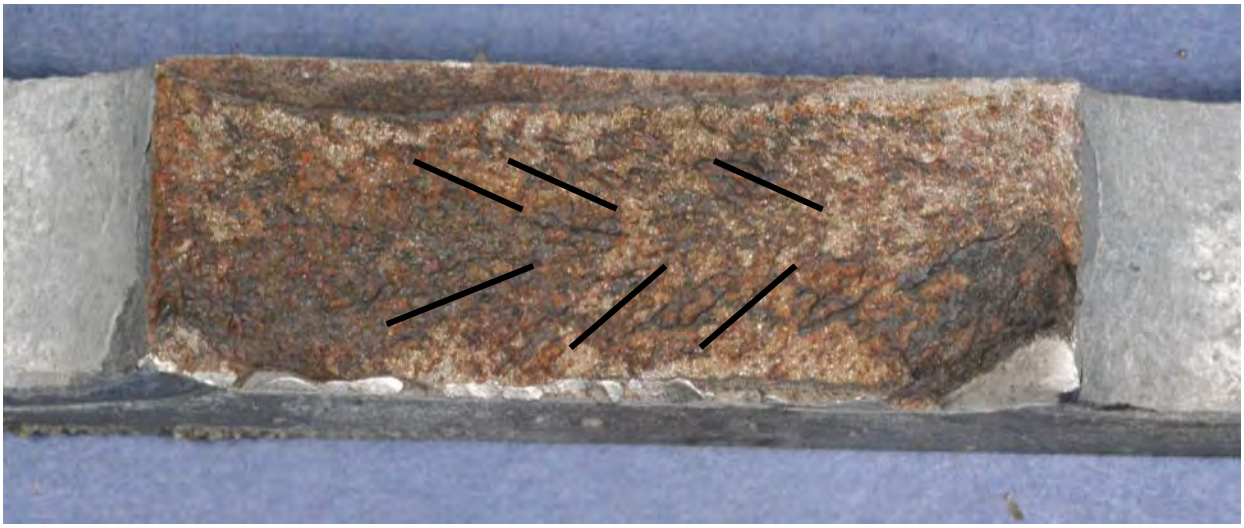

Figure 25. Photograph that shows representative chevron marks in Stub B. The dark lines help show the direction of the chevron marks.

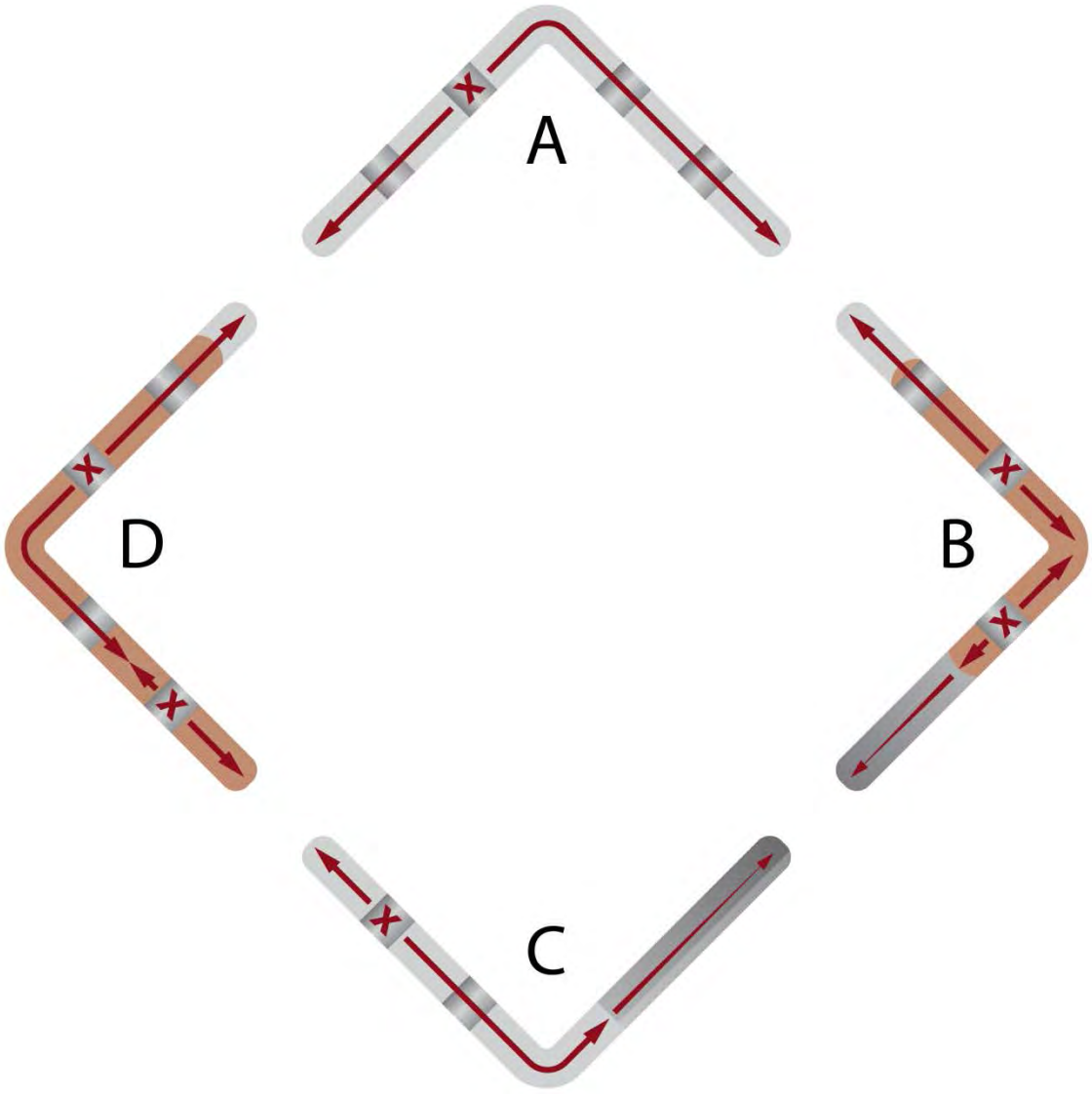


Figure 26. Schematic that shows fracture initiation locations and growth directions in each of the four stub bases, when viewed from above. “X” indicates fracture origin hole locations, red arrows show crack growth directions. Gray-colored areas are fractures that were created when the tower collapsed; orange areas are those that exhibited corrosion at the time of the collapse.

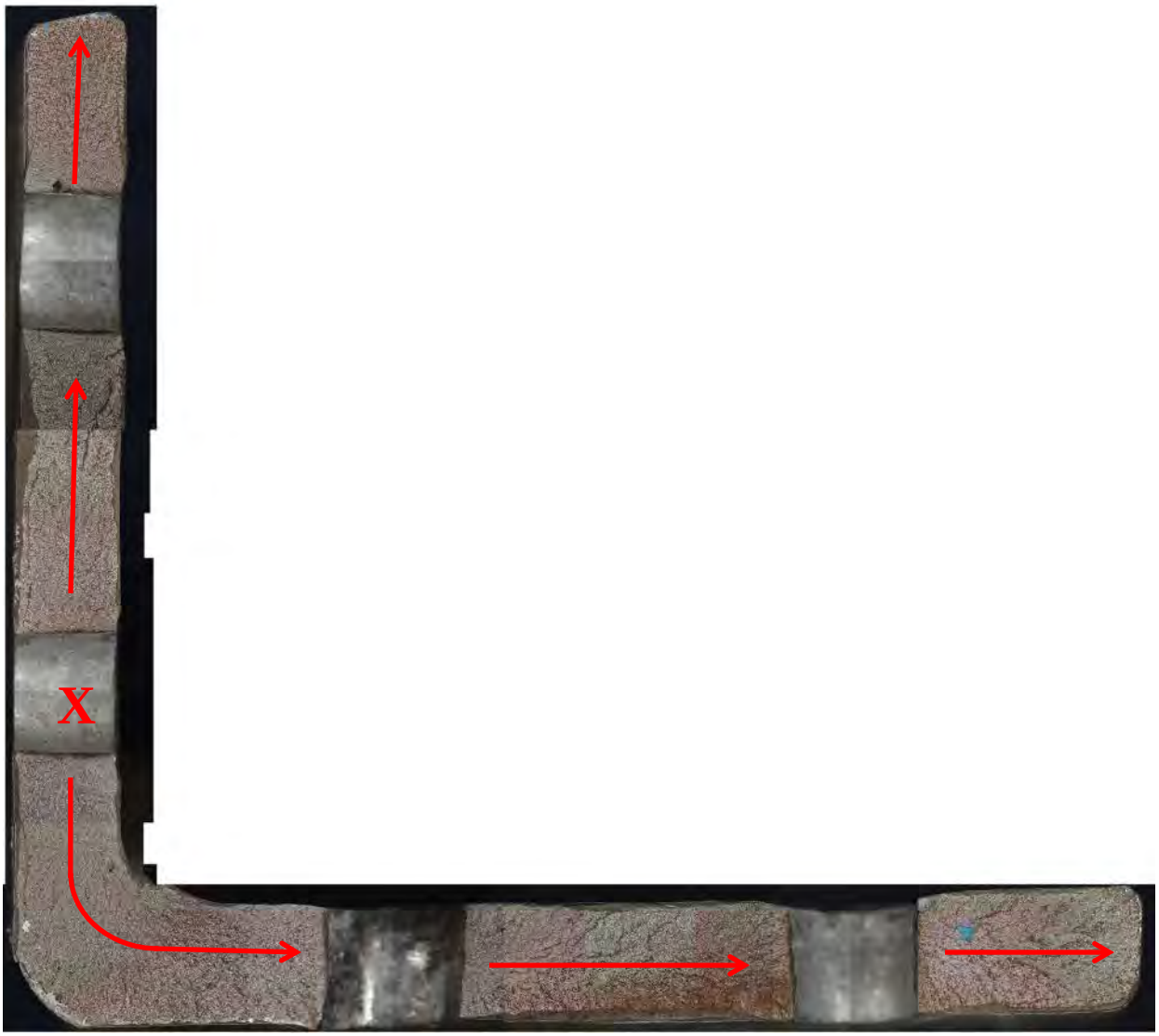


Figure 27. Stub A tower-side fracture surface montage, when viewed from below. “X” indicates the hole at the fracture origin, and red arrows show crack growth directions.

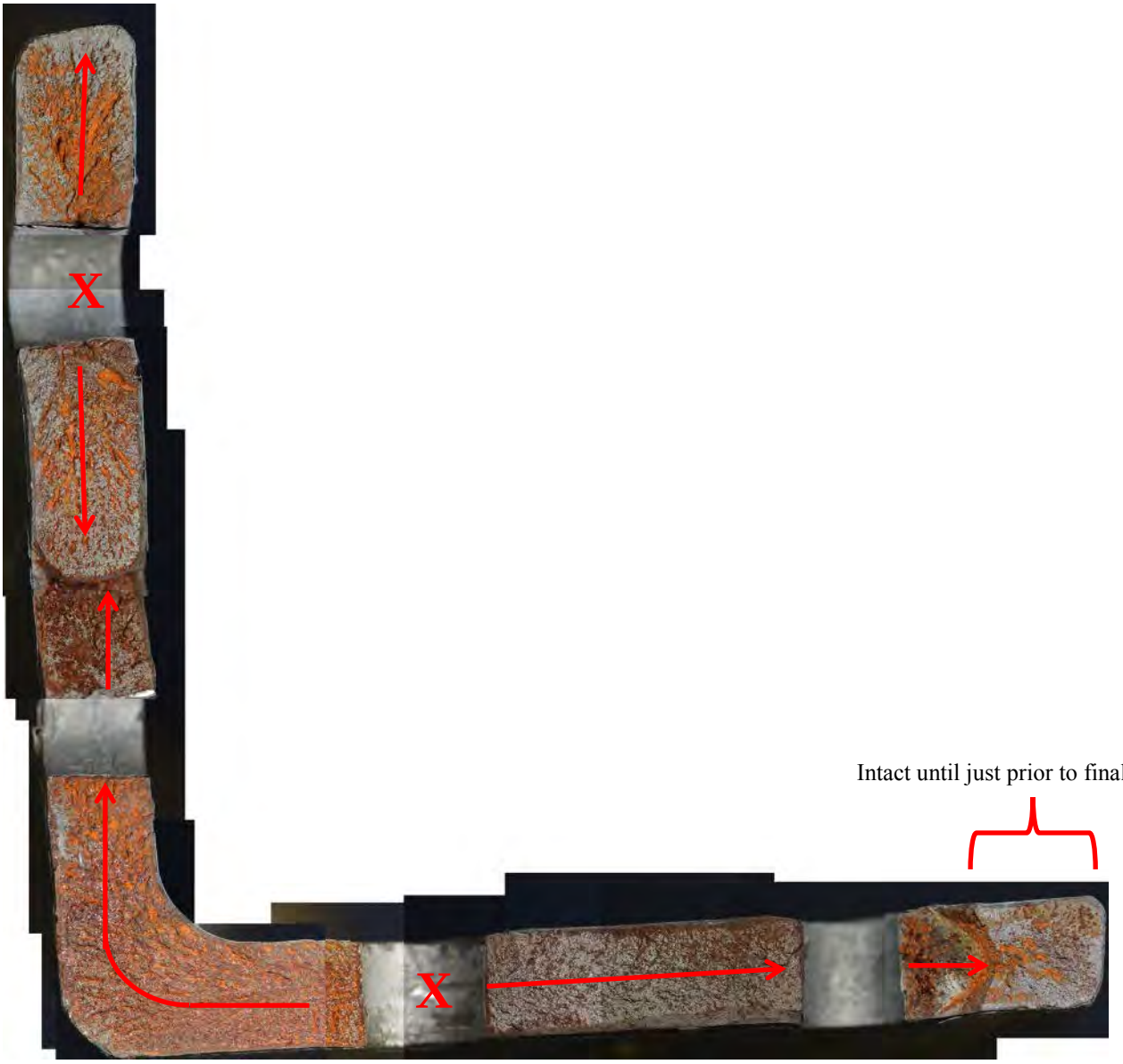


Figure 28. Stub D tower-side fracture surface montage, when viewed from below. "X" indicates the hole at the fracture origin, and red arrows show crack growth directions. The red bracket indicates the area that was intact until just before the final tower collapse.

## Scanning electron microscopy

Fracture origin areas from Stubs A and B were sectioned, cleaned, and examined using scanning electron microscopy (SEM) to confirm the fracture mode. SEM images of representative portions of Stub A and B fracture surfaces are shown in Figure 33. Both stubs exhibited cleavage fracture morphology, consistent with brittle overload fracture in carbon steels. The existence of cleavage fracture throughout the subject stubs confirms brittle fracture, and

indicates that the fractures all occurred at temperatures below the ductile-to-brittle-transition temperature for the tower steel. No evidence of progressive cracking, such as fatigue crack initiation and growth or environmentally-assisted cracking, such as stress-corrosion cracking (SCC) was observed.

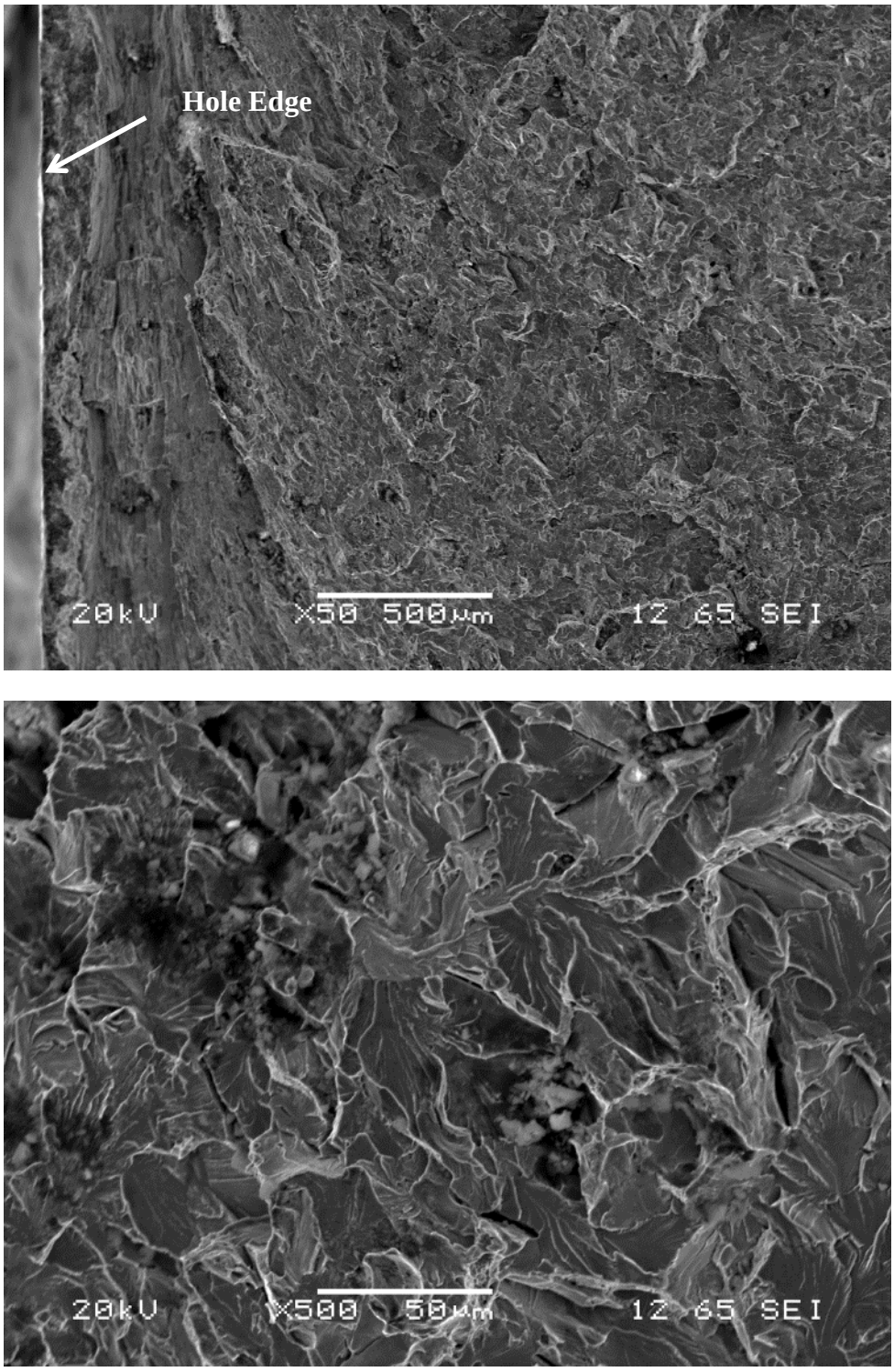


Figure 29. Representative SEM images from Stub A. Cleavage fracture morphology was observed throughout.

## Metallographic Examination

Specific locations of the incident stubs were cross sectioned, mounted, polished and etched for metallographic interpretation of the microstructure. The sectioning of the material surrounding the hole at the Stub A fracture origin, is shown in Figure 30. Metallographic examination showed significant plastic deformation at the holes, consistent with hole-punching with no subsequent reaming, as shown in Figure 31 and Figure 32. The base microstructure of the incident stubs was ferrite/ pearlite (Figure 33), as would be expected for this steel.

Microhardness traverses were taken that included material near and distant to the punched holes, including fracture origin locations. Plots from representative microhardness traverses are shown in Figure 34. Microhardness readings taken near the holes showed significant hardening, associated with the localized plastic deformation that occurs during the punching process. Further than approximately three millimeters from the holes, the zone of plastic deformation diminished, and the hardness values were roughly constant. The hardest areas adjacent to the holes were between roughly 350 and 400 on the Vickers scale, roughly equivalent to local tensile strengths of 160 to 200 ksi. The base metal hardness (away from the holes) was approximately 170 on the Vickers scale, predictive of a tensile strength of approximately 80 ksi; similar to strengths observed during tensile testing of each of the stubs.

Secondary cracks were observed at some of the holes examined metallographically, as shown in for both Stubs A and D in Figure 35. These cracks were typically less than one-millimeter in length, within the zone of hardened material from the punching process.

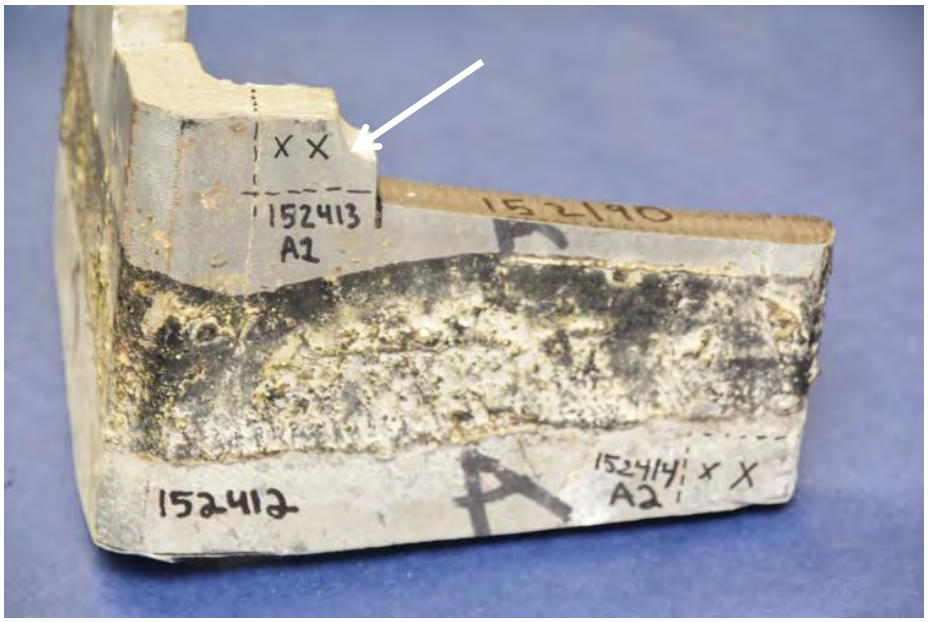


Figure 30. Photograph that shows representative sectioning location for metallographic analysis in Stub A (indicated by arrow). The “x x” indicates the metallographic section location.

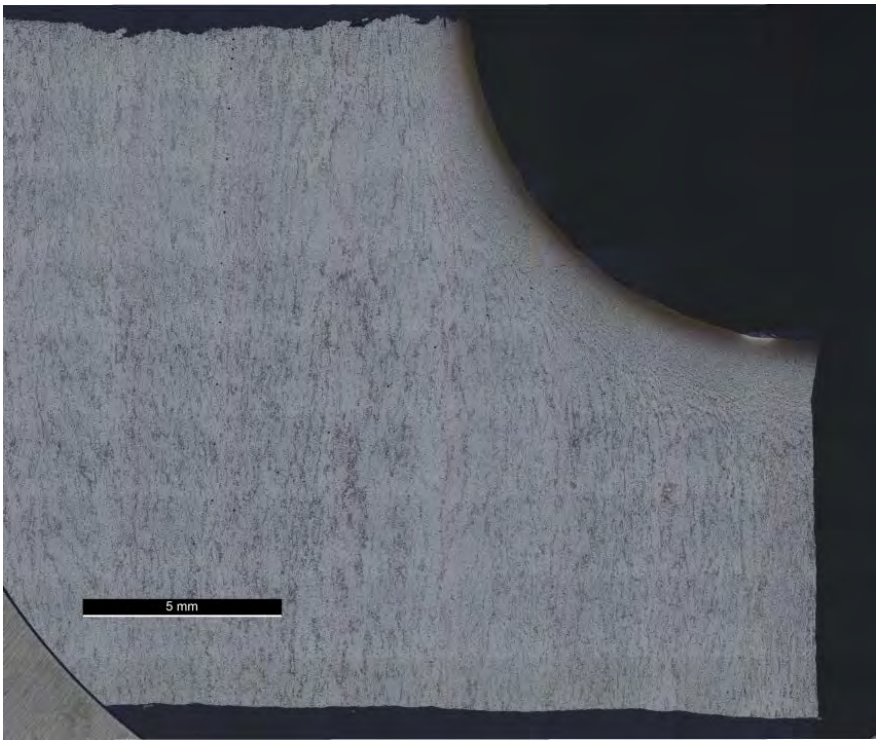


Figure 31. Low-magnification metallographic montage that shows microstructure at and away from one of the two Stub D punched-hole fracture origins.

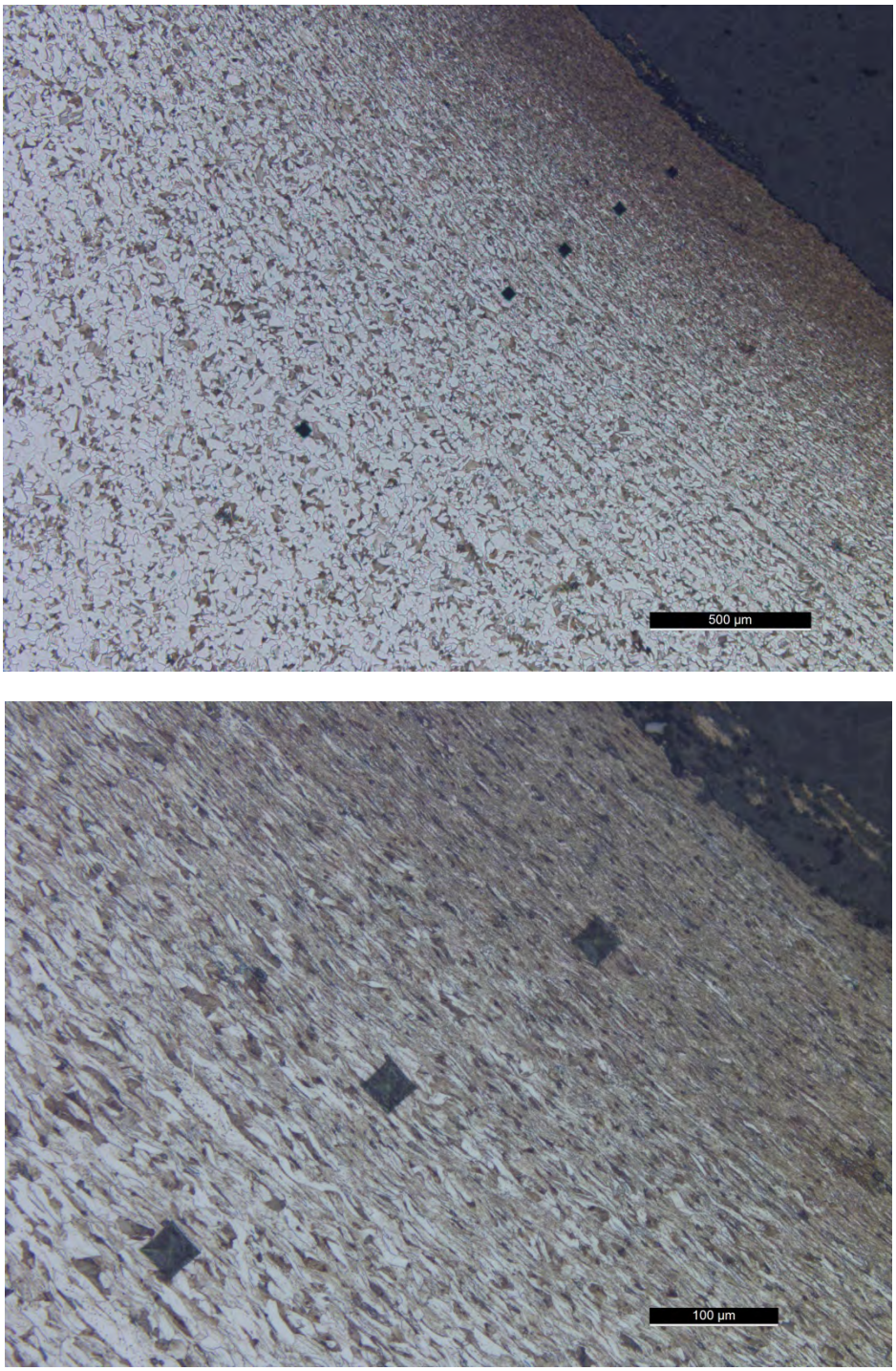


Figure 32. Metallographic image of the microstructure at a Stub D punched-hole fracture origin.

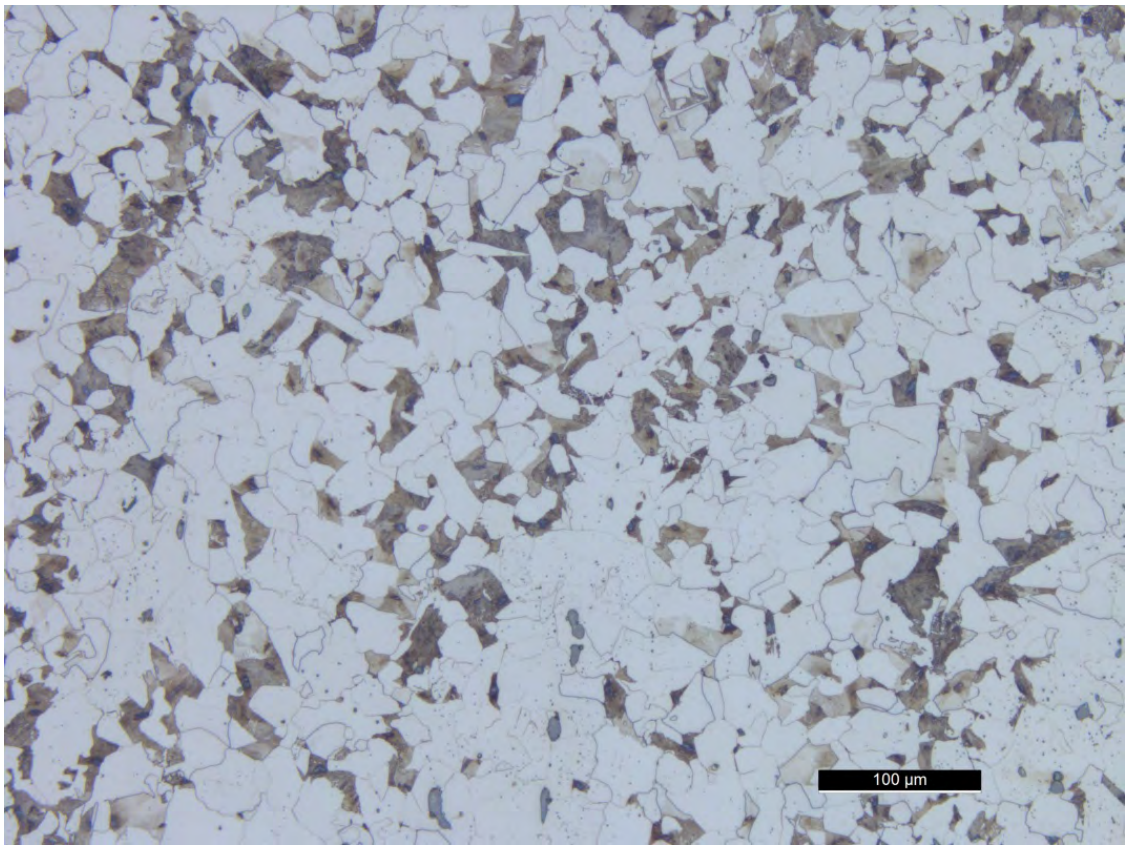


Figure 33. Representative metallographic images of the base metal microstructure observed in each of the stubs.

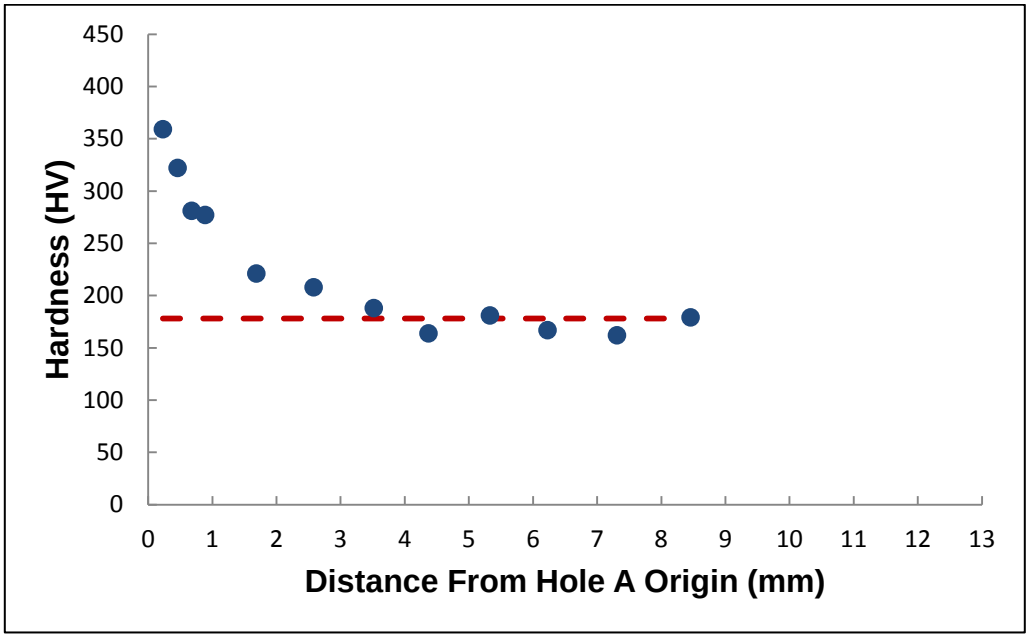


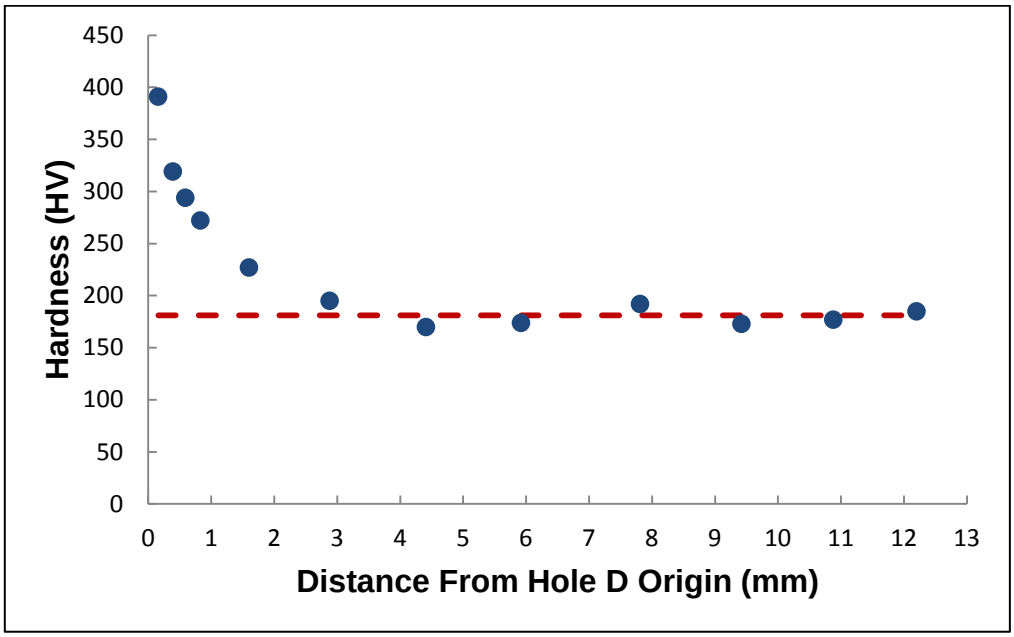


Figure 34. Microhardness profile plots for Stub A and D holes at fracture origin locations.

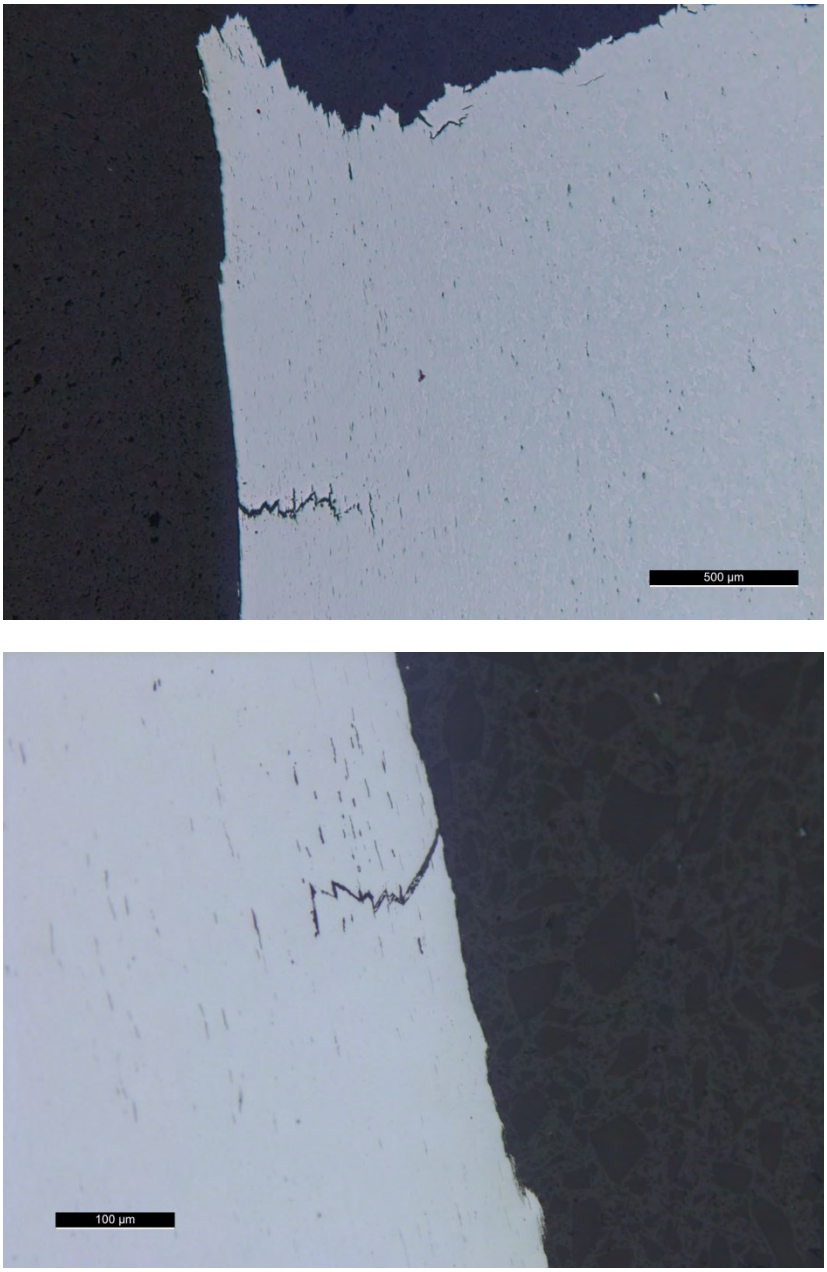


Figure 35. Metallographic images of secondary cracks observed along the hole surface in Stub A (top) and Stub D (bottom).

## Elemental Analysis

Samples were removed from each of the incident and exemplar stubs for elemental analysis. Results from the elemental analyses are shown in Table 2. PG&E indicated that the incident stubs were made from material purchased from Nucor. A 5/8/2014 Nucor Mill Certification for Nucor Multigrade Lot # PL420161901 was provided. The elemental ranges for each of the specifications listed in the Nucor Material Certification are shown in Table 3. The results show

that the incident and exemplar stub elemental compositions largely meet the specifications listed by the Nucor in Material Certification. The results also show that each of the incident stubs, as well as Exemplars 1 and 2 are likely from the same material lot. Elemental quantities in Exemplar 3 are slightly different than the others: it is likely that the Exemplar 3 material is from a different lot than the others. Sulfur has long been recognized as a tramp element that reduces steel toughness.[8] The sulfur content in the incident/ Exemplar 1 and 2 samples was just below the allowable levels for some of the Nucor-referenced standards, such as ASTM A572-2012. The 2015 version of ASTM A572 allows only 0.03 weight percent sulfur. Thus, none of the incident or exemplar samples would have met the current ASTM A572-15 requirements for maximum-allowable sulfur.

The base metal from each of the subject and exemplar stubs was also subjected to hydrogen analysis via inert gas fusion testing per ASTM E1447-09. Each of the samples contained three or four parts-per-million hydrogen. This amount of hydrogen is sufficient to embrittle hardened steel under sufficient stress.[9]

[8] G. Krauss, Steels: Processing, Structure, and Performance, ASM International, 2008, pp. 158-159.

[9] B. Pound, "Hydrogen Ingress During Corrosion", Encyclopedia of Electrochemistry, Vol. 4, (Stratmann, Frankel Editors), pg. 137.

**Table 2. Compositional analysis results for Incident Samples A, B, C, D and Exemplar Samples 1, 2, and 3. Composition was determined using spectrochemical analysis (ASTM E415-110). Some elements were analyzed using LECO combustion analysis (ASTM E1019-11), as indicated by an asterix. All results are reported in wt%.**

| Element | Incident Samples | | | | Exemplar Samples | | |
|---|---|---|---|---|---|---|---|
| | A | B | C | D | 1 | 2 | 3 |
| Aluminum | <0.005 | <0.005 | <0.005 | <0.005 | 0.01 | <0.005 | <0.005 |
| Carbon* | 0.21 | 0.21 | 0.21 | 0.21 | 0.21 | 0.21 | 0.18 |
| Chromium | 0.13 | 0.12 | 0.13 | 0.12 | 0.13 | 0.12 | 0.21 |
| Copper | 0.22 | 0.22 | 0.22 | 0.22 | 0.22 | 0.22 | 0.32 |
| Manganese | 0.73 | 0.73 | 0.73 | 0.73 | 0.73 | 0.72 | 0.72 |
| Molybdenum | 0.02 | 0.02 | 0.02 | 0.02 | 0.02 | 0.02 | 0.03 |
| Nickel | 0.09 | 0.09 | 0.09 | 0.09 | 0.09 | 0.09 | 0.12 |
| Nitrogen | 0.013 | 0.013 | 0.013 | 0.012 | 0.013 | 0.013 | 0.012 |
| Phosphorus | 0.012 | 0.011 | 0.012 | 0.011 | 0.012 | 0.011 | 0.014 |
| Silicon | 0.22 | 0.22 | 0.22 | 0.22 | 0.22 | 0.22 | 0.18 |
| Sulfur* | 0.044 | 0.047 | 0.047 | 0.047 | 0.046 | 0.046 | 0.033 |
| Titanium | <0.005 | <0.005 | <0.005 | <0.005 | <0.005 | <0.005 | <0.005 |
| Vanadium | 0.02 | 0.02 | 0.02 | 0.02 | 0.02 | 0.02 | 0.02 |

**Table 3. Compositional requirements for specifications listed in the NUCOR Mill Certification. All values are reported in wt%.**

| Element | ASTM A36 / A36M-12 | ASTM A529 / A529M-05 GR50 | ASTM A572 / A572M-12A GR50 | ASTM A709 / A709M-13 GR50 | CSA G40.21-13 GR44W (300W) | CSA G40.21-13 GR50W (350W) | AASHTO M270 / M270M-10 GR36 / GR50 | ASME SA36 / SA3636 M-07 |
|---|---|---|---|---|---|---|---|---|
| Carbon | <0.25 | <0.27 | <0.23 | <0.25 | <0.22 | <0.23 | <0.25 | <0.25 |
| Manganese | | <1.35 | <1.35 | | 0.5-1.5 | 0.5-1.5 | | |
| Phosphorus | <0.04 | <0.04 | <0.04 | <0.04 | <0.04 | <0.04 | <0.04 | <0.04 |
| Sulfur | <0.05 | <0.05 | <0.05 | <0.05 | <0.05 | <0.05 | <0.05 | <0.05 |
| Silicon | <0.40 | <0.40 | <0.40 | <0.40 | <0.40 | <0.40 | <0.40 | <0.40 |
| Copper | >0.20 | >0.20 | >0.20 | >0.20 | | | >0.20 | >0.20 |

## Mechanical Testing

Tensile and Charpy V-Notch (CVN) testing was conducted on each of the four incident stubs as well as three exemplars. None of the exemplars had punched holes. Exemplar 3 was galvanized, while Exemplars 1 and 2 were not.

Two tensile specimens were taken from each of the incident and the exemplar stubs. The tensile specimens were oriented such that their longitudinal direction matched that of the stubs: thus, the fracture plane in the tensile specimens was the same as that the incident stubs. The incident and exemplar tensile test results are shown in Table 4, and the requirements in the Nucor specification-referenced standards are shown in Table 5.

The tensile test results indicate that each of the incident stubs exhibited yield strengths at or greater than 50 ksi (one of the Stub D samples was slightly below 50 ksi yield), ultimate strengths all higher than 75 ksi, and more than 30-percent elongation. Based on these results, the incident stubs met the mechanical properties specified in each of the standards identified in the Nucor material certification document. The average yield strengths for Exemplars 1 and 2 were at or greater than 50 ksi, while both of the Exemplar 3 specimens exhibited yield strengths slightly below the 50 ksi minimum specified ASTM A529, A572, CSA G4-.21, and AAHSTO M270 standards in the Nucor materials certification.

CVN specimens were also taken from each of the four incident stubs, as well as from each of the three exemplars. CVN testing was performed per ASTM A370-14 specifications. CVN specimens were oriented in the L-T direction. Thus, like the tensile specimens, CVN specimen

fractures occurred along the same plane as the incident stub fractures. Review of PG&E purchasing records indicates that CVN testing was not required as part of the material certification process. Nucor indicated in their material certification document that CVN was not specified.

Specimens removed from Stub A were tested at a full series of temperatures ranging from -20°F to 140 °F. Specimens from Stubs B, C, D and Exemplars were tested at representative temperatures selected based on the test results of Stub A. The CVN impact energy of all incident samples were plotted versus test temperature (Figure 36), and curve-fit to the hyperbolic tangent equation (Figure 37) shown below as suggested by Standard API 579-1/ASME FFS-1 2007 Page F-14.

$$CVN = A_{cv} + B_{cv} \tanh\left[\frac{T - D_{cv}}{C_{cv}}\right]$$

The parameters of $A_{cv}$ and $B_{cv}$ were specified based on the upper and lower shelf of the Charpy transition-temperature curve. The upper shelf was selected as the maximum value at the highest test temperature (140 °F), while the lower shelf was the minimum at the lowest test temperature (-20 °F). The other two parameters, $C_{cv}$ and $D_{cv}$, were estimated by minimizing the sum of squares of the residual error (SSE), with statistical significance $P<0.05$ .

Similar analysis was performed on test results from exemplar specimens. The lower shelf was selected the same as the incident sample, while the upper shelf was selected based on the testing data of the exemplar at 140 °F and to reach a statistical significance of $P<0.05$.

Static fracture toughness ($K_{IC}$) at different temperatures was converted from the CVN impact energy by using $K_{IC} - CVN$ correlations as suggested by Standard API 579-1/ASME FFS-1 2007 Page F-14. The equation below was used to estimate the lower bound as recommended in WRC 265. The plot of static fracture toughness as a function of test temperature is shown in Figure 38.

$$K_{IC} = 9.35(CVN)^{0.63} \qquad (ksi\sqrt{in}, ft - lb)$$

All statistical calculations were performed using Minitab 17 software (Minitab Inc., PA, USA).

Comparison of ductile-to-brittle transition temperature (DBTT) behavior between the incident and exemplar stubs is shown in Figure 36 through Figure 38. The results show that the non-galvanized Exemplar Stubs 1 and 2 may have a slightly lower DBTT than the incident stubs. The small difference in toughness may be associated with strain aging that occurred during galvanizing of the incident stubs. Exemplar 3, which has lower carbon and sulfur levels, appears to have the best toughness/ transition behavior of all stubs. The DBTT of the incident stubs was approximately 70°F, above the estimated 55°F temperature at the time of the

collapse.[10] Based on the scatter found in our CVN testing, the critical fracture toughness $K_{IC}$ of the subject stubs may have been lower than 50 ksi√in at the time of the final collapse.

**Table 4. Tensile testing results for Incident Samples A, B, C, and D and Exemplar Samples 1, 2, and 3. Two tensile tests were performed and are reported for each Sample. Tensile testing was performed according to ASTM A370-14.**

| | Incident Samples | | | | | | | |
|---|---|---|---|---|---|---|---|---|
| | A | | B | | C | | D | |
| | Test 1 | Test 2 | Test 1 | Test 2 | Test 1 | Test 2 | Test 1 | Test 2 |
| Tensile Strength (ksi) | 78.5 | 78.4 | 78.2 | 78.0 | 77.9 | 78.1 | 77.7 | 77.6 |
| Yield Strength (ksi) | 51.0 | 50.8 | 51.5 | 50.0 | 51.0 | 51.4 | 49.4 | 50.4 |
| Elongation (%) | 32 | 32 | 32 | 32 | 32 | 31 | 31 | 31 |

| | Exemplar Samples | | | | | |
|---|---|---|---|---|---|---|
| | 1 | | 2 | | 3 | |
| | Test 1 | Test 2 | Test 1 | Test 2 | Test 1 | Test 2 |
| Tensile Strength (ksi) | 78.2 | 78.4 | 78.0 | 77.9 | 75.5 | 75.4 |
| Yield Strength (ksi) | 51.4 | 50.3 | 50.9 | 49.0 | 48.6 | 49.4 |
| Elongation (%) | 30.5 | 32 | 30 | 31.5 | 32 | 32 |

[10] See Figure 8

**Table 5. Tensile testing requirements for specifications listed in the NUCOR Mill Certification.**

| | ASTM A36 / A36M-12 | ASTM A529 / A529M-05 GR50 | ASTM A572 / A572M-12A GR50 | ASTM A709 / A709M-13 GR50 | CSA G40.21-13 GR44W (300W) | CSA G40.21-13 GR50W (350W) | AASHTO M270 / M270M-10 GR50 | ASME SA36 / SA3636M-07 |
|---|---|---|---|---|---|---|---|---|
| Tensile Strength (ksi) | 58-80 | 70-100 | >65 | >65 | 64-90 | 65-95 | >65 | 58-80 |
| Yield Strength (ksi) | >36 | >50 | >50 | >50 | >44 | >50 | >50 | >36 |
| Elongation (%) | >23 | >21 | >21 | >21 | >23 | >22 | >21 | >23 |

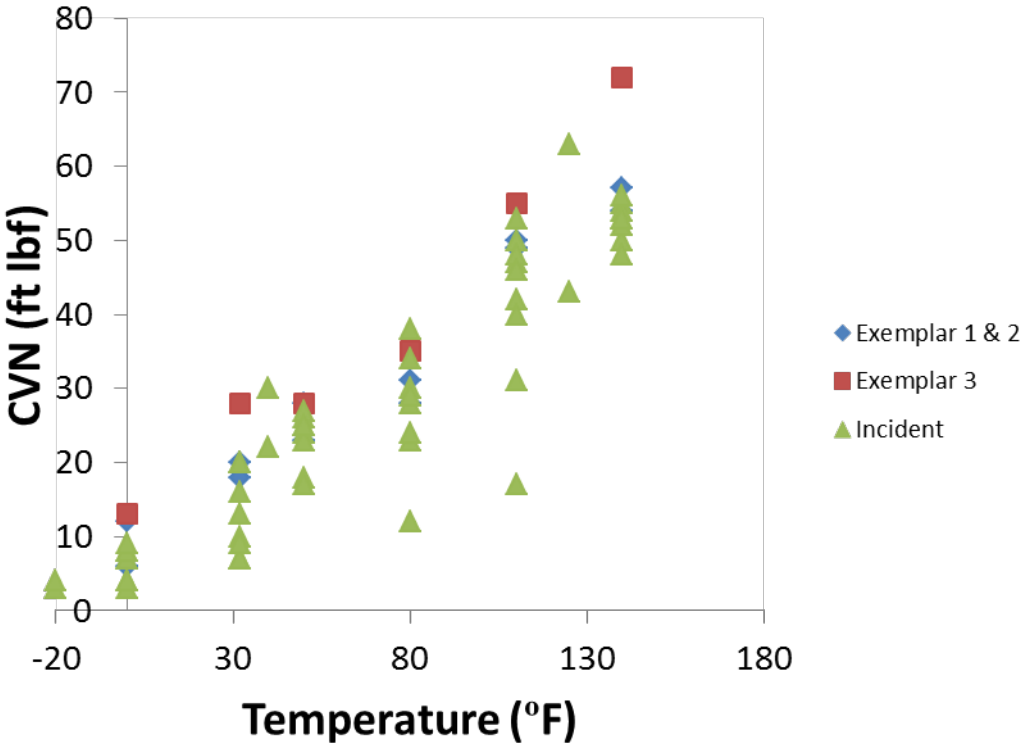


Figure 36. CVN data for each of the Incident stubs (A, B, C, D) and the three exemplar stubs.

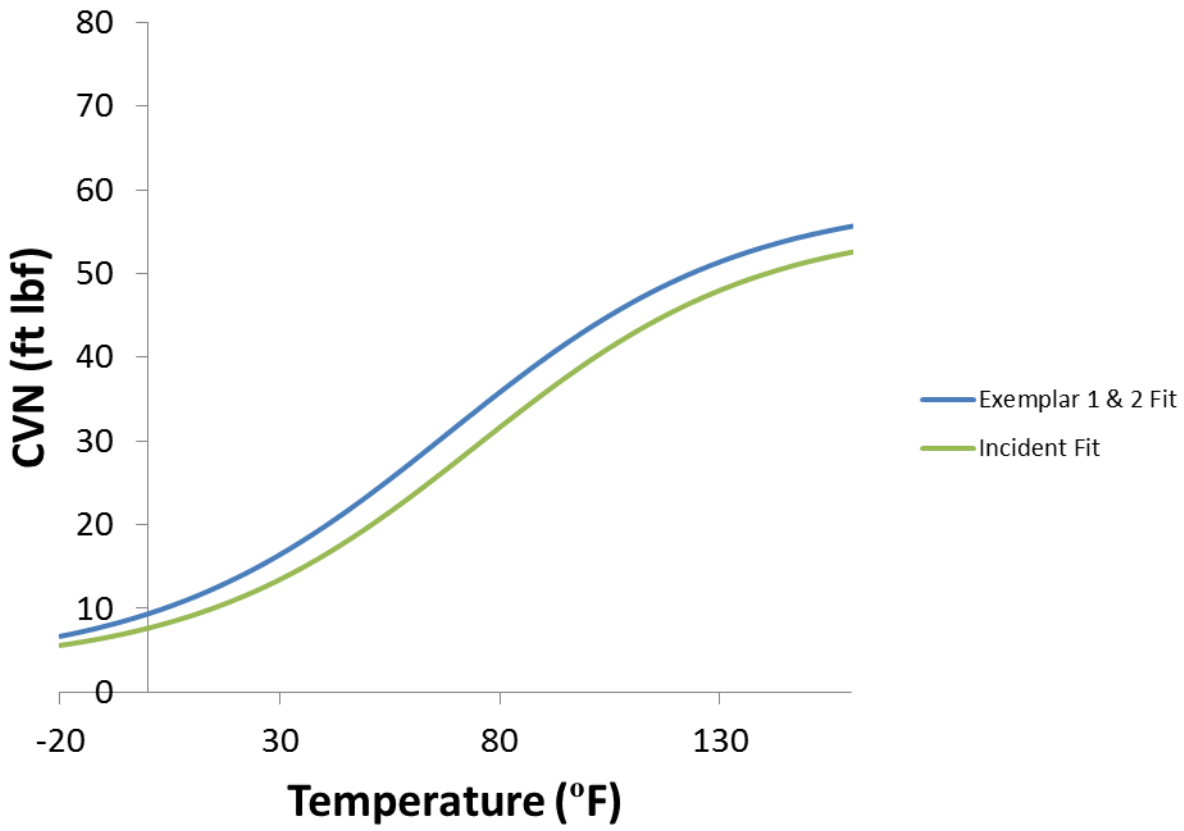


Figure 37. Hyperbolic tangent (per API 579) curve-fit CVN data as a function of test temperature for Incident and Exemplar 1 and 2 stubs.

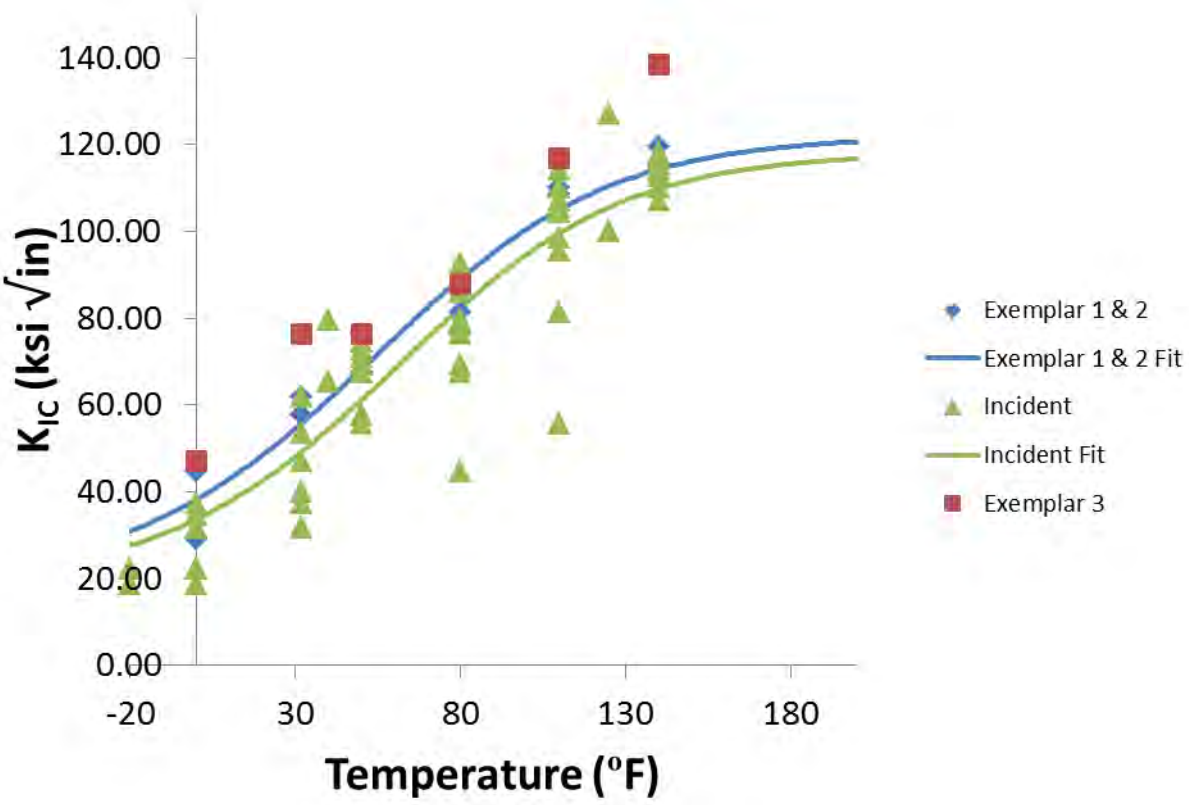


Figure 38. Stress intensity factor as a function of temperature converted from CVN test results.

# Stress and Fracture Mechanics Analysis

A three-dimensional finite element model was constructed to further investigate the stresses and fracture behavior associated with the Tower 61/268 collapse. The objective of the analysis was to calculate the stresses within the tower stubs given possible loading conditions observed during construction and the structural life of Tower 61/268. Using the resulting stress distributions combined with the fracture toughness measurements reported previously, a linear-elastic fracture mechanics analysis was performed to determine critical flaw sizes and critical load factors that would lead to tower stub fractures under various loading conditions.

## Finite Element Model Description

Abaqus 6.14-1 was used to generate the three-dimensional finite element model. Figure 39 shows the geometry of the un-cracked model (two-dimensional schematic shown in Figure 12), and was based on drawings provided by PG&E. The stub was modeled with linear-elastic properties for steel, assuming a Young's modulus of 29,000 ksi and a Poisson's ratio of 0.3.

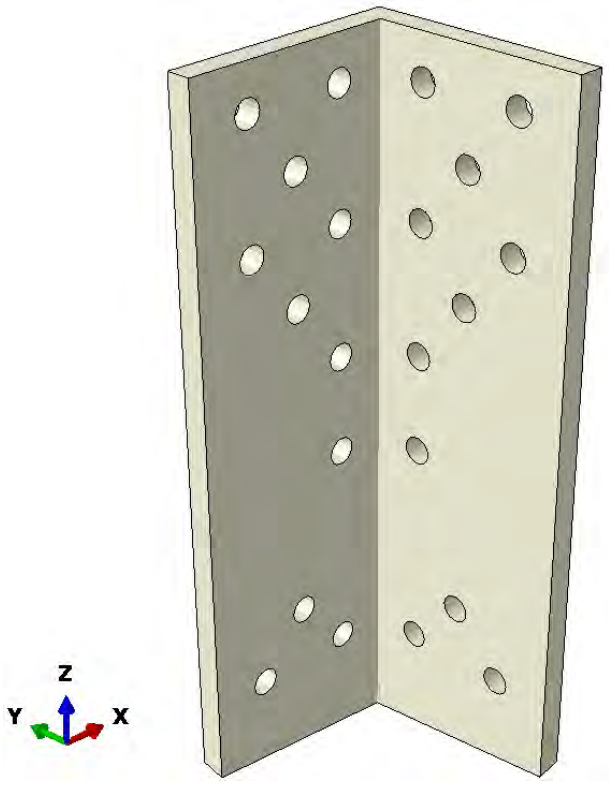


Figure 39. Stub finite element model geometry.

The stub model was fixed at the base where it was imbedded in the concrete footing. Two global structural load cases were analyzed: The first loading (nominal case) examined Stub D

with all conductors installed and all leg stubs fully intact. This load case is identified throughout this report as the "Stub-D case". The second loading condition examined Stub A with all lines installed, but assumed Stub D was completely fractured and could no longer support load. This case is identified as the "Stub-A case". The applied loads were extracted from the global structural analysis, as described in the *Structural Analysis* section. The idealized loading in the stub model consisted of three components: axial tension from the main structure leg, and two components from the diagonal struts. The idealized boundary conditions applied to the stub model are shown in Figure 40. Table 6 summarizes the applied load components for each case.

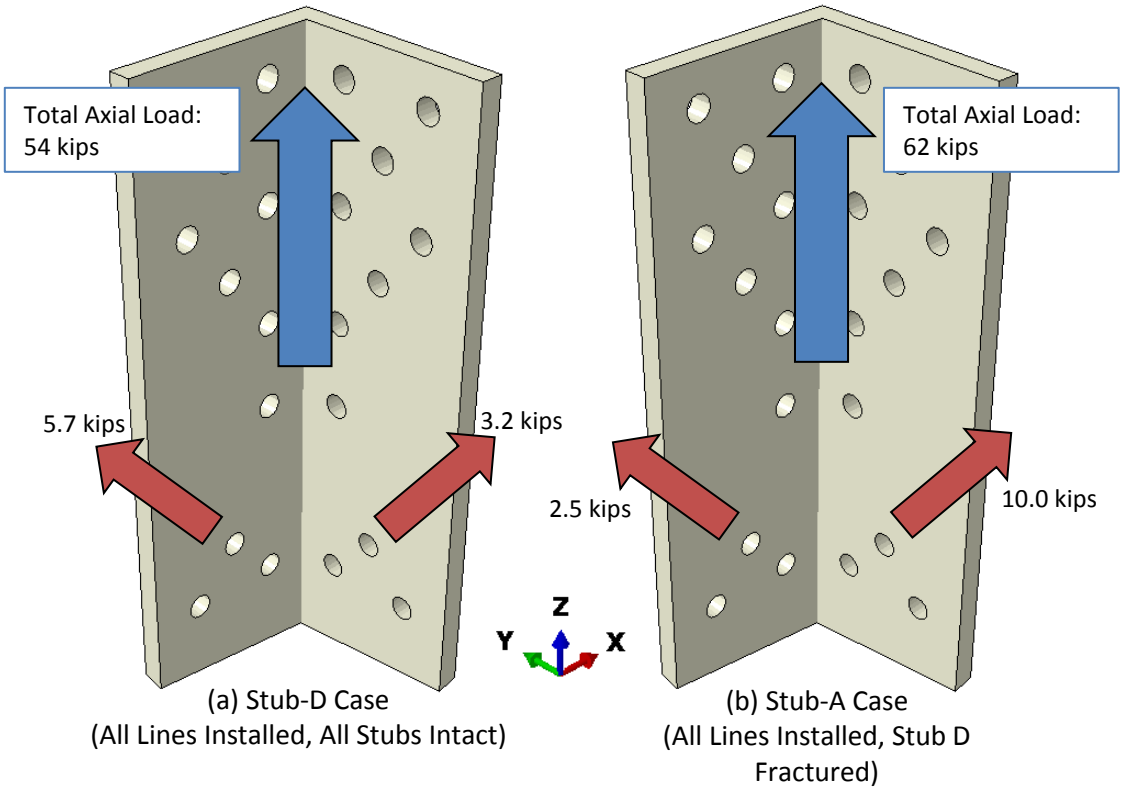


Figure 40. Applied load conditions based on global structural analysis for (a) "Stub-D case" and (b) "Stub-A case". In both cases the bottom of the stub is constrained.

**Table 6. Summary of applied load cases for stub fracture analysis.**

| Load Case | Axial Tension (kips) | Diagonal Tension I (kips) | Diagonal Tension II (kips) | Load Condition |
|---|---|---|---|---|
| "Stub-D" | 53.886 | 3.245 | 5.671 | All lines installed, no fractures |
| "Stub-A" | 62.198 | 9.986 | 2.454 | All lines installed / Stub D fractured |

Within the model, the applied loads for Stub-D and Stub-A cases were distributed among the bolt holes. It is expected that the actual stub experienced non-uniform loading through the bolt holes. To investigate the influence of bolt hole loading, two load distribution cases were analyzed. The first case assumed an even distribution of the axial load between the 22 bolt holes (Figure 41a). This condition provided a lower bound for the bolt loading. The second case consisted of distributing the axial load between the bottom six bolt holes (Figure 41b). For each case, the diagonal load on either side of the stub was split evenly between the respective bolt holes. For the diagonal bolt holes the axial load was combined with the diagonal component. Figure 41 shows the comparison between the two bolt hole loading distributions.

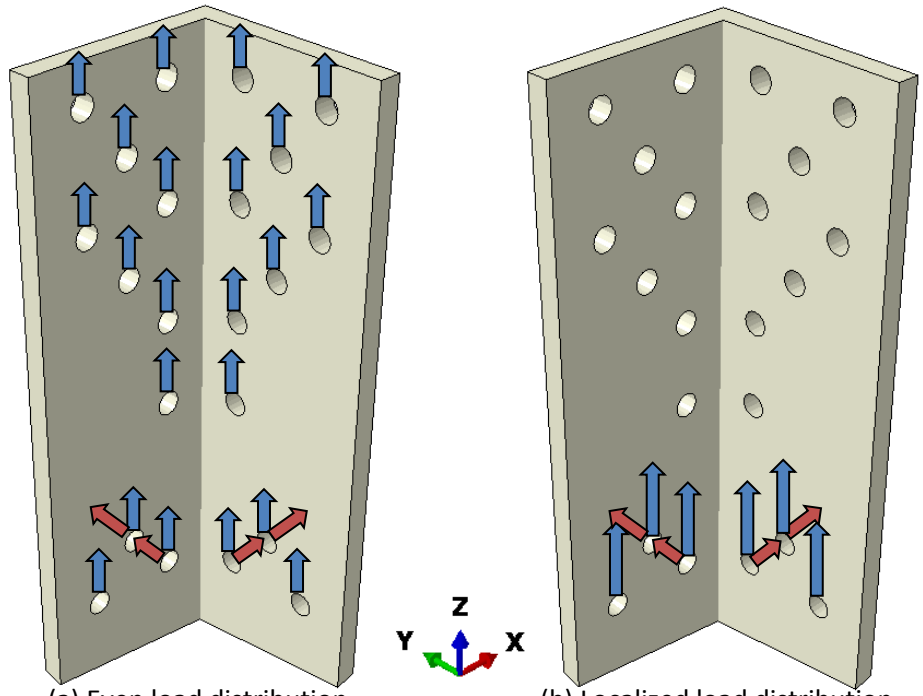


Figure 41. Schematic comparison between bolt-hole load distributions: (a) even between all 22 bolt holes, and (b) localized between lower six bolt holes.

A set of additional load cases was analyzed to investigate the behavior of the stub under bending moments. The moment analyses simulated stub behavior that could result from certain legs being pulled together during tower erection. Two moment application methods were considered. The first used the global structural analysis and beam bending theory to calculate effective moments that would initiate yielding of the stub material. These moments were applied at the top of the stub geometry. Figure 42 shows the top-down view of the stub and the applied moments. "Moment 1" was determined by assuming opposite legs were pulled together

(e.g. Leg B and Leg D). "Moment 2" was determined by assuming two adjacent legs were pulled together (e.g. Leg A and Leg D).

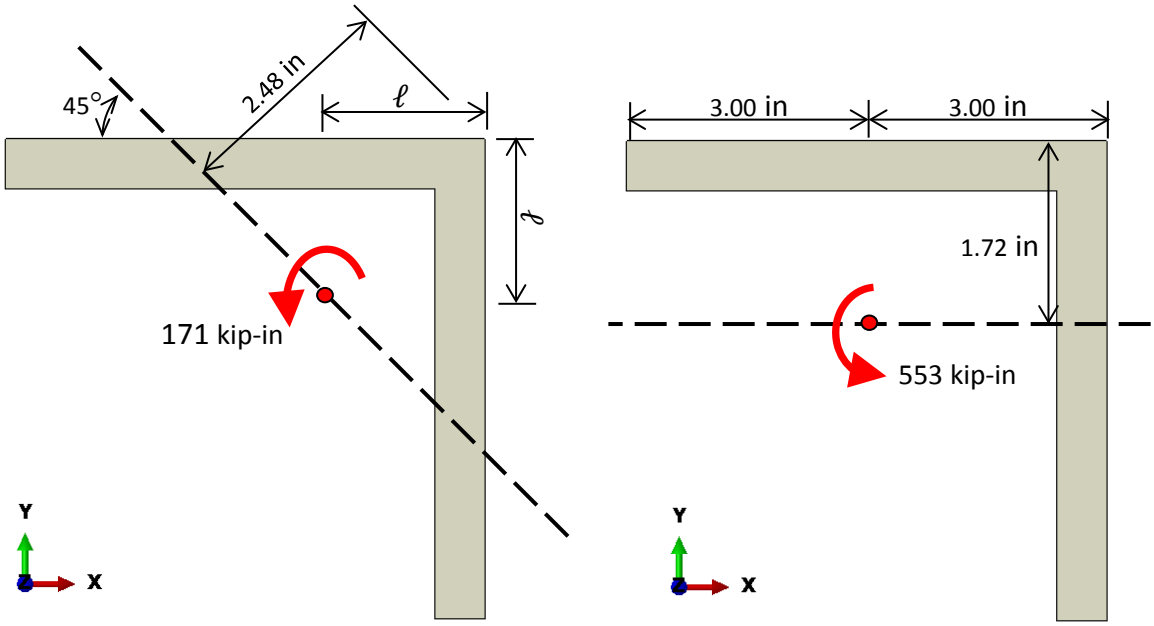


(a) Moment 1 (b) Moment 2

Figure 42. Top-down stub schematic showing applied (a) Moment 1 and (b) Moment 2.

The second moment application method idealized the stub-leg connection as a single structural member. The stub geometry was extended to a total length of approximately 18 feet and is shown in Figure 43. This dimension was based on the height at which the leg connects to the horizontal stringer spanning between adjacent legs. Horizontal displacements were applied in the directions of "Moment 1" and "Moment 2" at the top of the extended stub. This idealization allows bending behavior at the base of the stub to be transmitted through deflections of the leg above, as experienced during fit-up alignment. The induced moment is not transferred through the bolt holes in this modeling approach. Note, axial bolt-hole loadings were not included in the moment analysis cases (since the tower was not yet erected), and the stub geometry was constrained at the bottom, as previously described.

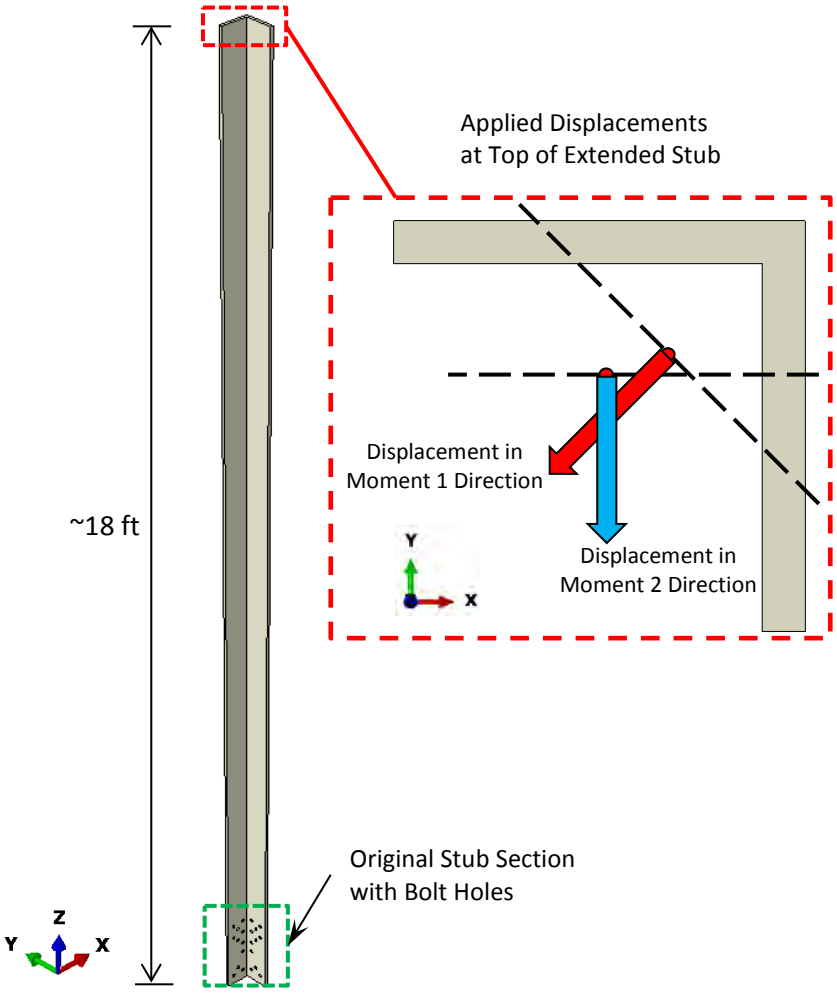


Figure 43. Geometry of extended-stub model.

## Linear-Elastic Fracture Mechanics Analysis

To determine potential crack growth conditions, geometrically-explicit through-cracks were inserted into the finite element models of the stub using the commercial fracture mechanics software, Franc3D. The cracked-model results were used to calculate stress intensity factors along the crack front that can be compared to fracture toughness data to evaluate the propensity for propagation.

The cracked bolt hole for the each load case, “Stub-D”, “Stub-A”, Moment 1 and Moment 2, was determined by identifying the bolt hole with the largest stress concentration in the un-cracked analysis. The locations of interest for the “Stub-D” and “Stub-A” cases correlated with the maximum diagonal tension load. The critical bolt hole for both Moment 1 and Moment 2 cases was the same as “Stub-D”. Figure 44 shows the crack locations for each load case.

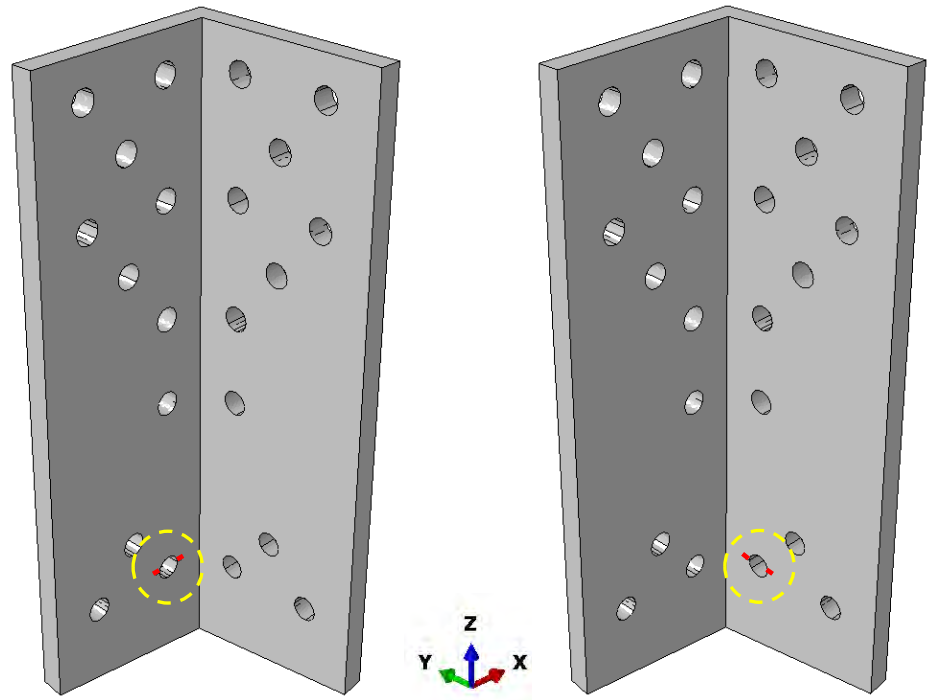


(a) Stub-D, Moment 1, Moment 2 (b) Stub-A

Figure 44. Cracked bolt-hole locations for load cases (a) “Stub-D” and (b) “Stub-A”.

In “Stub-D” and “Stub-A” load cases, four different crack depths were analyzed in an attempt to determine a critical flaw size associated with axial loading. The nominal crack depth of 4.0 mm was selected based on the conservative size of the hardened region surrounding the bolt hole (see Figure 34). The nominal-cracked model was also analyzed for three different load factors to determine the relationship between stress intensity factor and load. The moment analysis load cases were limited to crack sizes of 4.0 mm.

For each analysis, two cracks were inserted into the model. The cracks emanated, symmetrically, from either side of the selected bolt hole, perpendicular to the axial loading direction; an example is shown in Figure 45.

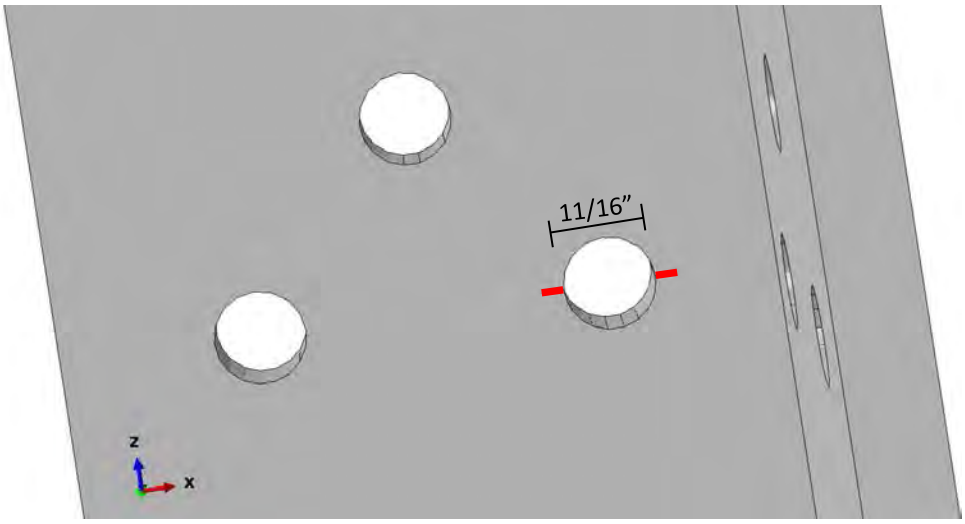


Figure 45. Example showing orientation of crack fronts (highlighted in red) emanating from a bolt hole. Crack depths of 4 mm (0.1575 in) are displayed. Bolt hole diameter is 0.6875 in.

Figure 46 shows an exemplar stress distribution near the crack front for the “Stub-D” configuration. Figure 47 provides a crack orientation schematic for the four load cases. Inner-crack (1) is located on the inside of the bolt hole, emanating in the direction towards the stub corner. Outer-crack (2) is located on the outside of the bolt hole, emanating towards the free edge of the stub.

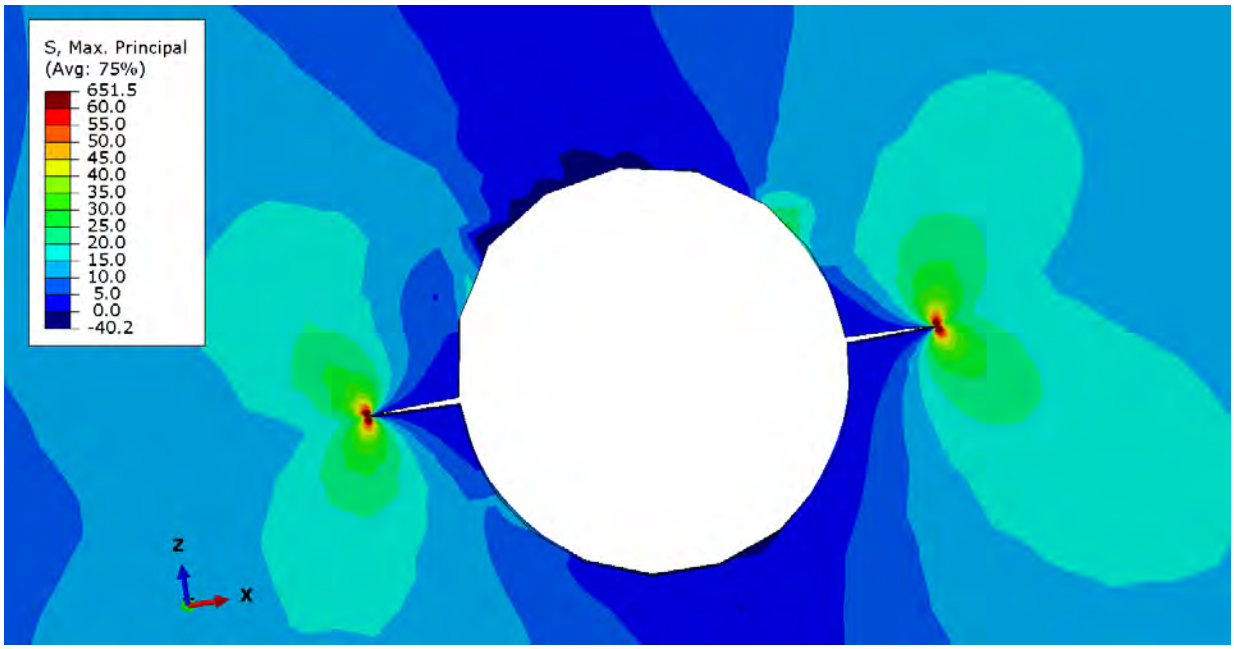


Figure 46. Stress concentrations located at the 4.0 mm crack fronts for “Stub-D” with an even bolt-load distribution. Deformation scale = 20.

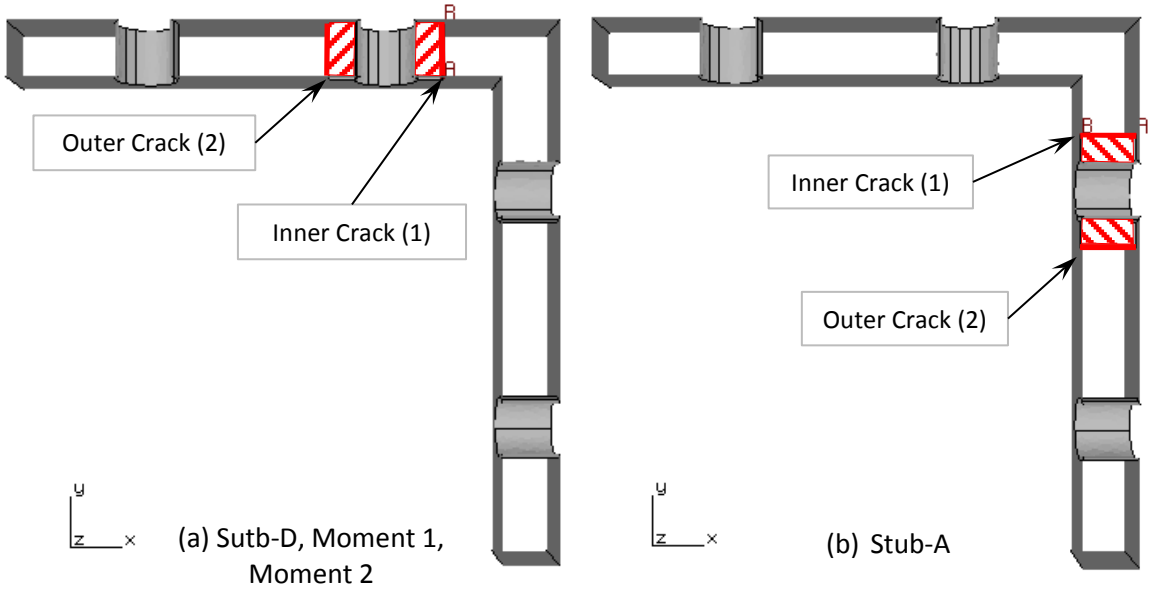


(a) Sutb-D, Moment 1, Moment 2

(b) Stub-A

Figure 47. Crack front orientation schematic for (a) “Stub-D”, Moment 1, Moment 2 and (b) “Stub-A”.

The axial “Stub-D” and “Stub-A” load cases are summarized in Figure 48-Figure 51. The maximum stress intensity factor along the crack front versus crack depth for the given nominal “Stub-D” and “Stub-A” load conditions are summarized in Figure 48 and Figure 49. The maximum stress intensity factor along the crack front versus load amplification factor for the given nominal crack depth of 4.0 millimeters are summarized in Figure 50 and Figure 51. Each summary plot shows the even axial bolt-load distribution (over 22 bolt holes, denoted by *b22*) and the localized bolt-load distribution (over the bottom 6 bolt holes, denoted by *b6*) results. Since the stub-only moment analysis involved a single crack depth (4.0 mm), Figure 52 plots the stress intensity factor distribution along the crack fronts for both Moment 1 and Moment 2 load cases. Stress intensity factors for the extended-stub analysis were calculated at displacement increments of one inch, up to a maximum displacement of 17 inches, for each moment load case direction. Figure 53 plots maximum stress intensity factor as a function of applied displacement for the extended-stub model. Stress intensity factors were calculated using a volume-integral approach within the Franc3D software.

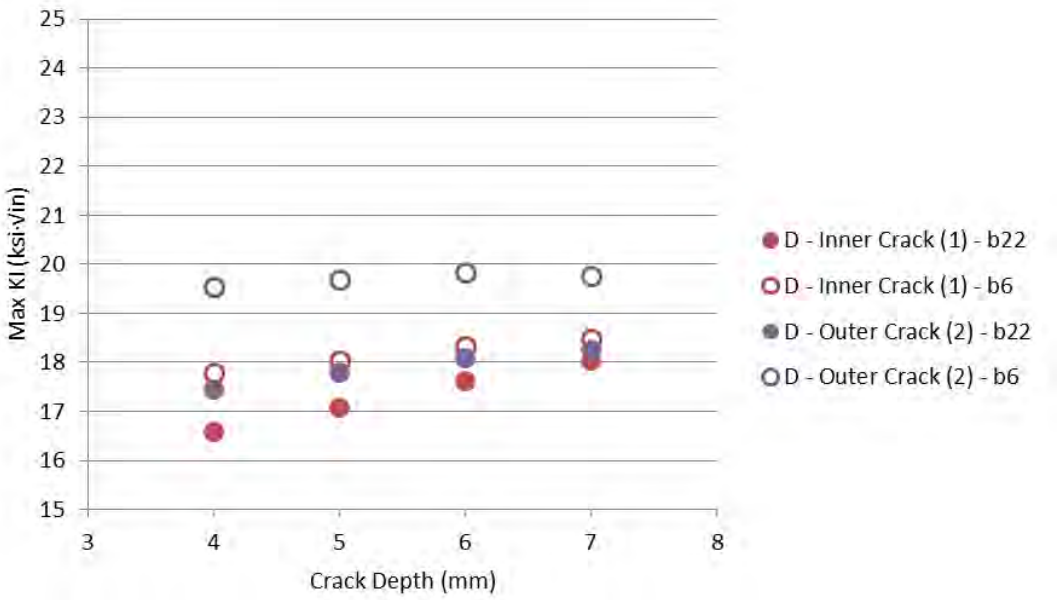


Figure 48. Maximum stress intensity factor vs. crack depth for the “Stub-D” condition (all tower stubs intact). ‘b22’ denotes even bolt-load distribution. ‘b6’ denotes localized bolt-load distribution.

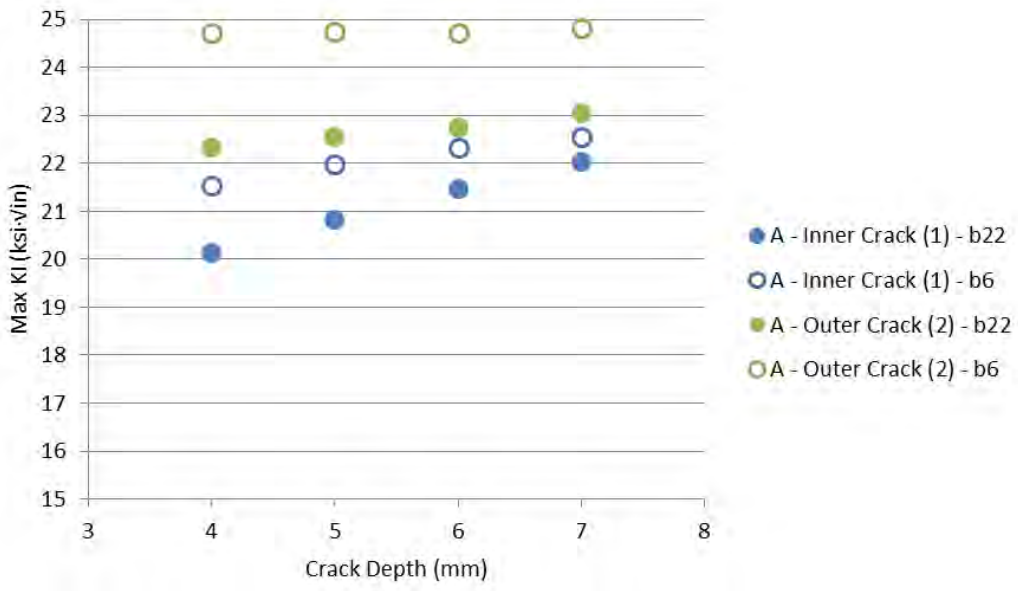


Figure 49. Maximum stress intensity factor vs. crack depth for the “Stub-A” condition (Stub D fractured). ‘b22’ denotes even bolt-load distribution. ‘b6’ denotes localized bolt-load distribution.

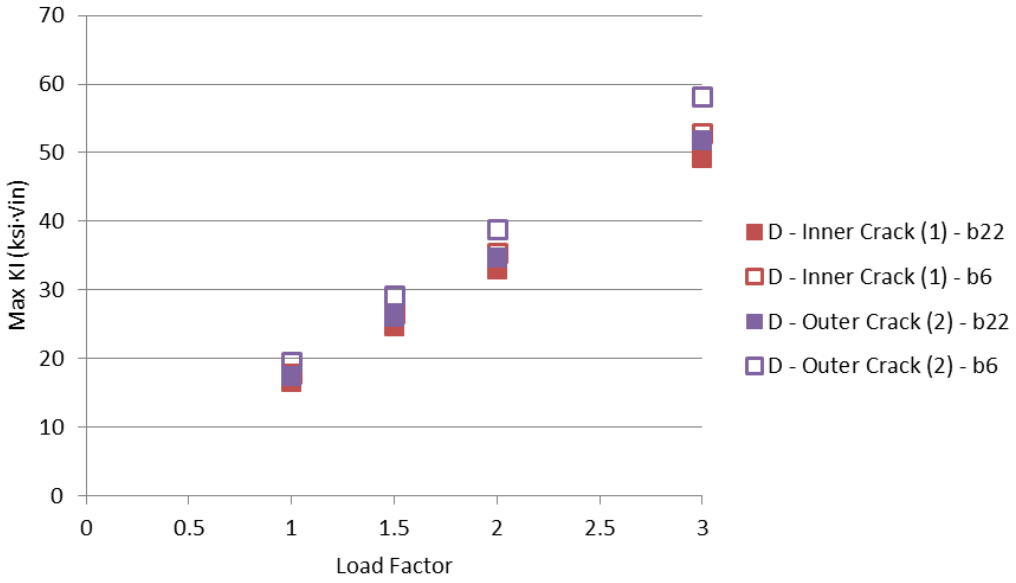


Figure 50. Maximum stress intensity factor vs. load factor for the “Stub-D” condition (all tower stubs intact). ‘b22’ denotes even bolt-load distribution. ‘b6’ denotes localized bolt-load distribution. Crack depth is 4.0 mm.

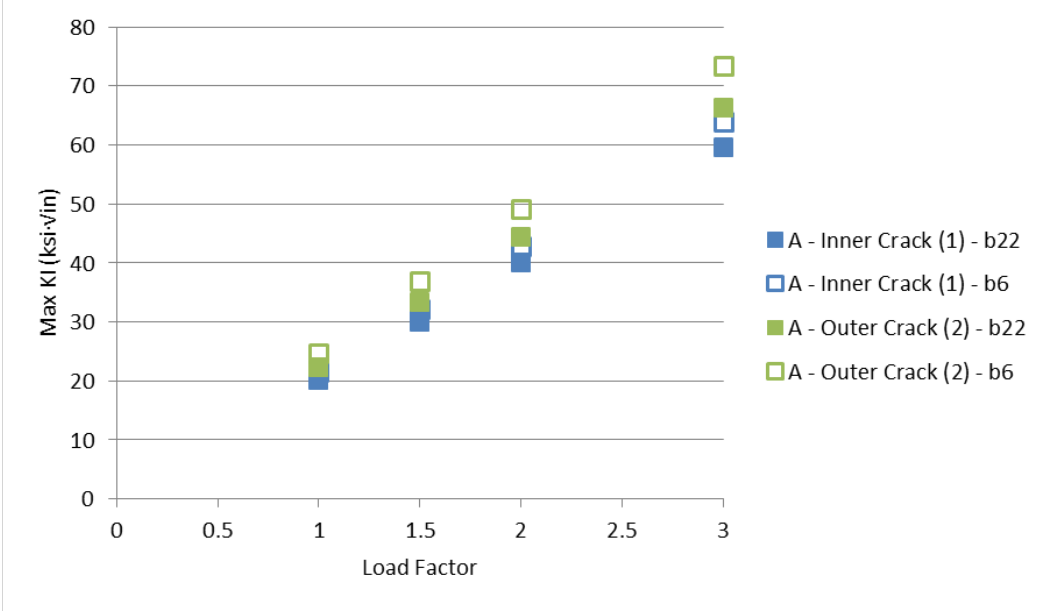


Figure 51. Maximum stress intensity factor vs. load factor for the “Stub-A” condition (Stub D fractured). ‘b22’ denotes even bolt-load distribution. ‘b6’ denotes localized bolt-load distribution. Crack depth is 4.0 mm.

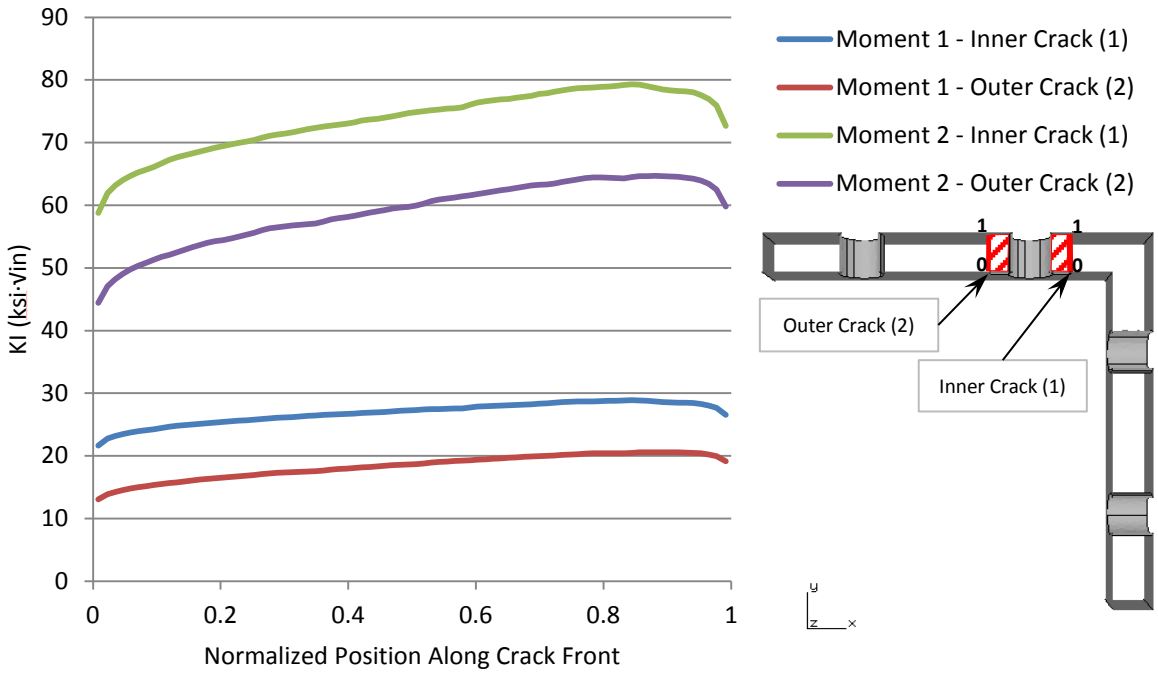


Figure 52. Stress intensity factor distributions along the crack fronts for stub-only Moment 1 and Moment 2 load cases. Normalized position along the crack front is plotted from the inside (0) to the outside (1) of the stub. Crack depth is 4.0 mm.

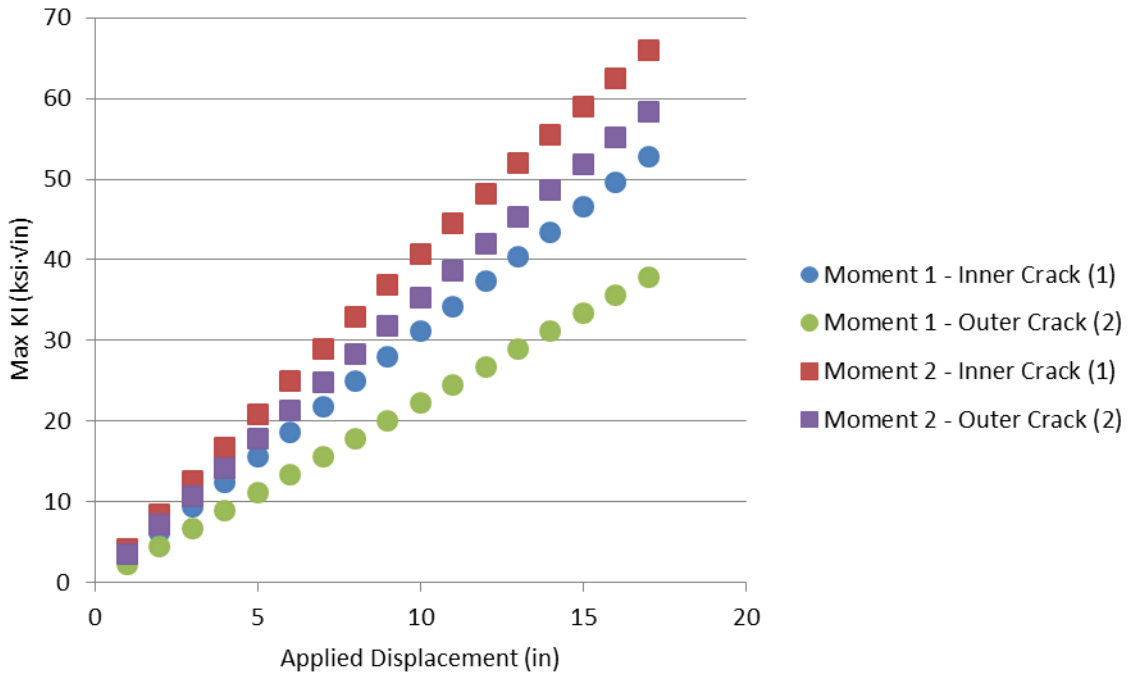


Figure 53. Maximum stress intensity factor vs. applied displacement for extended-stub Moment 1 and Moment 2 load cases. Crack depth is 4.0 mm.

# Discussion

Structural analysis of the subject tower indicates that the stub angles and bolted connection to the tower legs were appropriately designed to carry the expected tower loading up to the time of failure, with significant margin. Wind at the time of collapse was low and did not cause or measurably contribute to the failure. The sequence of fractures at the critical sections of Stub Angles B and D indicate a bending load was applied at the time of collapse. The orientation of that bending is consistent with forced fit-up during erection that would have been required to correct as-measured misalignment of the stub-angles and tower legs. As discussed below, apart from the bending failures on the inboard legs of the Stub Angles at B and C, the stub angle failures exhibited little or no plastic deformation that would be expected from construction steels that are overloaded in mild temperature conditions. That is, the subject steel did not have sufficient ductility to accommodate the forced fit-up during tower erection.

Instead, examination of the Tower 61/268 collapse indicated that the four incident stubs angles embedded in concrete piers fractured in a brittle manner. Two of stubs (B and D) had large cracks that were formed during tower assembly and pre-existed the October 18, 2015 collapse. Brittle fracture is never a desirable outcome for structural steel components, particularly for steel members only 5/8'' thick. The incident stubs were reportedly fabricated by PG&E from steel supplied by Nucor. Nucor specified that the steel met the requirements of: ASTM A36/36M-12, A529/A529M-05 – GR 50, A572/A572-12 – GR50, A709/A709M-13 GR36/50 (No CVN), CSA G40.21-13 GR44W (300W)/GR50W (350W), AASHTO M270/M270M-10 GR36/GR50, and ASME SA36/SA36M-07. Elemental and tensile testing indicated that the incident stubs all met the above specifications. However, Nucor did not certify toughness properties for the subject stubs. Toughness is the ability of an engineering material to absorb energy during the fracture process. Lower required energy for fracture indicates brittle behavior, while fractures that require relatively high energy input to drive the crack are characterized as ductile. Hence, toughness provides an indication of propensity for brittle fracture: high toughness materials will require more energy for fracture, while lower toughness materials will require less energy for crack propagation. While tensile testing provides an indication of the strength of a given material, it does not indicate the toughness.

CVN testing indicated that the subject stubs exhibited a relatively high ductile-to-brittle transition temperature (DBTT) of approximately 70ºF. Thus, given the air temperature the morning of the collapse[11] (approximately 55ºF) the subject stubs were susceptible to low energy, brittle fracture: they were below the ductile-to-brittle transition temperature. Conversion of the CVN toughness data to stress intensity (K) allows linear-elastic fracture mechanics-based analyses that can quantify and compare crack driving "force" and fracture toughness. This approach is therefore useful to assess whether various tower loading conditions would provide sufficient crack driving "force" to propagate assumed pre-existing cracks through steel with toughness values determined from our CVN testing.

[11] See Figure 8

Exponent's linear-elastic fracture mechanics analyses showed that even for relatively large assumed pre-existing cracks (assumed to extend the full depth of the hardened zone around each punched hole), loading several times the expected line-load and installation forces would be required to fracture the subject stubs. However, our results showed that the application of large bending moments associated with poor stub-to-leg fit up can easily result in crack driving "forces" sufficient to cause the stub fracture. For example, a deflection of approximately 12 inches (in the Moment 2 direction, Figure 53 ), would approach 50 ksi √in, a reasonably-assumed fracture toughness based on CVN testing (Figure 38). Additionally, given the expected nominal line-load and installation forces, the necessary crack driving "forces" would not be reached for a reasonable critical flaw size assuming a reasonable fracture toughness (50 ksi √in, Figure 48 and Figure 49). This supports the notion that the tower leg-stub connections were appropriately designed for the expected loading conditions given a potential existing flaw at a bolt hole. Had the incident stubs exhibited "tougher" behavior, the subject tower would have been significantly less notch-sensitive, and would have likely locally plastically deformed rather than fractured. For instance, based on the analyses shown in Figure 38 and Figure 53, had the subject stubs exhibited upper-shelf toughness behavior above 100 ksi√in, substantially more deflection would have been required to generate sufficient driving "force" for crack propagation. Thus, Exponent recommends that PG&E consider specifying toughness criteria for their transmission towers. A criterion such as specifying 15 ft-lbs at -20 ºF per ASCE Standard 48-11[12] (in the longitudinal direction) would result in substantially increased toughness compared to the subject and exemplar stubs. Further, Exponent recommends that PG&E specify maximum allowable sulfur elemental compositions below 0.030 weight percent, per the more recent ASTM A 572-15 specifications.

Metallographic analysis revealed substantial plastic deformation and hardening adjacent to the incident stub bolt holes. Areas around the holes had been work-hardened to levels above 350 HV (greater than the equivalent of 160 ksi local tensile strength). This indicates that the subject holes were cold-punched with no subsequent reaming. Cold-forming (such as hole punching) of structural steel produces an area of microstructural damage and potential cracking.[13,14,15, 16, 17] Galvanizing of hole-punched steel can increase the susceptibility to fracture, potentially by both strain aging and hydrogen embrittlement mechanisms.[13, 15, 16, 17, 18, 19] The plastic deformation

---

[12] American Society of Civil Engineers (ASCE) Standard 48-11, Design of Steel Transmission Pole Structures, Paragraph 5.2.1.3

[13] J.D. Brown, D.J. Lubitz, Y.C. Cekov, K.H. Frank, P.B. Keating, "Evaluation of Influence of Hole Making Upon the Performance of Structural Steel Plates and Connections", Center for Transportation Research, University of Texas at Austin, 2007

[14] G.K. Kulak, J.W. Fisher, J.H. Struik, "Guide to Design Criteria for Bolted and Riveted Joints", American Institute of Steel Construction, 2001

[15] G.W. Owens, P.J. Driver, G.J. Krige, "Punched Holes in Structural Steelwork", Journal of Construction Steel Research, Vol.1, No.3, May 1981.

[16] G.S. Bhuyan, D.H. Carter, "Fracture Properties of Ferrous Alloys Utilized for Transmission Line Hardware Components", Canadian Electrical Association, September 1994.

[17] G. Valtinat, H. Huhn, "Bolted Connections with Hot Dip Galvanized Steel Members with Punched Holes", Connections in Steel Structures V, Amsterdam, June 2004.

[18] G. Bhuyan, "Effect of Cold-Bending and Strain-Age-Embrittlement on the Fracture Behavior of CSA G40.21 M 350 WT Steel", Journal of Testing and Evaluation, Vol. 23, No. 3, May 1995

associated with punching results in local areas around holes that are significantly harder than the base metal: these hard areas are susceptible to strain aging that occurs at the elevated temperatures during galvanizing (associated with diffusion of carbon and nitrogen to dislocations formed by plastic deformation), as well as hydrogen embrittlement (associated with exposure to acid during the pre-galvanizing pickling process). Small cracks away from the main fractures were observed within the hardened zones that surrounded the incident punched holes, as shown in Figure 35.

PG&E G95 Tower drawing 5P17 from 1950 indicated that all holes galvanized plate greater than ½ inch be sub-punched and reamed (the plate in the incident stubs is 5/8-inches thick). Review of the literature indicates that sub punching and reaming is recommended for varying plate thicknesses, including between ½ and 1-inch (depending in part on steel strength);[15] ¾-inch;[19] or when the diameter of the hole is similar to or less than the plate thickness.[15] Thus, although punching without subsequent reaming created small cracks in subject stubs at the bolt holes, it was not unreasonable for PG&E cold-punch the subject 5/8-inch thick stubs.

Stubs B and D likely fractured at the time they were subjected to bending loads associated with poor fit-up. Stubs A and C fractured spontaneously at approximately 7am on October 18, 2015, approximately one week after the full conductor loads were applied. Based on available information, the winds at the time of the collapse were relatively light: higher winds had been experienced earlier in the subject tower's short life.[20] Further, lower temperatures had been experienced by the subject tower after being fully loaded the week earlier.[21] Our analysis indicates that the cause of the tower collapse at 7am on the 18th was likely from a combination of relatively low temperatures (which reduced the subject stubs' fracture toughness), sufficient time to allow diffusion of hydrogen to the high stress areas at the existing cracks within the cold-punch damage regions in Stubs A and C, and high stresses from poor fit-up. Hydrogen embrittlement is caused when susceptible material (such as work-hardened steel) contains sufficient atomic hydrogen and stress to result in fracture.[22] Delayed fractures at room temperature are typical in hydrogen embrittlement-induced failures in steels, as time (on the order of days to weeks) is required to allow sufficient interstitial hydrogen atoms to diffuse to high stress locations. Harder steels are more susceptible to hydrogen embrittlement,[19, 22] and the work-hardened regions around punched holes in steel plate are known to be prone to embrittlement.[19] The acid-pickling treatment used to clean the subject stubs is also known to be associated with hydrogen embrittlement in structural steels.[16, 19, 22] The pickling treatment used on the subject stubs was conducted in hydrochloric acid at ambient temperatures for times between 45 and 60 minutes (longer if there is substantial rust).[23] Reduction of these pickling times, if practical, will reduce the amount of hydrogen absorbed into PG&E plate steels during the galvanizing process. Hydrogen levels in the subject stubs were measured to be

---

[19] ASTM A143 "Standard Practice for Safeguarding Against Embrittlement of Hot-Dip Galvanized Structural Steel Products and Procedure for Detecting Embrittlement, ASTM International.

[20] See Figure 5 and Figure 6.

[21] See Figure 8.

[22] M.R. Louthan, "Hydrogen Embrittlement of Metals: A Primer for the Failure Analyst", Journal of Failure Analysis and Prevention, 2008, Vol. 8, pp. 289-301.

[23] 10/30/15 email from [redacted], PG&E, regarding Moore Quality Galvanizing process steps

approximately four parts-per-million (ppm), sufficient to result in hydrogen embrittlement in susceptible steel[9] (under sufficient stress).

Given that the steel from the Nucor Mill Certification in PG&E PO ST9919 (5/8/2014) has a proven propensity for low toughness, Exponent recommends that PG&E consider taking steps to minimize the chance of brittle fracture in current and future constructions using this material. One such step would be to sub-punch and ream any holes created for the subject 5/8-thick angle-plate material lot. This would minimize the creation of hardened areas and cracks adjacent to punched holes. In towers that have already constructed from the subject material lot, Exponent recommends non-destructive inspection be conducted. These examinations would include visual inspection of stubs and tower legs for misalignment, localized deformation that would indicate residual, "locked-in" stresses, as well as cracks (such as were present in incident Stubs B and D prior to collapse).

# Appendix A

## Anamet, Inc. Reports

13.7.2 (Rev. 8/90) CHEMICAL ANALYSIS FORM

Customer Exponent Lab No. 5005.2347 Date 10/22/15

INCIDENT - L-Bracket

| P W X (E) | | | A | B | C | D | Min. | Max. |
|---|---|---|---|---|---|---|---|---|
| | Aluminum | (Al) | <0.005 | <0.005 | <0.005 | <0.005 | | |
| | Antimony | Sb | | | | | | |
| | Arsenic | As | | | | | | |
| | Beryllium | Be | | | | | | |
| | Bismuth | Bi | | | | | | |
| | Boron | B | | | | | | |
| | Calcium | Ca | | | | | | |
| LECO | Carbon | (C) | 0.21 | 0.21 | 0.21 | 0.21 | | |
| | Chromium | (Cr) | 0.13 | 0.12 | 0.13 | 0.12 | | |
| | Cobalt | Co | | | | | | |
| | Columbium | Cb | | | | | | |
| | Copper | (Cu) | 0.22 | 0.22 | 0.22 | 0.22 | | |
| | Hydrogen | H | | | | | | |
| | Iron | Fe | | | | | | |
| | Lead | Pb | | | | | | |
| | Lithium | Li | | | | | | |
| | Magnesium | Mg | | | | | | |
| | Manganese | (Mn) | 0.73 | 0.73 | 0.73 | 0.73 | | |
| | Molybdenum | (Mo) | 0.02 | 0.02 | 0.02 | 0.02 | | |
| | Nickel | (Ni) | 0.09 | 0.09 | 0.09 | 0.09 | | |
| | Nitrogen | (N) | | | | | | |
| | Oxygen | O | | | | | | |
| | Phosphorus | (P) | 0.012 | 0.011 | 0.012 | 0.011 | | |
| | Selenium | Se | | | | | | |
| | Silicon | (Si) | 0.22 | 0.22 | 0.22 | 0.22 | | |
| | Silver | Ag | | | | | | |
| | Sodium | Na | | | | | | |
| LECO | Sulfur | (S) | 0.044 | 0.047 | 0.047 | 0.047 | | |
| | Tantalum | Ta | | | | | | |
| | Tin | Sn | | | | | | |
| | Titanium | (Ti) | <0.005 | <0.005 | <0.005 | <0.005 | | |
| | Tungsten | W | | | | | | |
| | Vanadium | (V) | 0.02 | 0.02 | 0.02 | 0.02 | | |
| | Zinc | Zn | | | | | | |
| | Zirconium | Zr | | | | | | |
| | | | | | | | | |
| | | | | | | | | |

Rush

Remarks _____ Technician _____ Date 10/28/15

13.7.2 (Rev. 8/90) CHEMICAL ANALYSIS FORM

Customer Exponent Lab No. 5005.2347 Date 10/22/15

EXEMPLAR L-Bracket

| P W X (E) | | | 1 | 2 | 3 | | Min. | Max. |
|---|---|---|---|---|---|---|---|---|
| | Aluminum | (Al) | 0.01 | <0.005 | <0.005 | | | |
| | Antimony | Sb | | | | | | |
| | Arsenic | As | | | | | | |
| | Beryllium | Be | | | | | | |
| | Bismuth | Bi | | | | | | |
| | Boron | B | | | | | | |
| | Calcium | Ca | | | | | | |
| LECO | Carbon | (C) | 0.21 | 0.21 | 0.18 | | | |
| | Chromium | (Cr) | 0.13 | 0.12 | 0.21 | | | |
| | Cobalt | Co | | | | | | |
| | Columbium | Cb | | | | | | |
| | Copper | (Cu) | 0.22 | 0.22 | 0.32 | | | |
| | Hydrogen | H | | | | | | |
| | Iron | Fe | | | | | | |
| | Lead | Pb | | | | | | |
| | Lithium | Li | | | | | | |
| | Magnesium | Mg | | | | | | |
| | Manganese | (Mn) | 0.73 | 0.72 | 0.72 | | | |
| | Molybdenum | (Mo) | 0.02 | 0.02 | 0.03 | | | |
| | Nickel | (Ni) | 0.09 | 0.09 | 0.12 | | | |
| | Nitrogen | (N) | | | | | | |
| | Oxygen | O | | | | | | |
| | Phosphorus | (P) | 0.012 | 0.011 | 0.014 | | | |
| | Selenium | Se | | | | | | |
| | Silicon | (Si) | 0.22 | 0.22 | 0.18 | | | |
| | Silver | Ag | | | | | | |
| | Sodium | Na | | | | | | |
| LECO | Sulfur | (S) | 0.046 | 0.046 | 0.033 | | | |
| | Tantalum | Ta | | | | | | |
| | Tin | Sn | | | | | | |
| | Titanium | (Ti) | <0.005 | <0.005 | <0.005 | | | |
| | Tungsten | W | | | | | | |
| | Vanadium | (V) | 0.02 | 0.02 | 0.02 | | | |
| | Zinc | Zn | | | | | | |
| | Zirconium | Zr | | | | | | |
| | | | | | | | | |
| | | | | | | | | |

Rush

Remarks _____ Technician _____ Date 10/28/15

13.7.1 (Rev. 8/7/13)

# TENSILE TEST FORM

Customer Exponent Lab. No. 5005. 2347 Date 10/22/15

Longitudinal Incident 2 - Bracket ASTM 370-14

| Temperature (room or as noted) (A) | 1 | 2 | | | |
|---|---|---|---|---|---|
| Dimensions of Specimen (in.): | | | | | |
| Width ⇨ | | | | | |
| Thickness ⇨ | | | | | |
| Diameter of Specimen (in.) ⇨ | 0.505 | 0.506 | | | |
| Area (in²) ⇨ | 0.200 | 0.201 | | | |
| Tensile Load (lbs) | 15,701 | 15,753 | | | |
| Tensile Strength (psi) ⇨ | 78,500 | 78,400 | | | |
| Yield Load (lbs)* | 10,200 | 10,200 | | | |
| Yield Strength (psi)* ⇨ | 51,000 | 50,800 | | | |
| Overall Length (in.): | | | | | |
| After | | | | | |
| Before | | | | | |
| Elongation (in.) | 0.63 | 0.64 | | | |
| Elongation in 2.0 Gage (%) ⇨ | 32 | 32 | | | |
| Final Diameter (in.) | 0.313 | 0.310 | | | |
| Reduction of Area (%) ⇨ | 62 | 62 | | | |
| Indicated Modulus of Elasticity (psi) ⇨ | | | | | |
| Fracture Location ⇨ | | | | | |
| Fracture Characteristic ⇨ | | | | | |

*Upper Yield Strength (formerly Y.P.)___ 0.2% offset X 0.5% E.U.L. ___.

Hardness Test

| Specimen | Result | Requirement |
|---|---|---|

Bend Test

| Angle | Diameter |
|---|---|

| Specimen | Result |
|---|---|

Remarks _____ Technician JB Date 10/30/15

13.7.1 (Rev. 8/7/13)

# TENSILE TEST FORM

Customer Exponent Lab. No. 5005. 2347 Date 10/22/15

Longitudinal Incident 2 - Bracket ASTM 370-14

| Temperature (room or as noted) (B) | 1 | 2 | | | |
|---|---|---|---|---|---|
| Dimensions of Specimen (in.): | | | | | |
| Width ⇨ | | | | | |
| Thickness ⇨ | | | | | |
| Diameter of Specimen (in.) ⇨ | 0.506 | 0.505 | | | |
| Area (in²) ⇨ | 0.201 | 0.200 | | | |
| Tensile Load (lbs) | 15,721 | 15,599 | | | |
| Tensile Strength (psi) ⇨ | 78,200 | 78,000 | | | |
| Yield Load (lbs)* | 10,350 | 10,000 | | | |
| Yield Strength (psi)* ⇨ | 51,500 | 50,000 | | | |
| Overall Length (in.): | | | | | |
| After | | | | | |
| Before | | | | | |
| Elongation (in.) | 0.63 | 0.63 | | | |
| Elongation in 2.0 Gage (%) ⇨ | 32 | 32 | | | |
| Final Diameter (in.) | 0.325 | 0.314 | | | |
| Reduction of Area (%) ⇨ | 59 | 61 | | | |
| Indicated Modulus of Elasticity (psi) ⇨ | | | | | |
| Fracture Location ⇨ | | | | | |
| Fracture Characteristic ⇨ | | | | | |

*Upper Yield Strength (formerly Y.P.)___ 0.2% offset X 0.5% E.U.L. ___.

Hardness Test

| Specimen | Result | Requirement |
|---|---|---|

Bend Test

| Angle | Diameter | Specimen | Result |
|---|---|---|---|

Remarks _____ Technician SB Date 10/30/15

13.7.1 (Rev. 8/7/13)

# TENSILE TEST FORM

Customer Exponent Lab. No. 5005. 2347 Date 10/22/15

Longitudinal Incident 2 - Bracket ASTM 370-14

| | | | | | |
|---|---|---|---|---|---|
| Temperature (room or as noted) (C) | 1 | 2 | | | |
| Dimensions of Specimen (in.): | | | | | |
| Width ⇨ | | | | | |
| Thickness ⇨ | | | | | |
| Diameter of Specimen (in.) ⇨ | 0.505 | 0.506 | | | |
| Area (in²) ⇨ | 0.200 | 0.201 | | | |
| Tensile Load (lbs) | 15,588 | 15,714 | | | |
| Tensile Strength (psi) ⇨ | 77,900 | 78,100 | | | |
| Yield Load (lbs)* | 10,200 | 10,337 | | | |
| Yield Strength (psi)* ⇨ | 51,000 | 51,400 | | | |
| Overall Length (in.): | | | | | |
| After | | | | | |
| Before | | | | | |
| Elongation (in.) | 0.64 | 0.62 | | | |
| Elongation in 2.0 Gage (%) ⇨ | 32 | 31 | | | |
| Final Diameter (in.) | 0.317 | 0.321 | | | |
| Reduction of Area (%) ⇨ | 61 | 58.2 | | | |
| Indicated Modulus of Elasticity (psi) ⇨ | | | | | |
| Fracture Location ⇨ | | | | | |
| Fracture Characteristic ⇨ | | | | | |

*Upper Yield Strength (formerly Y.P.)___ 0.2% offset X 0.5% E.U.L. ___.

Hardness Test

| Specimen | Result | Requirement |
|---|---|---|

Bend Test

| Angle | Diameter |
|---|---|

| Specimen | Result |
|---|---|

Remarks _____ Technician JM Date 10/30/15

13.7.1 (Rev. 8/7/13)

# TENSILE TEST FORM

Customer Exponent Lab. No. 5005.2347 Date 10/22/15

Longitudinal Incident 2 - Bracket ASTM 370-14

| Temperature (room or as noted) (D) | 1 | 2 | | | |
|---|---|---|---|---|---|
| Dimensions of Specimen (in.): | | | | | |
| Width ⇨ | | | | | |
| Thickness ⇨ | | | | | |
| Diameter of Specimen (in.) ⇨ | 0.507 | 0.508 | | | |
| Area (in²) ⇨ | 0.202 | 0.203 | | | |
| Tensile Load (lbs) | 15,688 | 15,732 | | | |
| Tensile Strength (psi) ⇨ | 77,700 | 77,600 | | | |
| Yield Load (lbs)* | 9970 | 10,218 | | | |
| Yield Strength (psi)* ⇨ | 49,400 | 50,400 | | | |
| Overall Length (in.): | | | | | |
| After | | | | | |
| Before | | | | | |
| Elongation (in.) | 0.62 | 0.62 | | | |
| Elongation in 2.0 Gage (%) ⇨ | 31 | 31 | | | |
| Final Diameter (in.) | 0.332 | 0.335 | | | |
| Reduction of Area (%) ⇨ | 56.9 | 56.2 | | | |
| Indicated Modulus of Elasticity (psi) ⇨ | | | | | |
| Fracture Location ⇨ | | | | | |
| Fracture Characteristic ⇨ | | | | | |

*Upper Yield Strength (formerly Y.P.)___ 0.2% offset X 0.5% E.U.L. ___.

Hardness Test

| Specimen | Result | Requirement |
|---|---|---|

Bend Test

| Angle | Diameter |
|---|---|

| Specimen | Result |
|---|---|

Remarks _____ Technician JM Date 10/30/15

13.7.1 (Rev. 8/7/13)

**TENSILE TEST FORM**

Customer Exponent Lab. No. 5005. 2347 Date 10/22/15

Longitudinal Exemplar L-Bracket ASTM 370-14

| Temperature (room or as noted) (1) | 1 | 2 | | | |
|---|---|---|---|---|---|
| Dimensions of Specimen (in.): | | | | | |
| Width ⇨ | | | | | |
| Thickness ⇨ | | | | | |
| Diameter of Specimen (in.) ⇨ | 0.507 | 0.507 | | | |
| Area (in²) ⇨ | 0.202 | 0.202 | | | |
| Tensile Load (lbs) | 15,780 | 15,836 | | | |
| Tensile Strength (psi) ⇨ | 78,200 | 78,400 | | | |
| Yield Load (lbs)* | 10,376 | 10,152 | | | |
| Yield Strength (psi)* ⇨ | 51,400 | 50,300 | | | |
| Overall Length (in.): | | | | | |
| After | | | | | |
| Before | | | | | |
| Elongation (in.) | 0.61 | 0.64 | | | |
| Elongation in 2.0 Gage (%) ⇨ | 30½ | 32 | | | |
| Final Diameter (in.) | 0.322 | 0.330 | | | |
| Reduction of Area (%) ⇨ | 59.5 | 55.9 | | | |
| Indicated Modulus of Elasticity (psi) ⇨ | | | | | |
| Fracture Location ⇨ | | | | | |
| Fracture Characteristic ⇨ | | | | | |

*Upper Yield Strength (formerly Y.P.)___ 0.2% offset X 0.5% E.U.L. ___.

Hardness Test

| Specimen | Result | Requirement |
|---|---|---|

Bend Test

| Angle | Diameter |
|---|---|

| Specimen | Result |
|---|---|

Remarks _____ Technician JM Date 10/30/15

13.7.1 (Rev. 8/7/13)

# TENSILE TEST FORM

Customer Exponent Lab. No. 5005. 23477 Date 10/22/15

Longitudinal Exemplar & Bracket ASTM 370-14

| Temperature (room or as noted) (2) | 1 | 2 | | | |
|---|---|---|---|---|---|
| Dimensions of Specimen (in.): | | | | | |
| Width ⇨ | | | | | |
| Thickness ⇨ | | | | | |
| Diameter of Specimen (in.) ⇨ | 0.507 | 0.505 | | | |
| Area (in²) ⇨ | 0.202 | 0.200 | | | |
| Tensile Load (lbs) | 15,740 | 15,611 | | | |
| Tensile Strength (psi) ⇨ | 78,000 | 77,900 | | | |
| Yield Load (lbs)* | 10,266 | 9,819 | | | |
| Yield Strength (psi)* ⇨ | 50,900 | 49,000 | | | |
| Overall Length (in.): | | | | | |
| After | | | | | |
| Before | | | | | |
| Elongation (in.) | 0.60 | 0.63 | | | |
| Elongation in 2.0 Gage (%) ⇨ | 30 | 31½ | | | |
| Final Diameter (in.) | 0.316 | 0.317 | | | |
| Reduction of Area (%) ⇨ | 61.0 | 60.8 | | | |
| Indicated Modulus of Elasticity (psi) ⇨ | | | | | |
| Fracture Location ⇨ | | | | | |
| Fracture Characteristic ⇨ | | | | | |

*Upper Yield Strength (formerly Y.P.)___ 0.2% offset X 0.5% E.U.L. ___.

Hardness Test

| Specimen | Result | Requirement |
|---|---|---|

Bend Test

| Angle | Diameter |
|---|---|

| Specimen | Result |
|---|---|

Remarks _____ Technician JM Date 10/30/15

13.7.1 (Rev. 8/7/13)

# TENSILE TEST FORM

Customer Exponent Lab. No. 5005. 2347 Date 10/22/15

Longitudinal Exemplar L-Bracket ASTM 370-14

| Temperature (room or as noted) (3) | 1 | 2 | | | |
|---|---|---|---|---|---|
| Dimensions of Specimen (in.): | | | | | |
| Width ⇨ | | | | | |
| Thickness ⇨ | | | | | |
| Diameter of Specimen (in.) ⇨ | 0.507 | 0.509 | | | |
| Area (in²) ⇨ | 0.202 | 0.204 | | | |
| Tensile Load (lbs) | 15,246 | 15,340 | | | |
| Tensile Strength (psi) ⇨ | 75,500 | 75,400 | | | |
| Yield Load (lbs)* | 9,804 | 10,058 | | | |
| Yield Strength (psi)* ⇨ | 48,600 | 49,400 | | | |
| Overall Length (in.): | | | | | |
| After | | | | | |
| Before | | | | | |
| Elongation (in.) | 0.64 | 0.64 | | | |
| Elongation in 2.0 Gage (%) ⇨ | 32 | 32 | | | |
| Final Diameter (in.) | 0.315 | 0.322 | | | |
| Reduction of Area (%) ⇨ | 61.2 | 59.5 | | | |
| Indicated Modulus of Elasticity (psi) ⇨ | | | | | |
| Fracture Location ⇨ | | | | | |
| Fracture Characteristic ⇨ | | | | | |

*Upper Yield Strength (formerly Y.P.)___ 0.2% offset X 0.5% E.U.L. ___.

Hardness Test

| Specimen | Result | Requirement |
|---|---|---|

Bend Test

| Angle | Diameter |
|---|---|

| Specimen | Result |
|---|---|

Remarks _____ Technician JM Date 10/30/15

Anamet, inc

Customer: Exponent
Laboratory No.: 5005.2347
Size: Charpy Dimensions: T x 10mm x 55mm
Orientation:

Date Received: 10-22-15
P. O. Number: Verbal
Sample I.D. :

## Incident Sample A CHARPY V-NOTCH IMPACT TEST

Charpy Specimen Thickness: 10 mm
Test Temperature: +/- ____ °F ____ °C

| Specimen I.D. | RESULTS Ft·Lbs | Lateral Expansion (Mils) | Shear (%) |
|---|---|---|---|
| +32 | 13, 10 | 15 | 23 |
| | 7 | 7 | 18 |
| +50 | 18, 22 | 16 | 18 |
| | 26 | 30 | 28 |
| | | | |

Charpy Specimen Thickness: 10 mm
Test Temperature: +/- ____ °F ____ °C

| Specimen I.D. | RESULTS Ft·Lbs | Lateral Expansion (Mils) | Shear (%) |
|---|---|---|---|
| 0 | 3 | 3 | 3 |
| | 7, 5 | 7 | 14 |
| +80 | 12 | 21 | 18 |
| | 34, 23 | 41 | 50 |
| | | | |

## CHARPY V-NOTCH IMPACT TEST

Charpy Specimen Thickness: 10 mm
Test Temperature: +/- ____ °F ____ °C

| Specimen I.D. | RESULTS Ft·Lbs | Lateral Expansion (Mils) | Shear (%) |
|---|---|---|---|
| -20 | 3 | 2 | <3 |
| | 4 | 3 | <3 |
| | | | |
| +110 | 17, 24 | 22 | 28 |
| | 31 | 31 | 38 |

Charpy Specimen Thickness: 10 mm
Test Temperature: +/- ____ °F ____ °C

| Specimen I.D. | RESULTS Ft·Lbs | Lateral Expansion (Mils) | Shear (%) |
|---|---|---|---|
| +140 | 55 | 71 | >98 |
| | 54 | 63 | * |
| | | | |
| +125 | 43 | 50 | 81 |
| | 63 | 65 | 95 |

* NO DISTINCTIVE CLEAVAGE AREA

Technician 4m Date: 10/30/15

Anamet, inc

Customer: Exponent

Laboratory No.: 5005.2347

Size: Charpy Dimensions: T x 10mm x 55mm

Orientation: _____

Date Received: 10.22.15

P. O. Number: Verbal

Sample I.D. : _____

## CHARPY V-NOTCH IMPACT TEST

A

Charpy Specimen Thickness: 10mm

Test Temperature: + / - _____ °F _____ °C

| Specimen I.D. | RESULTS | | |
|---|---|---|---|
| | Ft·Lbs | Lateral Expansion (Mils) | Shear (%) |
| +40 | 30 | 30 | 33 |
| | 22 | 24 | 40 |
| | | | |
| +110 | 50 | 60 | * |
| | | | |

Charpy Specimen Thickness: _____

Test Temperature: + / - _____ °F _____ °C

| Specimen I.D. | RESULTS | | |
|---|---|---|---|
| | Ft·Lbs | Lateral Expansion (Mils) | Shear (%) |
| | | | |
| | | | |
| | | | |
| | | | |
| | | | |

## CHARPY V-NOTCH IMPACT TEST

Charpy Specimen Thickness: _____

Test Temperature: + / - _____ °F _____ °C

| Specimen I.D. | RESULTS | | |
|---|---|---|---|
| | Ft·Lbs | Lateral Expansion (Mils) | Shear (%) |
| | | | |
| | | | |
| | | | |
| | | | |
| | | | |

Charpy Specimen Thickness: _____

Test Temperature: + / - _____ °F _____ °C

| Specimen I.D. | RESULTS | | |
|---|---|---|---|
| | Ft·Lbs | Lateral Expansion (Mils) | Shear (%) |
| | | | |
| | | | |
| | | | |
| | | | |
| | | | |

* NO DISTINCTIVE CLEAVAGE AREA.

Technician JM Date: 10/30/15

Anamet, inc

Customer: Exponent
Laboratory No.: 5005.2347
Size: Charpy Dimensions: T x 10mm x 55mm
Orientation: _____

Date Received: 10-22-15
P. O. Number: Verbal
Sample I.D. : _____

B

## CHARPY V-NOTCH IMPACT TEST

Charpy Specimen Thickness: 10mm
Test Temperature: +/- _____ °F _____ °C

| Specimen I.D. | RESULTS Ft·Lbs | Lateral Expansion (Mils) | Shear (%) |
|---|---|---|---|
| +32 | 20 | 23 | 18 |
| | 20 | 23 | 18 |
| | | | |
| +50 | 24 | 25 | 38 |
| | 25 | 28 | 33 |

Charpy Specimen Thickness: _____
Test Temperature: +/- _____ °F _____ °C

| Specimen I.D. | RESULTS Ft·Lbs | Lateral Expansion (Mils) | Shear (%) |
|---|---|---|---|
| | | | |
| | | | |
| | | | |
| | | | |
| | | | |

## CHARPY V-NOTCH IMPACT TEST

Charpy Specimen Thickness: _____
Test Temperature: +/- _____ °F _____ °C

| Specimen I.D. | RESULTS Ft·Lbs | Lateral Expansion (Mils) | Shear (%) |
|---|---|---|---|
| | | | |
| | | | |
| | | | |
| | | | |
| | | | |

Charpy Specimen Thickness: _____
Test Temperature: +/- _____ °F _____ °C

| Specimen I.D. | RESULTS Ft·Lbs | Lateral Expansion (Mils) | Shear (%) |
|---|---|---|---|
| | | | |
| | | | |
| | | | |
| | | | |
| | | | |

Technician _____ Date: _____

Anamet, inc

Customer: Exponent

Laboratory No.: 5005.2347

Size: Charpy Dimensions: T x 10mm x 55mm

Orientation: _____

Date Received: 10.22.15

P. O. Number: Verbal

Sample I.D. : _____

C

## CHARPY V-NOTCH IMPACT TEST

| Charpy Specimen Thickness: 10 mm | | | | Charpy Specimen Thickness: _____ | | | |
|---|---|---|---|---|---|---|---|
| Test Temperature: +/- _____ °F _____ °C | | | | Test Temperature: +/- _____ °F _____ °C | | | |
| Specimen I.D. | RESULTS | | | Specimen I.D. | RESULTS | | |
| | Ft·Lbs | Lateral Expansion (Mils) | Shear (%) | | Ft·Lbs | Lateral Expansion (Mils) | Shear (%) |
| +32 | 16 | 21 | 29 | | | | |
| | 10 | 15 | 23 | | | | |
| | | | | | | | |
| +50 | 27 | 31 | 37 | | | | |
| | 23 | 29 | 29 | | | | |

## CHARPY V-NOTCH IMPACT TEST

| Charpy Specimen Thickness: _____ | | | | Charpy Specimen Thickness: _____ | | | |
|---|---|---|---|---|---|---|---|
| Test Temperature: +/- _____ °F _____ °C | | | | Test Temperature: +/- _____ °F _____ °C | | | |
| Specimen I.D. | RESULTS | | | Specimen I.D. | RESULTS | | |
| | Ft·Lbs | Lateral Expansion (Mils) | Shear (%) | | Ft·Lbs | Lateral Expansion (Mils) | Shear (%) |
| | | | | | | | |
| | | | | | | | |
| | | | | | | | |
| | | | | | | | |
| | | | | | | | |

Technician_____ Date:_____

Anamet, inc

Customer: Exponent
Laboratory No.: 5005.2347
Size: Charpy Dimensions: T x 10mm x 55mm
Orientation: _____

Date Received: 10-22-15
P. O. Number: Verbal
Sample I.D. : _____

D

## CHARPY V-NOTCH IMPACT TEST

| Charpy Specimen Thickness: 10mm | | | | Charpy Specimen Thickness: _____ | | | |
|---|---|---|---|---|---|---|---|
| Test Temperature: +/- _____ °F _____ °C | | | | Test Temperature: +/- _____ °F _____ °C | | | |
| Specimen I.D. | RESULTS | | | Specimen I.D. | RESULTS | | |
| | Ft·Lbs | Lateral Expansion (Mils) | Shear (%) | | Ft·Lbs | Lateral Expansion (Mils) | Shear (%) |
| +32 | 7 | 8 | 14 | | | | |
| | 9 | 10 | 23 | | | | |
| | | | | | | | |
| +50 | 17 | 22 | 33 | | | | |
| | 25 | 20 | 33 | | | | |

## CHARPY V-NOTCH IMPACT TEST

| Charpy Specimen Thickness: _____ | | | | Charpy Specimen Thickness: _____ | | | |
|---|---|---|---|---|---|---|---|
| Test Temperature: +/- _____ °F _____ °C | | | | Test Temperature: +/- _____ °F _____ °C | | | |
| Specimen I.D. | RESULTS | | | Specimen I.D. | RESULTS | | |
| | Ft·Lbs | Lateral Expansion (Mils) | Shear (%) | | Ft·Lbs | Lateral Expansion (Mils) | Shear (%) |
| | | | | | | | |
| | | | | | | | |
| | | | | | | | |
| | | | | | | | |
| | | | | | | | |

Technician _____ Date: _____

Anamet, inc

Customer: Exponent

Laboratory No.: 5005.2347

Size: Charpy Dimensions: T x 10mm x 55mm

Orientation: _____

Date Received: 10-22-15

P. O. Number: Verbal

Sample I.D. : _____

## CHARPY V-NOTCH IMPACT TEST

E1

Charpy Specimen Thickness: 10mm

Test Temperature: + / - _____ °F _____ °C

| Specimen I.D. | RESULTS | | |
|---|---|---|---|
| | Ft·Lbs | Lateral Expansion (Mils) | Shear (%) |
| +32 | 18 | 23 | 23 |
| | | | |
| +50 | 28 | 31 | 29 |
| | | | |
| | | | |

Charpy Specimen Thickness: _____

Test Temperature: + / - _____ °F _____ °C

| Specimen I.D. | RESULTS | | |
|---|---|---|---|
| | Ft·Lbs | Lateral Expansion (Mils) | Shear (%) |
| | | | |
| | | | |
| | | | |
| | | | |
| | | | |

## CHARPY V-NOTCH IMPACT TEST

Charpy Specimen Thickness: _____

Test Temperature: + / - _____ °F _____ °C

| Specimen I.D. | RESULTS | | |
|---|---|---|---|
| | Ft·Lbs | Lateral Expansion (Mils) | Shear (%) |
| | | | |
| | | | |
| | | | |
| | | | |
| | | | |

Charpy Specimen Thickness: _____

Test Temperature: + / - _____ °F _____ °C

| Specimen I.D. | RESULTS | | |
|---|---|---|---|
| | Ft·Lbs | Lateral Expansion (Mils) | Shear (%) |
| | | | |
| | | | |
| | | | |
| | | | |
| | | | |

Technician _____ Date: _____

Anamet, inc

Customer: Exponent

Laboratory No.: 5005.2347

Size: Charpy Dimensions: T x 10mm x 55mm

Orientation: _____

Date Received: 10.22.15

P. O. Number: Verbal

Sample I.D. : _____

E2

## CHARPY V-NOTCH IMPACT TEST

| Charpy Specimen Thickness: 10mm | | | | Charpy Specimen Thickness: _____ | | | |
|---|---|---|---|---|---|---|---|
| Test Temperature: +/- _____ °F _____ °C | | | | Test Temperature: +/- _____ °F _____ °C | | | |
| Specimen I.D. | RESULTS | | | Specimen I.D. | RESULTS | | |
| | Ft·Lbs | Lateral Expansion (Mils) | Shear (%) | | Ft·Lbs | Lateral Expansion (Mils) | Shear (%) |
| +32 | 20 | 23 | 25 | | | | |
| | | | | | | | |
| +50 | 23 | 29 | 33 | | | | |
| | | | | | | | |
| | | | | | | | |

## CHARPY V-NOTCH IMPACT TEST

| Charpy Specimen Thickness: _____ | | | | Charpy Specimen Thickness: _____ | | | |
|---|---|---|---|---|---|---|---|
| Test Temperature: +/- _____ °F _____ °C | | | | Test Temperature: +/- _____ °F _____ °C | | | |
| Specimen I.D. | RESULTS | | | Specimen I.D. | RESULTS | | |
| | Ft·Lbs | Lateral Expansion (Mils) | Shear (%) | | Ft·Lbs | Lateral Expansion (Mils) | Shear (%) |
| | | | | | | | |
| | | | | | | | |
| | | | | | | | |
| | | | | | | | |
| | | | | | | | |

Technician_____ Date:_____

Anamet, inc

Customer: Exponent

Laboratory No.: 5005.2347

Size: Charpy Dimensions: T x 10mm x 55mm

Orientation: _____

Date Received: 10.22.15

P. O. Number: Verbal

Sample I.D. : _____

E3

## CHARPY V-NOTCH IMPACT TEST

| Charpy Specimen Thickness: 10mm | | | | Charpy Specimen Thickness: _____ | | | |
|---|---|---|---|---|---|---|---|
| Test Temperature: +/- _____ °F _____ °C | | | | Test Temperature: +/- _____ °F _____ °C | | | |
| Specimen I.D. | RESULTS | | | Specimen I.D. | RESULTS | | |
| | Ft·Lbs | Lateral Expansion (Mils) | Shear (%) | | Ft·Lbs | Lateral Expansion (Mils) | Shear (%) |
| +32 | 28 | 33 | 25 | | | | |
| | | | | | | | |
| +50 | 28 | 32 | 29 | | | | |
| | | | | | | | |
| | | | | | | | |

## CHARPY V-NOTCH IMPACT TEST

| Charpy Specimen Thickness: _____ | | | | Charpy Specimen Thickness: _____ | | | |
|---|---|---|---|---|---|---|---|
| Test Temperature: +/- _____ °F _____ °C | | | | Test Temperature: +/- _____ °F _____ °C | | | |
| Specimen I.D. | RESULTS | | | Specimen I.D. | RESULTS | | |
| | Ft·Lbs | Lateral Expansion (Mils) | Shear (%) | | Ft·Lbs | Lateral Expansion (Mils) | Shear (%) |
| | | | | | | | |
| | | | | | | | |
| | | | | | | | |
| | | | | | | | |
| | | | | | | | |

Technician _____ Date: _____

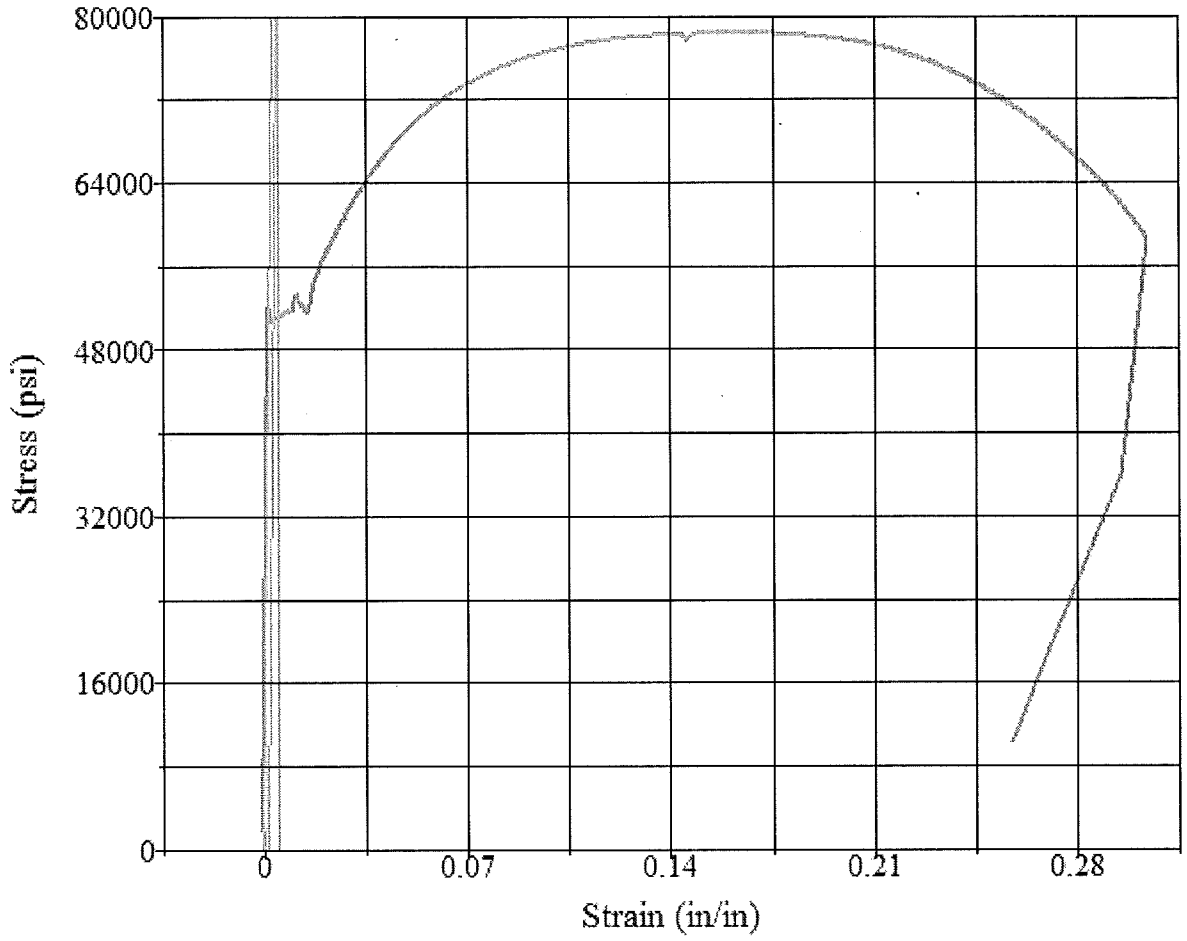


**Test Summary**

| | |
|---|---|
| Counter: | 9960 |
| Elapsed Time: | 00:02:25 |
| Anamet Job Number: | 5005.2347 |
| Specimen Identification: | A1 |
| Operator: | jb |
| Procedure Name: | Tensile MTS2in. Ext. |
| Start Date: | 10/30/2015 |
| Start Time: | 10:58:29 AM |
| End Date: | 10/30/2015 |
| End Time: | 11:00:54 AM |
| Workstation: | ANAMET-PC |
| Tested By: | James |
| Customer: | Exponent |

**Test Results**

| | |
|---|---|
| Area: | 0.2003 in² |
| Tensile Strength: | 78400 psi |
| Peak Load: | 15701 lbf |
| Load at Offset: | 10156.4500 lbf |
| Stress at Offset: | 50706.1900 psi |
| Young's Modulus: | 2.58e+007 psi |
| Load at EUL: | 10238.0700 lbf |
| Stress at EUL: | 51113.6800 psi |
| Halt of Force Yield: | 10459.0000 lbf |
| Diameter: | 0.5050 in |

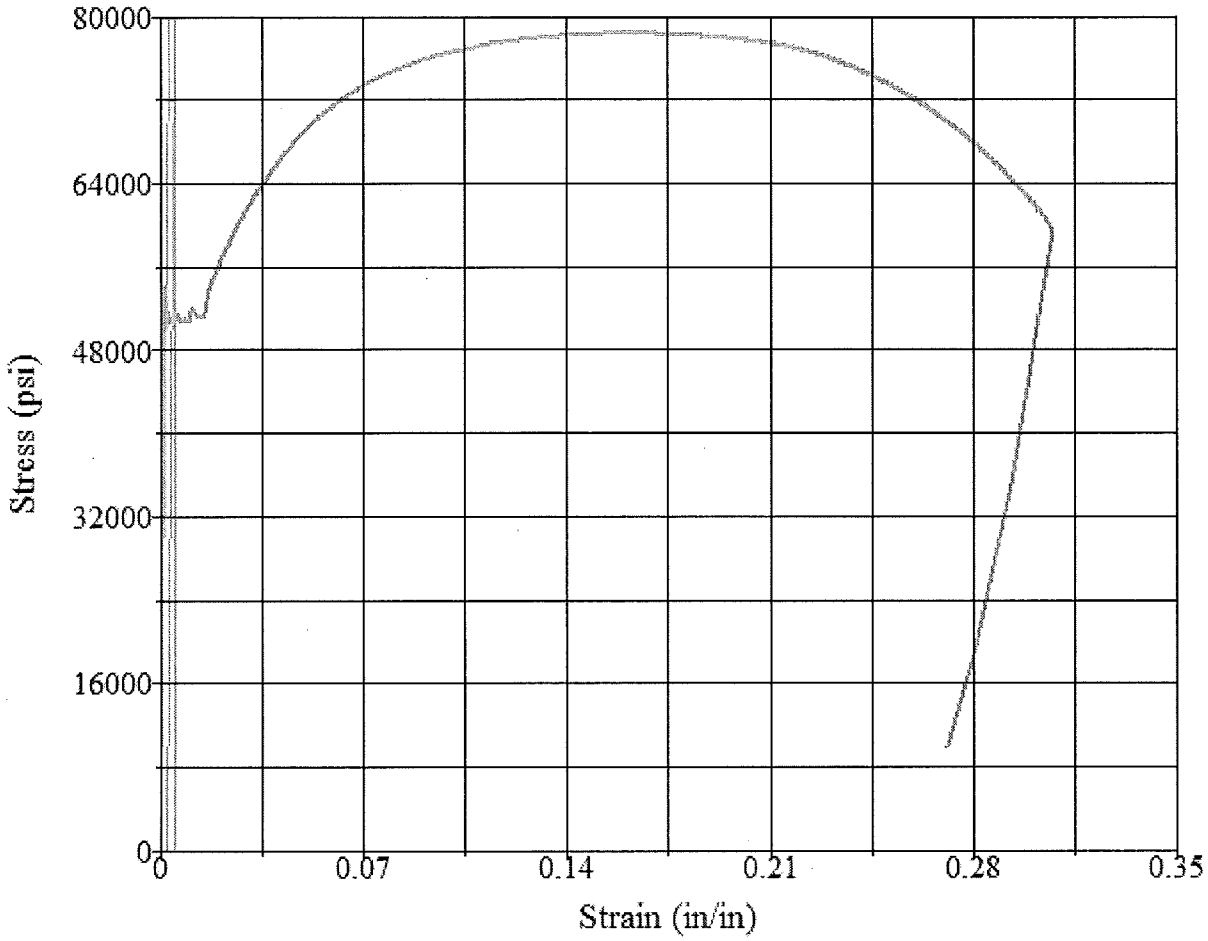


**Test Summary**

| | |
|---|---|
| Counter: | 9961 |
| Elapsed Time: | 00:02:28 |
| Anamet Job Number: | 5005.2347 |
| Specimen Identification: | A2 |
| Operator: | jb |
| Procedure Name: | Tensile MTS2in. Ext. |
| Start Date: | 10/30/2015 |
| Start Time: | 11:10:44 AM |
| End Date: | 10/30/2015 |
| End Time: | 11:13:12 AM |
| Workstation: | ANAMET-PC |
| Tested By: | James |
| Customer: | Exponent |

**Test Results**

| | |
|---|---|
| Area: | 0.2011 in² |
| Tensile Strength: | 78300 psi |
| Peak Load: | 15753 lbf |
| Load at Offset: | 10184.5400 lbf |
| Stress at Offset: | 50644.1700 psi |
| Young's Modulus: | 2.78e+007 psi |
| Load at EUL: | 10349.7700 lbf |
| Stress at EUL: | 51465.8000 psi |
| Halt of Force Yield: | 10916.0000 lbf |
| Diameter: | 0.5060 in |

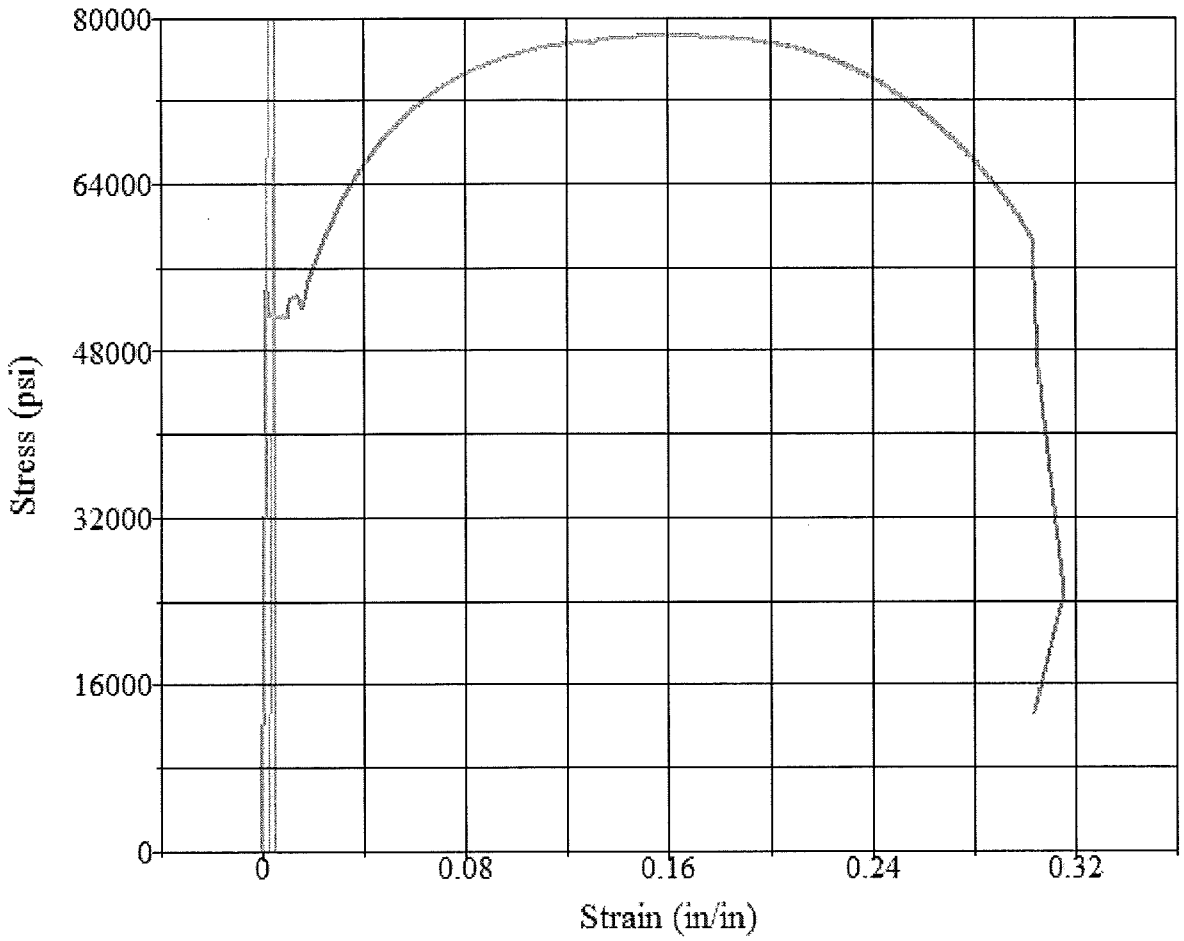


**Test Summary**

| | |
|---|---|
| Counter: | 9962 |
| Elapsed Time: | 00:02:33 |
| Anamet Job Number: | 5005.2347 |
| Specimen Identification: | B1 |
| Operator: | jb |
| Procedure Name: | Tensile MTS2in. Ext. |
| Start Date: | 10/30/2015 |
| Start Time: | 11:29:35 AM |
| End Date: | 10/30/2015 |
| End Time: | 11:32:08 AM |
| Workstation: | ANAMET-PC |
| Tested By: | James |
| Customer: | Exponent |

**Test Results**

| | |
|---|---|
| Area: | 0.2011 in² |
| Tensile Strength: | 78200 psi |
| Peak Load: | 15721 lbf |
| Load at Offset: | 10350.0300 lbf |
| Stress at Offset: | 51467.0600 psi |
| Young's Modulus: | 3.27e+007 psi |
| Load at EUL: | 10314.9800 lbf |
| Stress at EUL: | 51292.7800 psi |
| Halt of Force Yield: | 10836.0000 lbf |
| Diameter: | 0.5060 in |

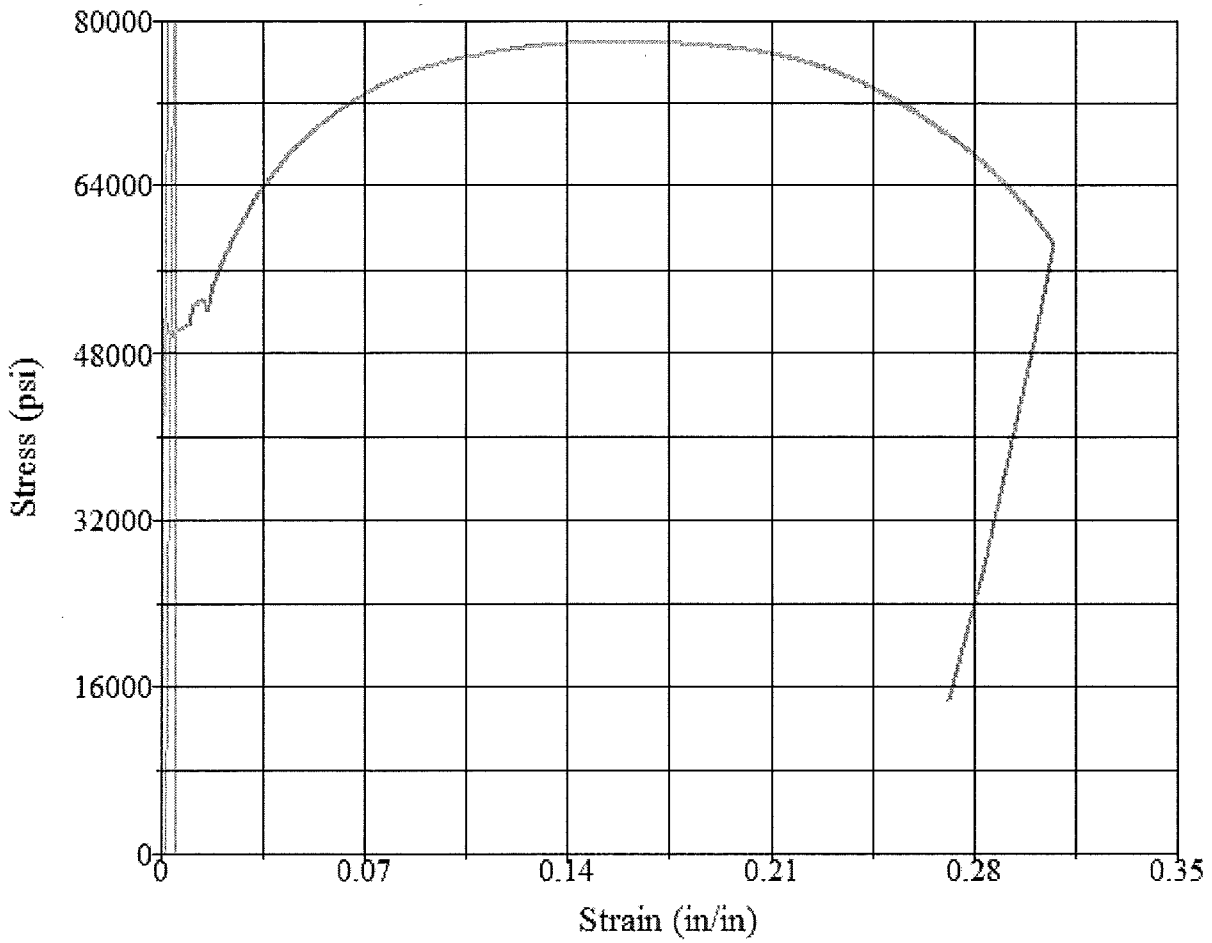


**Test Summary**

| | |
|---|---|
| Counter: | 9963 |
| Elapsed Time: | 00:02:32 |
| Anamet Job Number: | 5005.2347 |
| Specimen Identification: | B2 |
| Operator: | jb |
| Procedure Name: | Tensile MTS2in. Ext. |
| Start Date: | 10/30/2015 |
| Start Time: | 1:07:18 PM |
| End Date: | 10/30/2015 |
| End Time: | 1:09:50 PM |
| Workstation: | ANAMET-PC |
| Tested By: | James |
| Customer: | Exponent |

**Test Results**

| | |
|---|---|
| Area: | 0.2003 in² |
| Tensile Strength: | 77900 psi |
| Peak Load: | 15599 lbf |
| Load at Offset: | 10030.4700 lbf |
| Stress at Offset: | 50077.2400 psi |
| Young's Modulus: | 3.09e+007 psi |
| Load at EUL: | 10008.1600 lbf |
| Stress at EUL: | 49965.8600 psi |
| Halt of Force Yield: | 10298.0000 lbf |
| Diameter: | 0.5050 in |

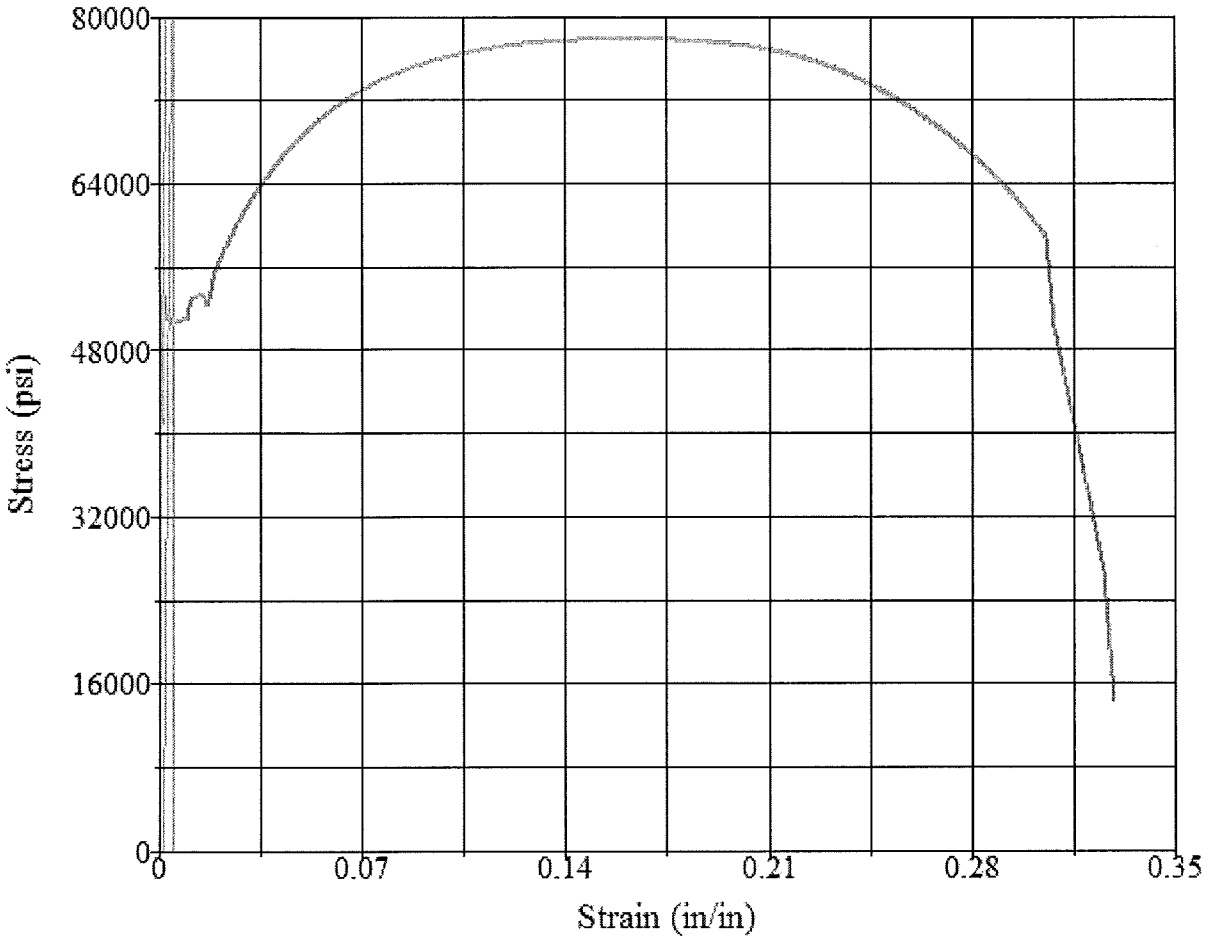


**Test Summary**

| | |
|---|---|
| Counter: | 9964 |
| Elapsed Time: | 00:02:29 |
| Anamet Job Number: | 5005.2347 |
| Specimen Identification: | C1 |
| Operator: | jb |
| Procedure Name: | Tensile MTS2in. Ext. |
| Start Date: | 10/30/2015 |
| Start Time: | 1:25:32 PM |
| End Date: | 10/30/2015 |
| End Time: | 1:28:01 PM |
| Workstation: | ANAMET-PC |
| Tested By: | James |
| Customer: | Exponent |

**Test Results**

| | |
|---|---|
| Area: | 0.2003 in² |
| Tensile Strength: | 77800 psi |
| Peak Load: | 15588 lbf |
| Load at Offset: | 10214.4000 lbf |
| Stress at Offset: | 50995.5200 psi |
| Young's Modulus: | 2.98e+007 psi |
| Load at EUL: | 10135.0000 lbf |
| Stress at EUL: | 50599.1000 psi |
| Halt of Force Yield: | 10663.0000 lbf |
| Diameter: | 0.5050 in |

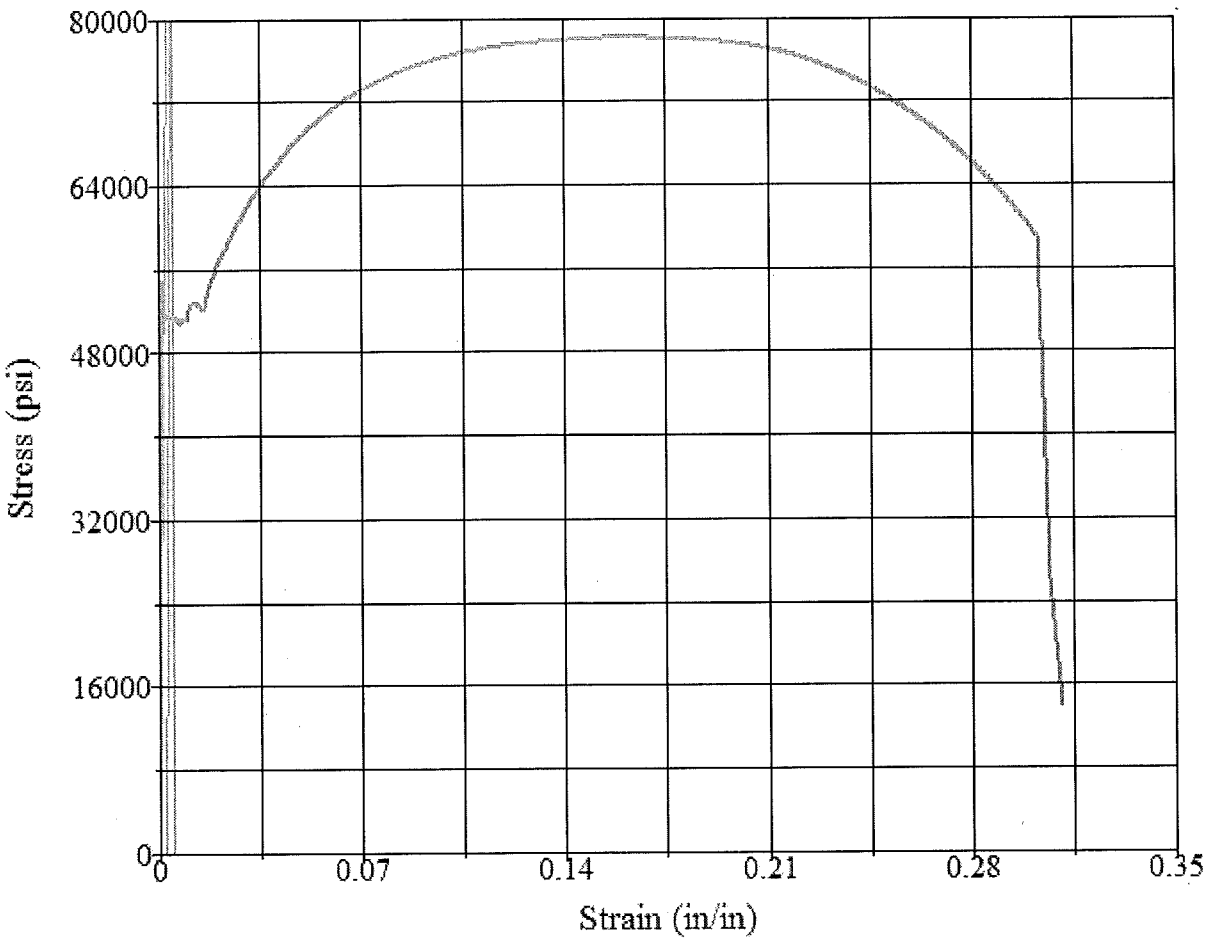


**Test Summary**

| | |
|---|---|
| Counter: | 9965 |
| Elapsed Time: | 00:02:30 |
| Anamet Job Number: | 5005.2347 |
| Specimen Identification: | C2 |
| Operator: | jb |
| Procedure Name: | Tensile MTS2in. Ext. |
| Start Date: | 10/30/2015 |
| Start Time: | 1:43:37 PM |
| End Date: | 10/30/2015 |
| End Time: | 1:46:07 PM |
| Workstation: | ANAMET-PC |
| Tested By: | James |
| Customer: | Exponent |

**Test Results**

| | |
|---|---|
| Area: | 0.2011 in² |
| Tensile Strength: | 78100 psi |
| Peak Load: | 15714 lbf |
| Load at Offset: | 10337.2500 lbf |
| Stress at Offset: | 51403.5500 psi |
| Young's Modulus: | 3.02e+007 psi |
| Load at EUL: | 10329.9700 lbf |
| Stress at EUL: | 51367.3500 psi |
| Halt of Force Yield: | 11054.0000 lbf |
| Diameter: | 0.5060 in |

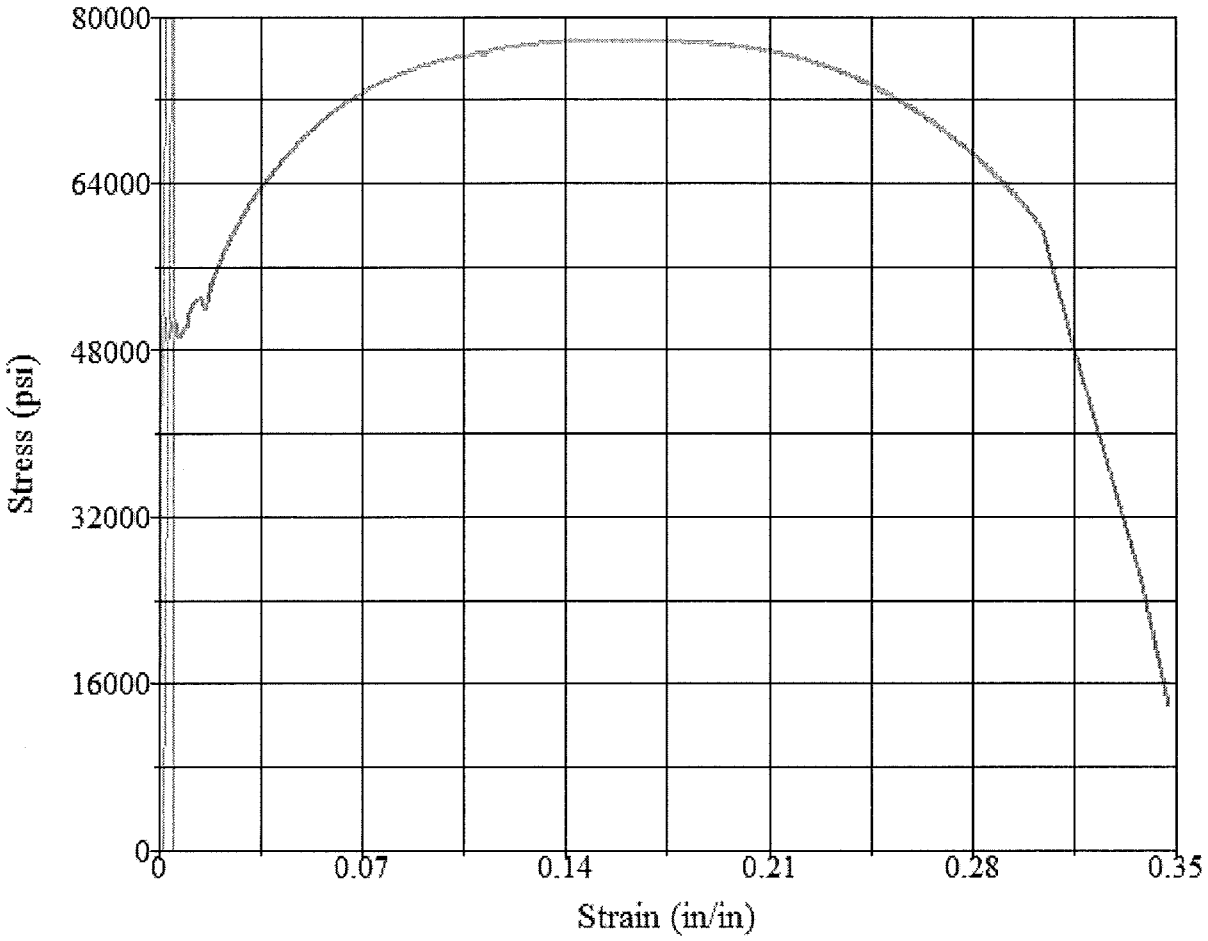


**Test Summary**

| | |
|---|---|
| Counter: | 9966 |
| Elapsed Time: | 00:02:26 |
| Anamet Job Number: | 5005.2347 |
| Specimen Identification: | D1 |
| Operator: | jm |
| Procedure Name: | Tensile MTS2in. Ext. |
| Start Date: | 10/30/2015 |
| Start Time: | 1:59:45 PM |
| End Date: | 10/30/2015 |
| End Time: | 2:02:11 PM |
| Workstation: | ANAMET-PC |
| Tested By: | James |
| Customer: | Exponent |

**Test Results**

| | |
|---|---|
| Area: | 0.2019 in² |
| Tensile Strength: | 77700 psi |
| Peak Load: | 15688 lbf |
| Load at Offset: | 9970.8590 lbf |
| Stress at Offset: | 49385.1400 psi |
| Young's Modulus: | 3.06e+007 psi |
| Load at EUL: | 10208.8400 lbf |
| Stress at EUL: | 50563.8600 psi |
| Halt of Force Yield: | 10372.0000 lbf |
| Diameter: | 0.5070 in |

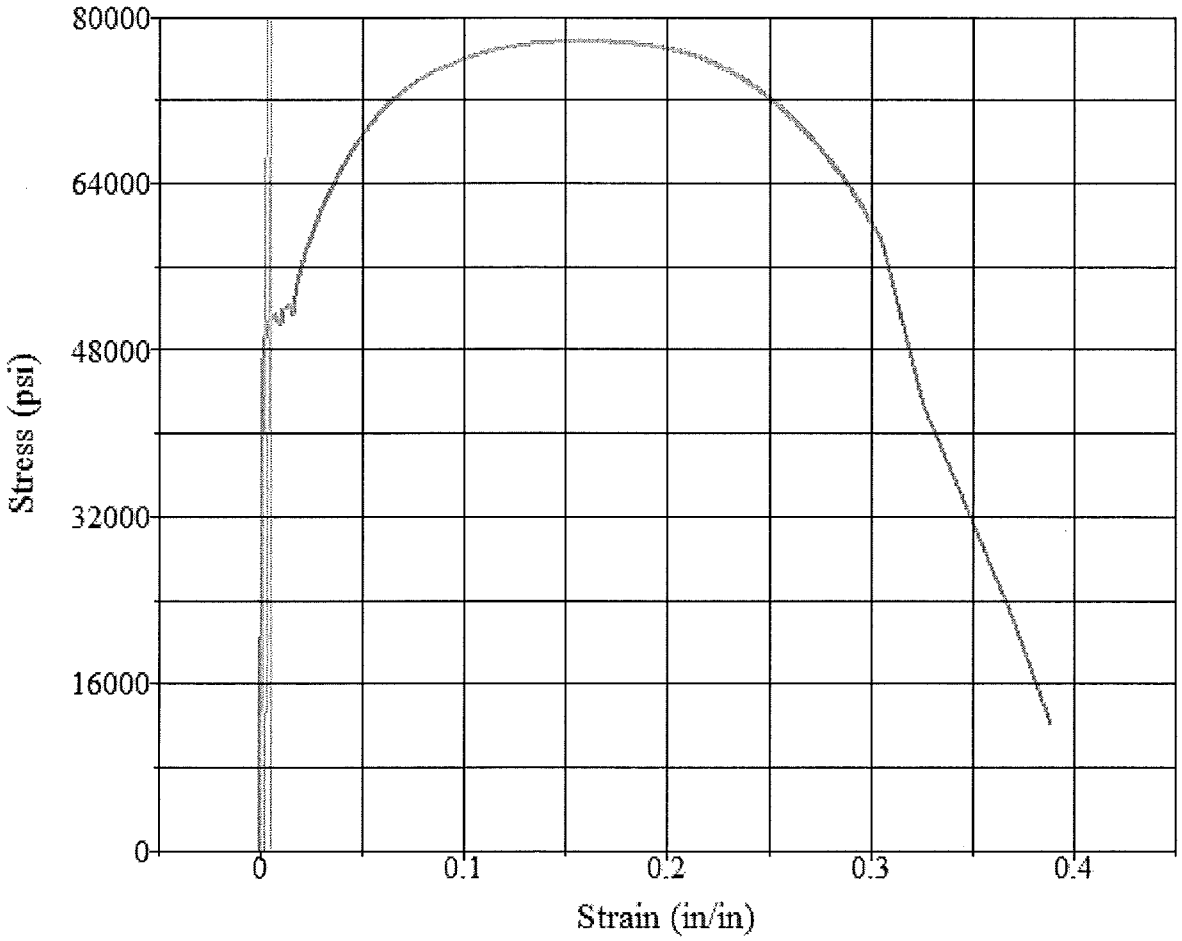


**Test Summary**

| | |
|---|---|
| Counter: | 9967 |
| Elapsed Time: | 00:02:26 |
| Anamet Job Number: | 5005.2347 |
| Specimen Identification: | D2 |
| Operator: | jm |
| Procedure Name: | Tensile MTS2in. Ext. |
| Start Date: | 10/30/2015 |
| Start Time: | 2:09:44 PM |
| End Date: | 10/30/2015 |
| End Time: | 2:12:10 PM |
| Workstation: | ANAMET-PC |
| Tested By: | James |
| Customer: | Exponent |

**Test Results**

| | |
|---|---|
| Area: | 0.2027 in² |
| Tensile Strength: | 77600 psi |
| Peak Load: | 15732 lbf |
| Load at Offset: | 10218.6700 lbf |
| Stress at Offset: | 50412.7800 psi |
| Young's Modulus: | 2.98e+007 psi |
| Load at EUL: | 10347.2700 lbf |
| Stress at EUL: | 51047.2300 psi |
| Halt of Force Yield: | 9905.0000 lbf |
| Diameter: | 0.5080 in |

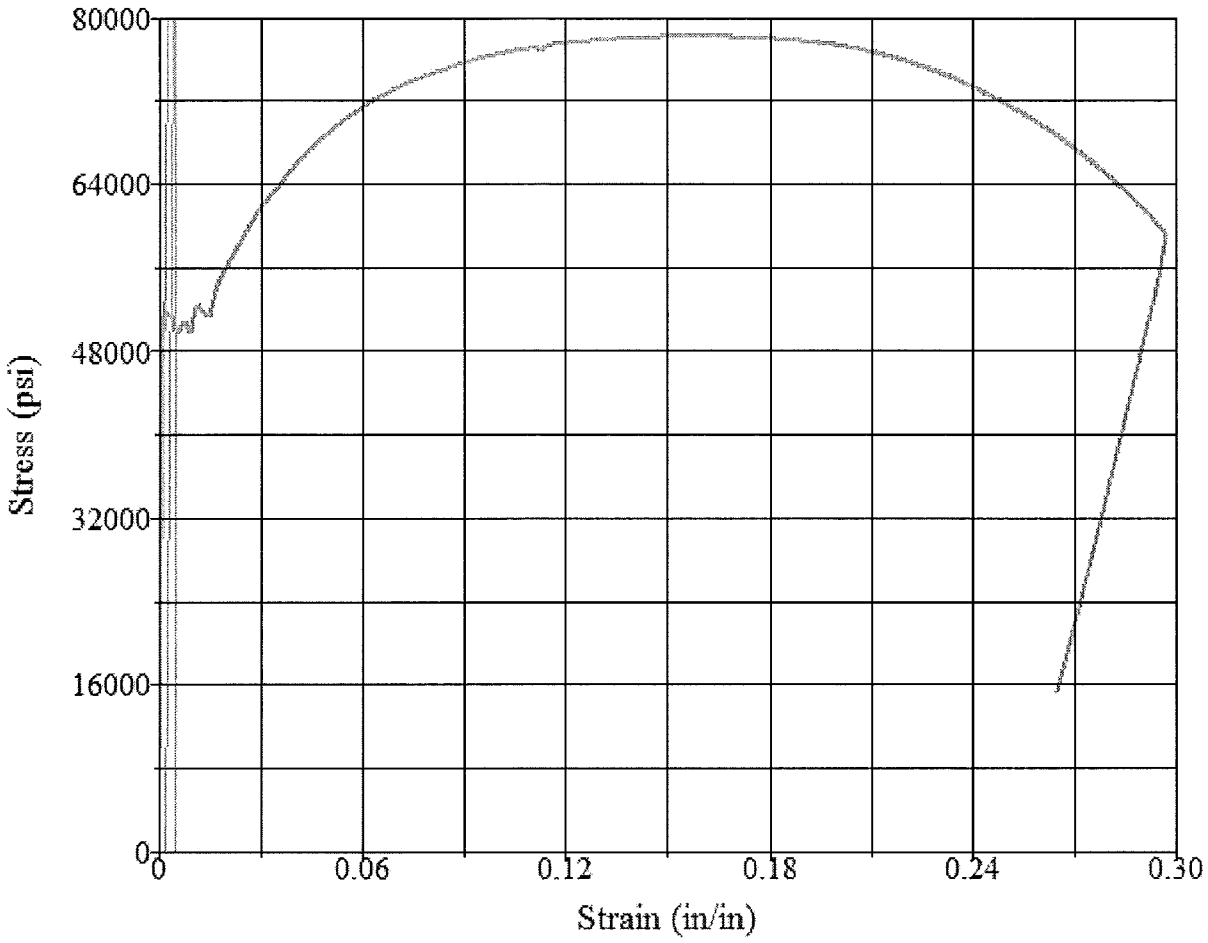


**Test Summary**

| | |
|---|---|
| Counter: | 9973 |
| Elapsed Time: | 00:02:27 |
| Anamet Job Number: | 5005.2347 |
| Specimen Identification: | E1-1 |
| Operator: | jm |
| Procedure Name: | Tensile MTS2in. Ext. |
| Start Date: | 10/30/2015 |
| Start Time: | 3:06:29 PM |
| End Date: | 10/30/2015 |
| End Time: | 3:08:56 PM |
| Workstation: | ANAMET-PC |
| Tested By: | James |
| Customer: | Exponent |

**Test Results**

| | |
|---|---|
| Area: | 0.2019 in² |
| Tensile Strength: | 78200 psi |
| Peak Load: | 15780 lbf |
| Load at Offset: | 10376.1700 lbf |
| Stress at Offset: | 51392.6200 psi |
| Young's Modulus: | 3.15e+007 psi |
| Load at EUL: | 10131.9700 lbf |
| Stress at EUL: | 50183.1100 psi |
| Halt of Force Yield: | 10649.0000 lbf |
| Diameter: | 0.5070 in |

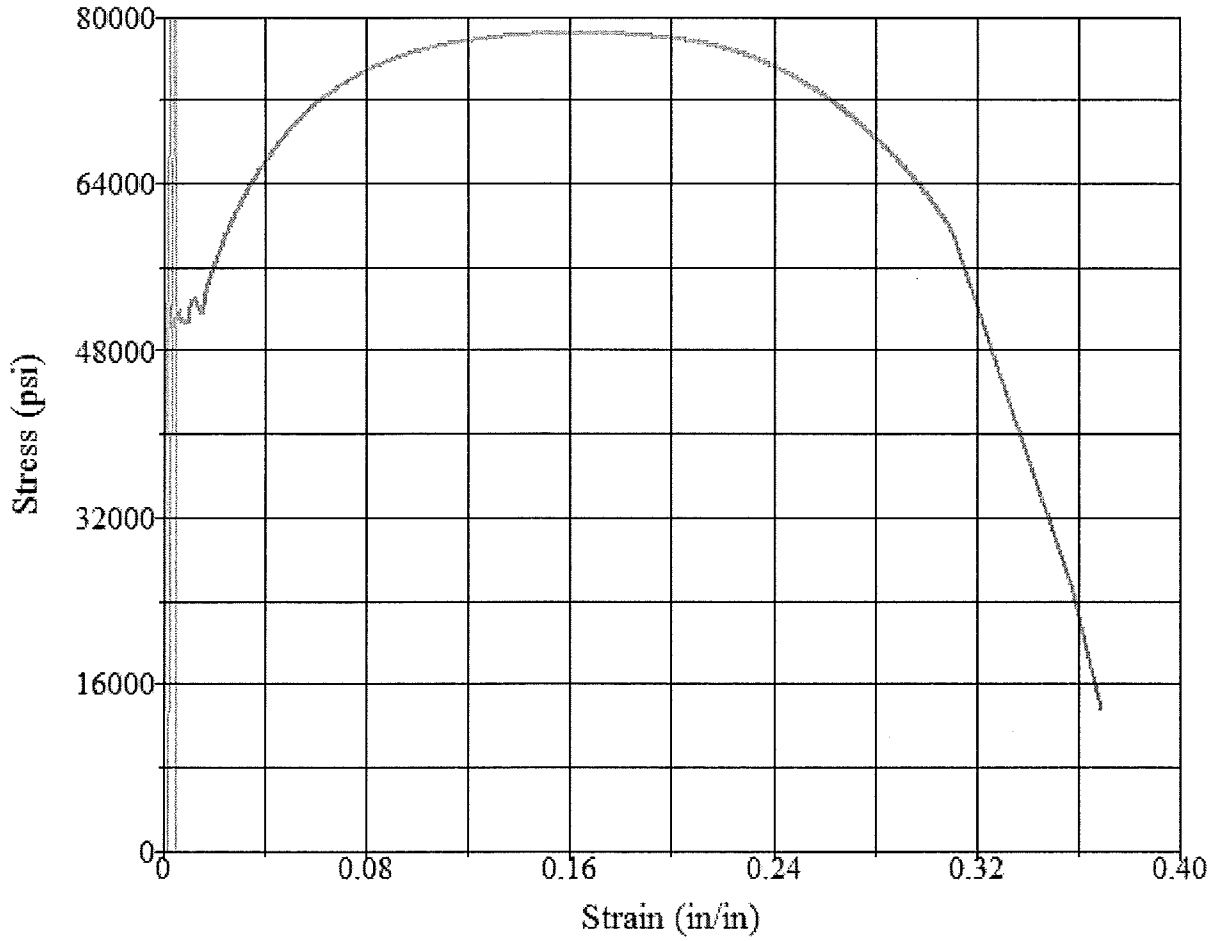


**Test Summary**

| | |
|---|---|
| Counter: | 9968 |
| Elapsed Time: | 00:02:29 |
| Anamet Job Number: | 5005.2347 |
| Specimen Identification: | E1-2 |
| Operator: | jm |
| Procedure Name: | Tensile MTS2in. Ext. |
| Start Date: | 10/30/2015 |
| Start Time: | 2:19:25 PM |
| End Date: | 10/30/2015 |
| End Time: | 2:21:54 PM |
| Workstation: | ANAMET-PC |
| Tested By: | James |
| Customer: | Exponent |

**Test Results**

| | |
|---|---|
| Area: | 0.2019 in² |
| Tensile Strength: | 78400 psi |
| Peak Load: | 15836 lbf |
| Load at Offset: | 10152.0100 lbf |
| Stress at Offset: | 50282.3500 psi |
| Young's Modulus: | 3.34e+007 psi |
| Load at EUL: | 10236.4500 lbf |
| Stress at EUL: | 50700.6200 psi |
| Halt of Force Yield: | 10589.0000 lbf |
| Diameter: | 0.5070 in |

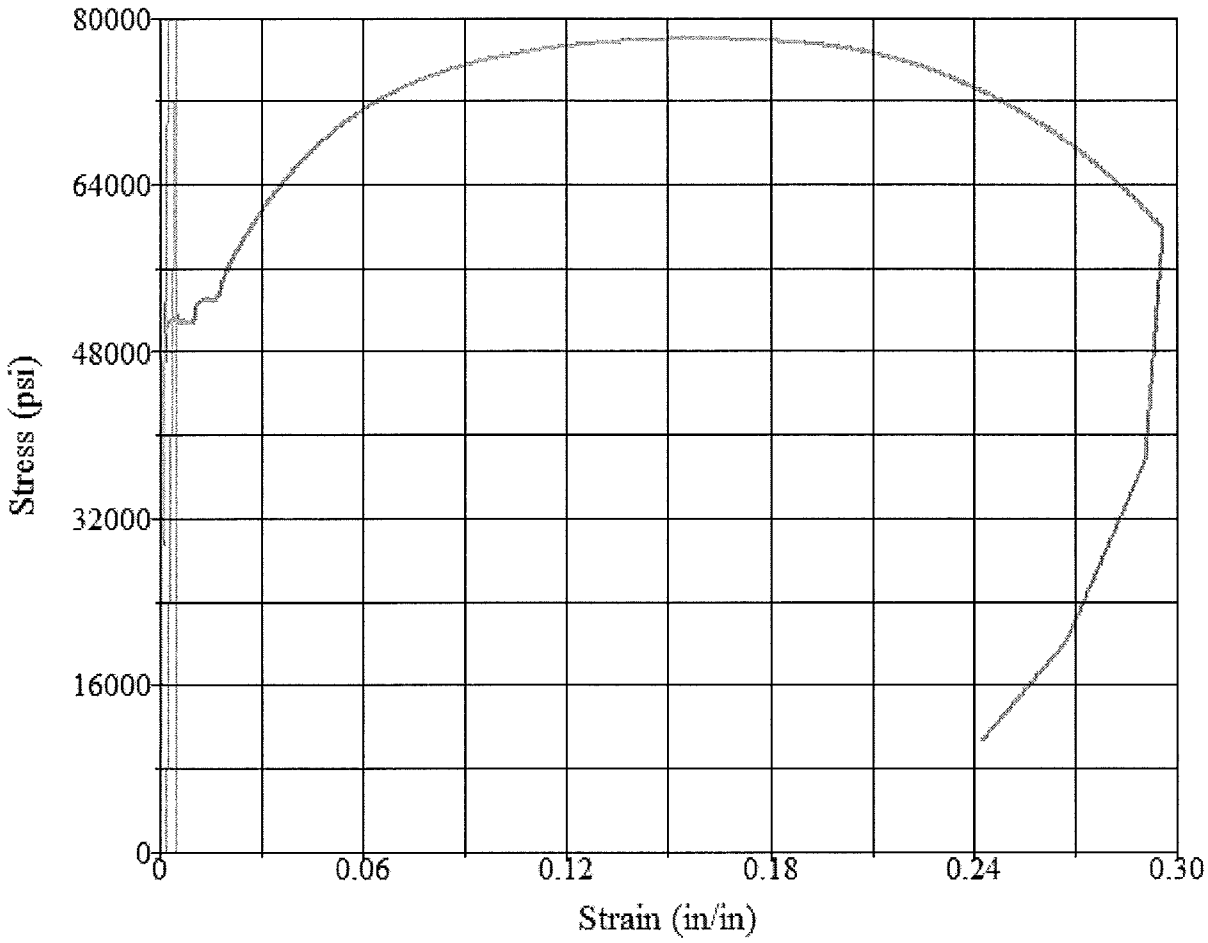


**Test Summary**

| | |
|---|---|
| Counter: | 9969 |
| Elapsed Time: | 00:02:27 |
| Anamet Job Number: | 5005.2347 |
| Specimen Identification: | E2-1 |
| Operator: | jm |
| Procedure Name: | Tensile MTS2in. Ext. |
| Start Date: | 10/30/2015 |
| Start Time: | 2:31:51 PM |
| End Date: | 10/30/2015 |
| End Time: | 2:34:18 PM |
| Workstation: | ANAMET-PC |
| Tested By: | James |
| Customer: | Exponent |

**Test Results**

| | |
|---|---|
| Area: | 0.2019 in² |
| Tensile Strength: | 78000 psi |
| Peak Load: | 15740 lbf |
| Load at Offset: | 10266.8300 lbf |
| Stress at Offset: | 50851.0600 psi |
| Young's Modulus: | 2.89e+007 psi |
| Load at EUL: | 10357.0000 lbf |
| Stress at EUL: | 51297.6700 psi |
| Halt of Force Yield: | 10633.0000 lbf |
| Diameter: | 0.5070 in |

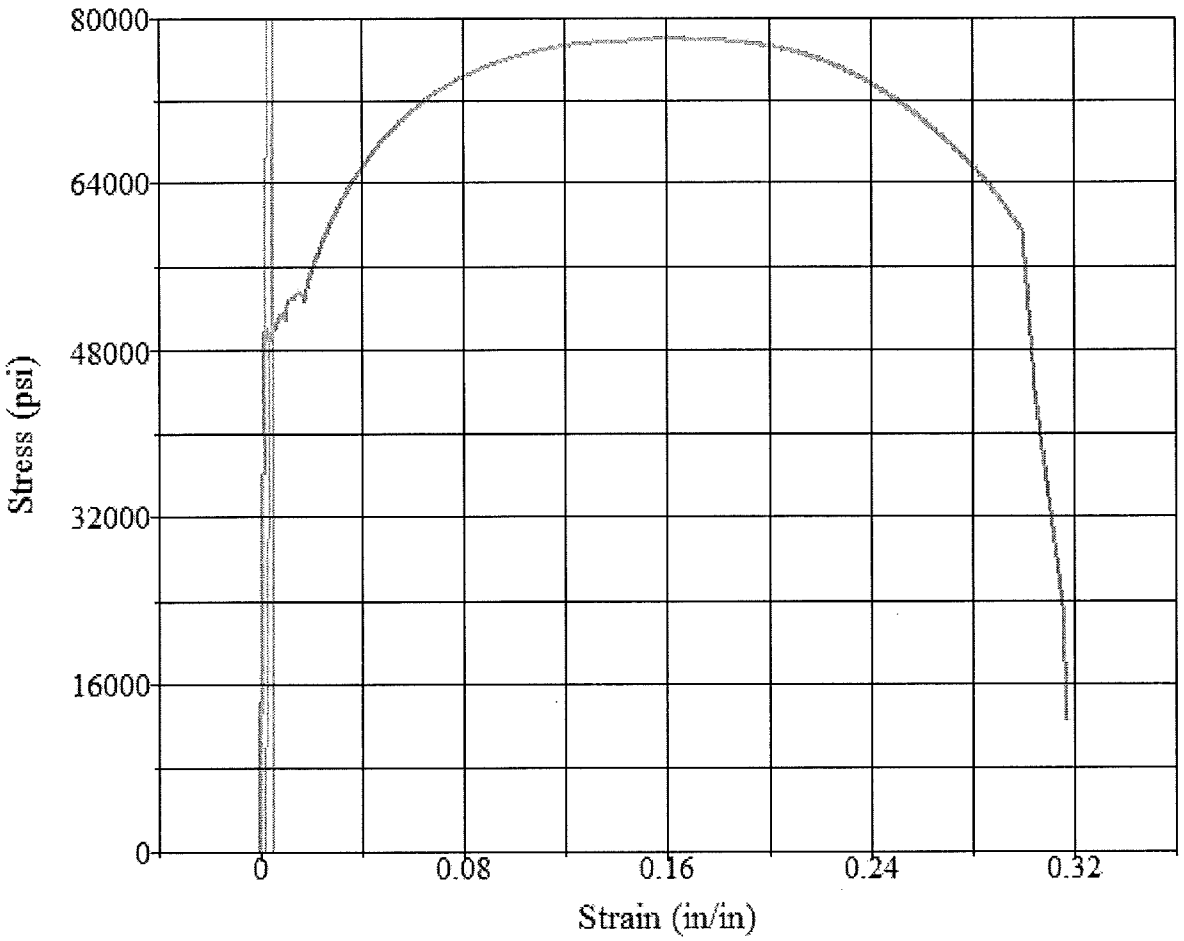


**Test Summary**

| | |
|---|---|
| Counter: | 9970 |
| Elapsed Time: | 00:02:27 |
| Anamet Job Number: | 5005.2347 |
| Specimen Identification: | E2-2 |
| Operator: | jm |
| Procedure Name: | Tensile MTS2in. Ext. |
| Start Date: | 10/30/2015 |
| Start Time: | 2:41:34 PM |
| End Date: | 10/30/2015 |
| End Time: | 2:44:01 PM |
| Workstation: | ANAMET-PC |
| Tested By: | James |
| Customer: | Exponent |

**Test Results**

| | |
|---|---|
| Area: | 0.2003 in² |
| Tensile Strength: | 77900 psi |
| Peak Load: | 15611 lbf |
| Load at Offset: | 9819.2780 lbf |
| Stress at Offset: | 49022.8600 psi |
| Young's Modulus: | 2.88e+007 psi |
| Load at EUL: | 9986.8340 lbf |
| Stress at EUL: | 49859.3800 psi |
| Halt of Force Yield: | 10040.0000 lbf |
| Diameter: | 0.5050 in |

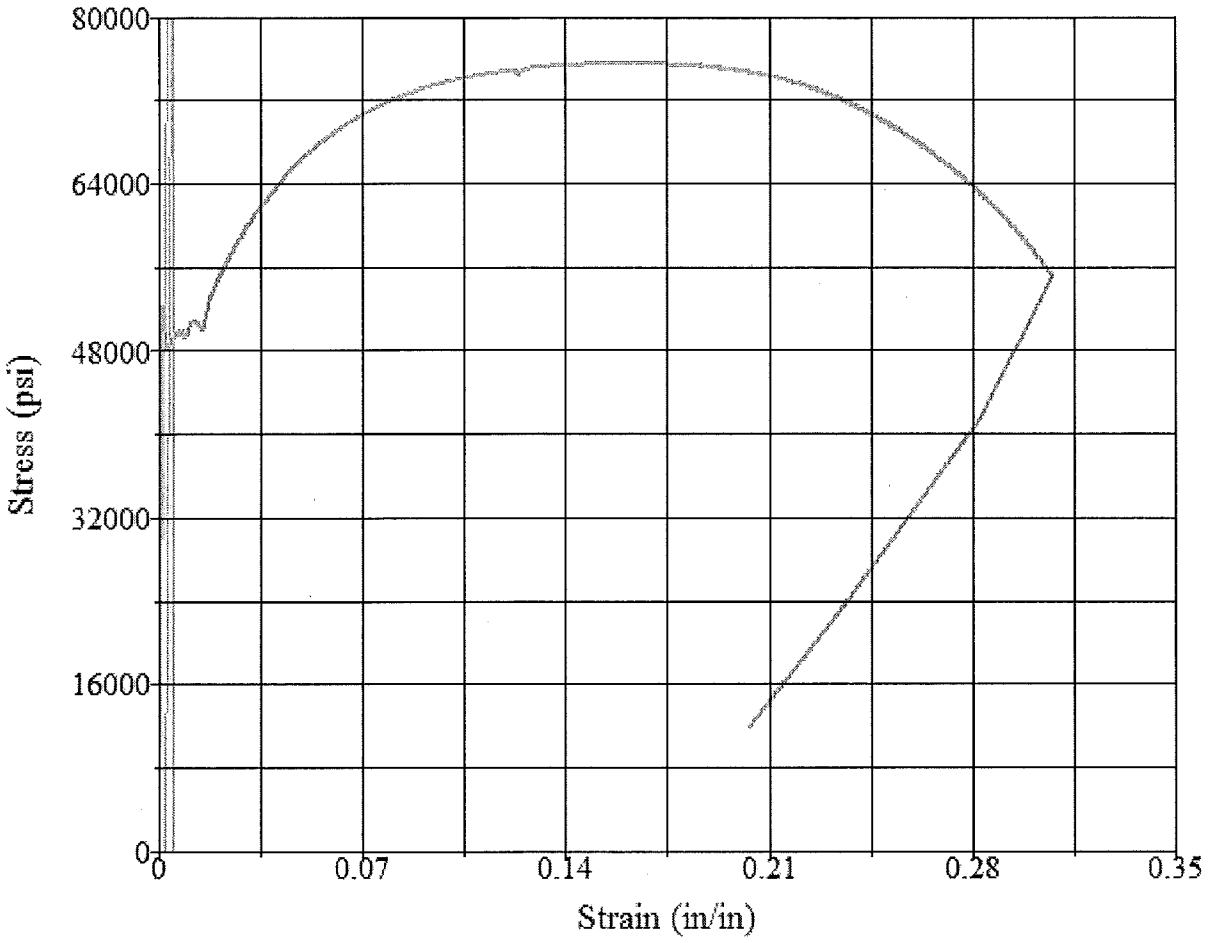


**Test Summary**

| | |
|---|---|
| Counter: | 9971 |
| Elapsed Time: | 00:02:25 |
| Anamet Job Number: | 5005.2347 |
| Specimen Identification: | E3-1 |
| Operator: | jm |
| Procedure Name: | Tensile MTS2in. Ext. |
| Start Date: | 10/30/2015 |
| Start Time: | 2:48:07 PM |
| End Date: | 10/30/2015 |
| End Time: | 2:50:32 PM |
| Workstation: | ANAMET-PC |
| Tested By: | James |
| Customer: | Exponent |

**Test Results**

| | |
|---|---|
| Area: | 0.2019 in² |
| Tensile Strength: | 75500 psi |
| Peak Load: | 15246 lbf |
| Load at Offset: | 9804.4800 lbf |
| Stress at Offset: | 48561.0700 psi |
| Young's Modulus: | 2.99e+007 psi |
| Load at EUL: | 9946.4000 lbf |
| Stress at EUL: | 49264.0000 psi |
| Halt of Force Yield: | 10563.0000 lbf |
| Diameter: | 0.5070 in |

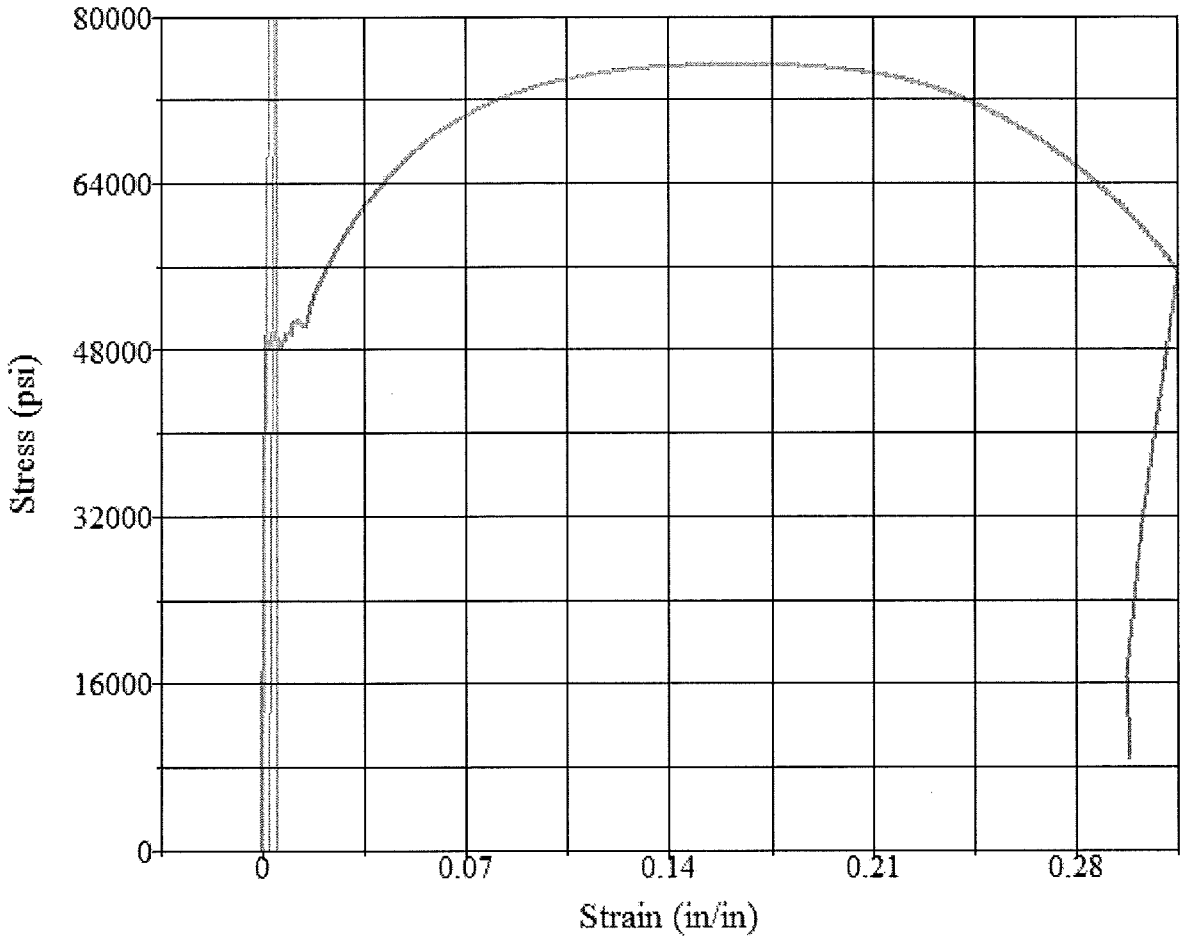


**Test Summary**

| | |
|---|---|
| Counter: | 9972 |
| Elapsed Time: | 00:02:30 |
| Anamet Job Number: | 5005.2347 |
| Specimen Identification: | E3-2 |
| Operator: | jm |
| Procedure Name: | Tensile MTS2in. Ext. |
| Start Date: | 10/30/2015 |
| Start Time: | 3:00:23 PM |
| End Date: | 10/30/2015 |
| End Time: | 3:02:53 PM |
| Workstation: | ANAMET-PC |
| Tested By: | James |
| Customer: | Exponent |

**Test Results**

| | |
|---|---|
| Area: | 0.2035 in² |
| Tensile Strength: | 75400 psi |
| Peak Load: | 15340 lbf |
| Load at Offset: | 10058.7600 lbf |
| Stress at Offset: | 49428.8000 psi |
| Young's Modulus: | 3.31e+007 psi |
| Load at EUL: | 10037.4000 lbf |
| Stress at EUL: | 49323.8200 psi |
| Halt of Force Yield: | 10055.0000 lbf |
| Diameter: | 0.5090 in |

# Appendix B

## CVs of key personnel

Exponent
Failure Analysis Associates®

Exponent
149 Commonwealth Drive
Menlo Park, CA 94025

telephone 650-326-9400
facsimile 650-326-8072
www.exponent.com

# Brian M. McDonald, Ph.D., S.E.
**Principal Engineer and Practice Director**

## Professional Profile

Dr. Brian McDonald is a Principal Engineer and the Director of Exponent's Buildings and Structures practice, which investigates and remedies performance problems ranging from leaking building envelopes to structural collapse. Dr. McDonald specializes in structural analysis and design, material behavior, and construction technology with focus on issues surrounding structural damage assessment and repair methods. During more than 20 years at Exponent, he has led evaluations of damaged wood frame, reinforced concrete, post-tensioned concrete and steel buildings as well as bridges, tunnels, industrial structures, power transmission lines, communication towers, cable-supported and fabric structures. Dr. McDonald has investigated structures damaged by wind, snow, explosion, fire, construction problems, design defects, decay and corrosion, as well as hundreds of structures damaged by the Loma Prieta, Northridge, San Simeon and Hawaii earthquakes. In addition to damage investigations, Dr. McDonald also provides peer review services for structural design of complex structures, including safety-critical nuclear power plant structures. Dr. McDonald's work often includes nonlinear and dynamic structural analysis; instrumentation and full-scale testing of structures; seismic risk assessment and retrofit; and material failures including fracture and plasticity analyses.

Dr. McDonald has held several positions in the fields of structural engineering and software design, most recently as Chief Analyst at Krawinkler, Luth, and Associates, a leading structural design firm. Dr. McDonald teaches a graduate level course in Finite Element Analysis at Stanford University.

## Academic Credentials and Professional Honors

Ph.D., Civil Engineering, University of Wisconsin, Madison, 1988
M.S., Engineering Mechanics, University of Wisconsin, Madison, 1989
M.S., Civil Engineering, University of Wisconsin, Madison, 1984
B.S., Civil Engineering, University of Wisconsin, Madison (*with distinction*), 1982

Awarded 1996 Grand Prize Award from the American Concrete Institute for restoration of a concrete façade of a Philadelphia high-rise; serves on University of Wisconsin Alumni Advisory Board

## Licenses and Registrations

Registered Professional Civil Engineer, California, #C47585; Registered Structural Engineer, California, #S4330; Registered Civil and Structural Engineer, New Mexico, #19925; Washington, #37689; Registered Structural Engineer, Illinois, #081-006025; Registered

Professional Civil Engineer, Wisconsin, #35893-006; Registered Professional Civil Engineer, New York, #081314; Registered Professional Civil Engineer, Hawaii, #12310-S; Registered Professional Civil Engineer Oklahoma, #22510; Registered Professional Engineer, Colorado, #41875; Registered Professional Civil Engineer, Alabama, #29048-E; Registered Professional Engineer, Maryland, #33587; Missouri, #PE-2008014092; Registered Structural Engineer, Oregon, #81321; Registered Civil Engineer, Maine, #11734; Registered Structural Engineer, Nevada, #021563; Registered Professional Engineer, Georgia #PE039137

**Academic Appointments**

- Adjunct Professor, Stanford University, 2006–2007

**Professional Affiliations**

- American Society of Civil Engineers (member #270581)
- Structural Engineers Association of Northern California (Member SE, Chair of the Existing Buildings Committee, past Chair of the Research Committee, past Chair of Nonductile Concrete Subcommittee)
- American Concrete Institute (member #00121237)
- American Institute of Steel Construction (member #064972)

**Publications**

Bishop CD, Uriz P, McDonald BM. Stability of column rebar cages for buildings under construction. Proceedings, Annual Stability Conference, Structural Stability Research Council, Nashville, TN, March 24–27, 2015.

Maison B, McDonald B, McCormick D, Schotanus M, Buckalew J. Commentary on FEMA P-807: Seismic evaluation and retrofit of multi-unit wood-frame buildings with weak first stories. Structural Engineers Association of Northern California Existing Buildings Committee Report, January 2014.

Maison B, McDonald B, Schotanus M. Pounding of San Francisco–Type soft-story midblock buildings. Earthquake Spectra August 2013, 29(3):1069-1089.

Morgan TA, McDonald BM. Design for uniform risk to standardized nuclear power plants using seismic isolation. Transactions, Structural Mechanics in Reactor Technology (SMiRT-22), San Francisco, CA, 2013.

Morgan TA, McDonald BM. Design for uniform risk to standardized nuclear power plants using seismic isolation. Proceedings, 10th CUEE Conference, Tokyo, Japan, 2013.

McDonald B, Hunt J. Thermal load-induced failure of steel space frame structure. Proceedings, 6th Congress on Forensic Engineering, San Francisco, CA, October 31–November 3, 2012.

Uriz P, Osteraas J, McDonald B. Using ASTM E1155 to determine finished floor quality: background and areas for consideration. Proceedings, 6th Congress on Forensic Engineering, San Francisco, CA, October 31, 2012.

Krawinkler H, Osteraas J, McDonald B, Hunt J. Development of damage fragility functions for URM chimneys and parapets. Proceedings, 15th World Conference on Earthquake Engineering, Lisbon Portugal, September 23–28, 2012.

Maison B, McDonald B, Schotanus M. Pounding of San Francisco-type soft-story midblock buildings. Structural Engineers Association of Northern California Existing Buildings Committee Report, September 2012.

Osteraas J, Krawinkler H, McDonald B, Hunt J. ATC-58 Fragility of masonry chimneys. Applied Technology Council, Redwood City, CA, March 2011.

McDonald B, Hunt J, Krawinkler H, Osteraas J. ATC-58 Fragility of masonry parapets. Applied Technology Council, Redwood City, CA, March 2011.

McDonald B, Ross B, Carnahan RA. The Bellevue crane disaster. Engineering Failure Analysis 2011 Oct; 18(7):1621–1636.

McCann DJ, Corr D, McDonald B. Lessons learned from Marcy Bridge collapse. ASCE 5th Congress on Forensic Engineering, Washington DC, November 11–14 2009.

McDonald B. The art and science of designing structures to resist earthquakes. Silicon Valley Engineering Council Journal 2009; 1.

Gupta A, McDonald BM. Performance of building structures during the October 15, 2006 Hawaii earthquake. The 14th World Conference on Earthquake Engineering, Beijing, China, October 12–17, 2008.

Luth G, Supriya S, Krawinkler H, McDonald B. USC School of Cinema: An example of reparable performance based design. Proceedings, 77th Annual Structural Engineers Association of California (SEAOC) Convention, Hawaii, 2008.

Osteraas J, Gupta, A, Griffith, M, McDonald, B. Woodframe seismic response analysis—Benchmarking with buildings damaged during the Northridge Earthquake. Proceedings, 2008 ASCE Structures Conference, Vancouver BC Canada, April 24–26, 2008.

Ross B, McDonald BM, Saraf V. Big blue goes down. The Miller Park crane accident. Engin Failure Anal 2007; 14(6):942–961.

McDonald BM, Gupta A, Alavi B, Osteraas J. Rational seismic evaluation and retrofit of a multistory RC shear wall structure. 100th Anniversary Earthquake Conference Commemorating the 1906 San Francisco Earthquake, San Francisco, CA, April 18–22, 2006.

Gupta A, McDonald BM, Griffith M, Osteraas J. Displacement coefficients for conventional residential wood-frame structures. 100th Anniversary Earthquake Conference Commemorating the 1906 San Francisco Earthquake, San Francisco, CA, April 18–22, 2006.

Meldrum J, Gupta A, McDonald BM. Investigation of structural damage in a corrosive environment. Proceedings, 5th International Conference on Case Histories in Geotechnical Engineering, New York, NY, April 2004.

McDonald BM, Luth G, Osteraas J. Review of safety factors for assessing column stability in existing braced frame buildings. Proceedings, 2004 Structures Congress, The Structural Engineering Institute of the American Society of Civil Engineers, Nashville, TN, May 22–26, 2004.

Osteraas J, Bonowitz D, Gupta A McDonald BM. Development of guidelines for assessment and repair of earthquake damage in woodframe construction. 13th World Conference on Earthquake Engineering, Paper No. 1580, Vancouver, BC, Canada, August 1–6, 2004

Ross B, McDonald BM, Saraf V. Big Blue goes down: The Miller Park crane accident. Proceedings, 6th International Symposium on Risk, Economy and Safety, Failure Minimization and Analysis, Capetown, South Africa, March 8–12, 2004.

McDonald BM, Saraf V, Ross B. A spectacular collapse: The Koror-Babeldaob (Palau) balanced cantilever prestressed post-tensioned bridge. Indian Concrete J 2003; 77(3). Also in Proceedings, 27th Conference on Our World in Concrete and Structures, XXI:57–68, August 29–30, 2002.

Osteraas J, Shusto L, McDonald BM. Forensic aspects of earthquake engineering: Protocols for earthquake damage assessment and repair. Proceedings, 2nd Forensic Engineering Congress, American Society of Civil Engineers, San Juan, Puerto Rico, May 19–23, 2000.

Rau G, Meldrum J, Medley E, McDonald BM. Forensic investigations of the soil-structure kind (wind & settlement failures). Proceedings, 2nd Forensic Engineering Congress, American Society of Civil Engineers, San Juan, Puerto Rico, May 19–23, 2000.

McDonald BM, Bozorgnia Y, Osteraas J. Structural damage claims attributed to aftershocks. Proceedings, 2nd Forensic Engineering Congress, American Society of Civil Engineers, San Juan, Puerto Rico, May 19–23, 2000.

Osteraas J, Shusto L, McDonald BM. Engineering involvement in post-Northridge damage assessment and repair of wood-frame dwellings. 12th World Conference on Earthquake Engineering, New Zealand Society of Earthquake Engineering, Auckland, New Zealand, February 2000.

Moncarz PD, McDonald BM, Caligiuri RD. Earthquake failures of welded building connections. Proceedings, 6th Pan American Congress of Applied Mechanics and 8th International Conference on Dynamic Problems in Mechanics, Rio de Janeiro, Brazil, January 4–8, 1999.

Moncarz PD, Caligiuri RD, McDonald BM, Sire RA, Borduin WP. Ultimate moment capacity of many steel connections: Failure in design, materials or workmanship? EUROMAT '98 Conference on Materials in Oceanic Environment, Lisbon, Portugal, July 22–24, 1998.

McDonald BM, Sire RA, Caligiuri RD. Ductile initiation of cleavage fractures in welded moment frame connections. 12th Engineering Mechanics Conference, American Society of Civil Engineers, La Jolla, CA, May 17–20, 1998.

Moncarz PD, Caligiuri RD, McDonald BM, Sire RA. Failures in steel frame building connections—A multi-billion dollar example of professional wishful thinking. 8th Annual International Federation for Information Processing (IFIP) Working Conference on Reliability and Optimization of Structural Systems, Krakow, Poland, May 11–13, 1998.

Johnston P, Shusto L, McDonald BM. Correlating torsional response to engine performance parameters. Presentation, International Off-Highway and Power Plant Congress and Exposition, Society of Automotive Engineering, Milwaukee, WI, September 1993.

Luth GP, McDonald BM, Jain D. Qualitative formulation of load paths through a functional description of structures. Proceedings, 5th International Conference on Computing in Civil and Building Engineering, Anaheim, CA, 1993.

McDonald BM, Burke M, Moncarz PD. The effects of natural aging on a polymer modified glass fiber reinforced concrete. Proceedings, 8th Biennial Congress of the Glassfibre Reinforced Cement Association, Maastricht, Netherlands, October 1991.

McDonald BM, Peyrot A. Generalized sag-tension calculations valid for any line geometry. J Struct Div, Am Soc Civil Engin 1990; 116(9).

McDonald BM, Peyrot A. Analysis of cable suspended in sheaves. J Struct Div, Am Soc Civil Engin 1988; 114(3).

McDonald BM. Analysis of cables suspended by sheaves. Dissertation, University of Wisconsin, Madison, WI, 1988.

Peyrot AH, Dagher HJ, McDonald BM. Reliability based design of transmission line structures—Theoretical user's manual for descal, reliability analysis and design of transmission line structures. EPRI Report for Project 1352-2, January 1986.

Saul W, McDonald BM. Microcomputer-aided structural analysis. In: Computer-Aided Processes in Instruction and Research. Beakley G, Haden C (eds), Academic Press Inc., Orlando, FL, 1985.

Saul W, Tuan CY-B, McDonald BM. Loads due to human movement. In: Structural Safety Studies. Yao JTP, Corotis R, Brown CB, Moses F (eds), American Society of Civil Engineers, New York, NY, 1985.

McDonald BM. The dynamic loading due to stadium crowds: A statistical measure of the coherency of crowd movements. Thesis, University of Wisconsin, Madison, WI, 1984.

Exponent
Failure Analysis Associates

Exponent
149 Commonwealth Drive
Menlo Park, CA 94025

telephone 650-326-9400
facsimile 650-326-8072
www.exponent.com

# Brad James, Ph.D., P.E., FASM

**Corporate Vice President, Practice Director, and Principal Engineer**

## Professional Profile

Dr. Brad James is a Corporate Vice President, the Director of Exponent's Materials and Corrosion Engineering practice, and a Principal Engineer. Dr. James specializes in failure analysis, failure prevention, and integrity assessment of engineering structures and components. His specific expertise includes metallurgy, materials science, fracture, fatigue, material degradation, corrosion, life prediction, and design.

In his many years of engineering experience, Dr. James has conducted hundreds of failure analysis investigations on widely varying engineering structures, ranging from miniscule medical devices to power-plant components. Dr. James also helps clients from various industries prevent failures, assess the integrity of their designs or equipment, as well as interact with governmental agencies. Dr. James has special interest in fractography, fracture mechanics, wear, corrosion, embrittlement phenomena, microstructural development, heat treatment, material selection, and welding and joining. The common thread in each of Dr. James' investigations is the application of metallurgical, materials science, and engineering mechanics fundamentals to help understand and solve complex problems.

Dr. James has taught several graduate-level fracture mechanics and failure analysis courses at Stanford and Santa Clara Universities. He has also taught several courses for The American Society for Materials (ASM International) involving failure analysis, design, and life prediction/validation of medical devices, and has been a Visiting Lecturer at San Jose State University. Dr. James was the co-Chairman of the 2011 ASM International Materials and Processes for Medical Devices (MPMD) conference. Prior to joining Exponent, Dr. James was employed as a Research Engineer, Materials Performance Division, at the Babcock and Wilcox R&D Center.

## Academic Credentials and Professional Honors

Ph.D., Metallurgical and Materials Engineering, Colorado School of Mines, 1994
B.S., Metallurgical Engineering, University of Washington, 1988

ASM International Fellow, 2011

## Licenses and Certifications

Registered Professional Engineer, California, #MT1867
Registered Professional Engineer, New York, 090492-1
Registered Professional Engineer, Minnesota, 49620
Registered Professional Engineer, Texas, 116334

## Publications

Hudgins A, James B. Fatigue of threaded fasteners, Advanced Materials & Processes, ASM International 2014 Aug; 172(8):18–22.

Guyer E, James B. Surgical tool failure analyses, Journal of Failure analysis and Prevention, Vol. 13, Issue 6, December 2013; DOI 10.1007/s11668-013-9763-5.

Briant P, Lieberman S, James B. Residual stress distribution in MP35N due to plastic deformation and comparison to finite element analysis. International Medical Device Conference and Expo, Chicago, IL, October 5–6, 2011.

Briant P, Siskey R, Rau C, Easley S, James B. Effect of strain rate on nitinol constitutive modeling in the clinically relevant strain range. Proceedings, ASM Materials and Processes for Medical Devices, Minneapolis, MN, August 8–10, 2011.

James B, Lieberman S. Analysis of a brake cylinder failure. Journal of Failure Analysis and Prevention 2011; 11:193–196.

James B, McVeigh C, Rosenbloom S, Guyer E, Lieberman S. Ultrasonic cleaning-induced failures in medical devices. Journal of Failure Analysis and Prevention 2010; 10(3): 223–227.

James B, Sire R. Fatigue-life assessment and validation techniques for metallic vascular implants. Biomaterials 2010; 31:181–186.

Fasching A, Kuş E, James B, Bhargava Y, Eiselstein L. The effects of heat treatment, surface condition and strain on nickel-leaching rates and corrosion performance in nitinol wires. Materials and Processes for Medical Devices, ASM International, Minneapolis MN, August 2009.

James B, Sire R, Caligiuri R. Determination of the failure mode and the rupture pressure in a mechanically damaged pipeline. Journal of Failure Analysis and Prevention 2008; 8(3):223–230.

Eiselstein L, Sire R, James B. Review of fatigue and fracture behavior of nitinol. ASM Symposium on Materials and Processes for Medical Devices, ASM International, pp. 135–147, Boston, MA, November 14–16, 2005.

James B, Eiselstein L, Foulds J. Failure analysis of NiTi wires used in medical applications. ASM International Journal of Failure Analysis and Prevention 2005; 5(5):82–87; Materials and Processes for Medical Devices, ASM International, pp. 44–49, St. Paul, MN, August 2004.

Eiselstein L, James B. Medical device failures—Can we learn from our mistakes? Proceedings, Materials & Processes for Medical Devices Conference, ASM International, pp. 3–11, August 2004.

James B, Wood L, Murray S, Eiselstein L, Foulds J. Compressive damage-induced cracking in nitinol. Proceedings, International Conference on Shape Memory and Superelastic Technologies, ASM International, pp. 117–124, Baden Baden, Germany, October 2004.

James B, Murray S, Saint S. Fracture characterization in nitinol. Proceedings, International Conference on Shape Memory and Superelastic Technologies, SMST Society, pp. 321–329, May 2003.

James B, Matlock D, Krauss G. Interactive effects of phosphorus and tin on carbide evolution and fatigue properties of 5160 Steel. 38th Mechanical Working and Steel Processing Conference, Vol. XXXIV, pp. 579–590, October 1996.

Jones D, Hoppe R, Hechmer J, James B. An experimental study on the effects of compressive stress on the fatigue crack growth of low-alloy steel. Journal of Pressure Vessel Technology 1994; 116:317–324.

James B. Interactive effects of phosphorus and tin on carbide evolution and fatigue and fracture properties in 5160 steel. Ph.D. Thesis, Colorado School of Mines, 1994.

Merlano N, James B, Matlock D, Krauss G. Effects of tempering and residual element content on mechanical properties of 5160H steel. Proceedings, Gilbert R. Speich Symposium, Iron and Steel Society, pp. 101–109, Montreal, Canada, October 1992.

James B, Paul L, Miglin M. Low cycle fatigue crack initiation in SA-210 A1 carbon steel boiler tubing in contaminated boiler water. Proceedings, Pressure Vessels and Piping Conference, ASME-PVP Vol. 195, pp. 13–19, Nashville, TN, June 1990.

**Presentations, Seminars, and Published Abstracts**

James B, Briant P. Fatigue design and validation for medical devices: What we learned from Portico. Invited Lecture, St. Jude Medical Materials Summit, September 29, 2015.

Briant P, James B, Easley S, Kennett S, Schaffer J, Kay L. The effect of crimp strain on the fatigue performance of nitinol. Shape Memory and Superelastic Transformation (SMST) Conference, May 22, 2015.

Ganot G, Birringer R, James B. Failure Analysis of Bone Plates and Screws, Materials Science and Technology Conference, October 16, 2014.

Lemberg J, Gibbs J, Birringer R, James B, Eiselstein L. Fire Cracking of Lead-Free Brasses for Use in Water, Oil and Gas Applications, Materials Science and Technology Conference, October 15, 2014.

James B. Medical device failure prevention and analysis, San Jose State University, March 6, 2014.

James B. Surgical tools failure analysis: causes and prevention, Materials Science and Technology Conference, Montreal, Canada, November 2013.

James B., Medical device failure analysis, Fort Wayne Metals, IN, September 2013.

James B. Medical device design and failure analysis, ASM International, Materials Park, OH, November 2012.

James B. Pipeline rupture failure mechanisms and prevention, IMECA, Pacific Grove, CA, October 2012.

James B. Pipeline Ruptures: Review of common metallurgical failure mechanisms, Materials Science and Technology Conference, Pittsburgh, PA, October 2012.

James B. Pipeline ruptures: Causes and prevention. Natural Gas Claims and Litigation Association, San Diego, CA, April 2012.

James B. Fracture, fatigue, corrosion and failure analysis of medical devices, Health Canada, Ottawa, Canada, March 2012.

James B. Medical device failure modes: Learning from unexpected outcomes. Plenary Speaker, Bay Area Biomedical Device Conference, San Jose State University, March 2012.

James B. Failure analysis for medical device engineers, ASM MPMD lecture, Medtronic, Minneapolis, MN, January 2012.

James B. Fracture fatigue and corrosion for medical device engineers, ASM MPMD lecture, Medtronic, Minneapolis, MN, January 2012.

James B. Nitinol processing, properties and design, ASM MPMD lecture, Medtronic, Minneapolis, MN, January 2012.

James B. Nitinol processing, properties and design. ASM MPMD lecture, Medtronic Vascular, Galway, Ireland, December 2010.

James B. Fracture, fatigue and corrosion for medical device engineers. ASM MPMD lecture, Medtronic Vascular, Galway, Ireland, December 2010.

James B. Failure analysis for medical device engineers. ASM MPMD lecture, Medtronic Vascular, Galway Ireland, December 2010.

James B. Fracture surface interpretation. Invited lecture, St. Jude Medical Cardiac Rhythm Management Division, Sylmar, CA, September 2010.

James B. Medical device fatigue design. Invited lecture, Medtronic Cardiovascular Innovation Seminar (CVIS), Santa Rosa, CA, July 2010.

James B. Fatigue design and validation of implantable medical devices. Invited lecture, St. Jude Medical, Cardiovascular Division, Maple Grove, MN, January 2010.

James B. Ultrasonic cleaning-induced failures in medical devices. Materials and Processes for Medical Devices, ASM International, Minneapolis MN, August 2009.

James B. Fatigue design and validation of implantable medical devices. Invited lecture, United States Food and Drug Administration (USFDA) Office of Science and Engineering Laboratories (OSEL) Science Seminar, June 2009.

James B. Medical device failures—Lessons learned. Invited lecture, Bio2Device Group, Sunnyvale, CA, March 2009.

James B. Medical device design validation and failure analysis. Materials and Processes for Medical Devices, ASM International Educational Course, 2008–present.

James B. Medical device failure analysis—Practice and pitfalls. Invited lecture, ASM International, Materials and Processes for Medical Devices Conference, Cleveland Clinic, August 2008.

James B. Medical device failure analysis. Invited lecture, San Jose State University, April 2008.

James B. Failure analysis for the medical device engineer. Materials and Processes for Medical Devices, ASM International Educational Course, 2005–2007.

James B. Fracture, fatigue and corrosion for the medical device engineer. Materials and Processes for Medical Devices, ASM International Educational Course, 2005–2007.

James B. Engineering design for medical device fracture, fatigue and corrosion performance. ASM International, Materials and Processes for Medical Devices Conference, Cleveland Clinic, October 2006.

James B. Medical device failure analysis. Invited lecture, San Jose State University, July 2006.

James B. Nitinol fatigue and fracture—Beyond the fundamentals. Invited lecture, International conference on shape memory and superelastic technologies, Monterey, CA, May 7, 2006.

James B. Compressive damage-induced cracking in nitinol. International Conference on Shape Memory and Superelastic Technologies, ASM International, Baden Baden, Germany, October 2004.

James B. Failure analysis of NiTi wires used in medical applications. Materials and Processes for Medical Devices, ASM International, St. Paul, MN, August 2004.

James B. Metallurgical failure analysis. Invited lecture, Stanford University, April, 2004.

James B. Fracture characterization in nitinol. International Conference on Shape Memory and Superelastic Technologies, SMST Society, May 2003.

James B. Interactive effects of phosphorus and tin on carbide evolution and fatigue properties of 5160 Steel. 38th Mechanical Working and Steel Processing Conference, Cleveland OH, October 1996.

James B. Effects of tempering and residual element content on mechanical properties of 5160H steel. Gilbert R. Speich Symposium, Iron and Steel Society, Montreal, Canada, October 1992.

James B. Low cycle fatigue crack initiation in SA-210 A1 carbon steel boiler tubing in contaminated boiler water. Pressure Vessels and Piping Conference, ASME, Nashville, TN, June 1990.

**Book Chapters**

James B, Hudgins A. Failure analysis of oil and gas transmission lines. Handbook of Materials Failure Analysis with Case Studies from the Oil and Gas Industry, Elsevier, 2015.

James B. Medical device failure analysis. ASM Handbook, Volume 23, Materials for Medical Devices, ASM International 2012.

**Editorial Boards**

- *Journal of Failure Analysis and Prevention*

**Peer Review**

- ASM Handbook, Volume 19, *Fatigue and Fracture*
- *Journal of Failure Analysis and Prevention*
- *Biomaterials*
- *Materials Engineering and Performance*
- *Acta Biomaterialia*

## Professional Affiliations

- ASM International (Fellow)
- International Organization on Shape Memory and Superelastic Technologies (member)
- ASTM International, Committees E08 – Fatigue and Fracture, F04 – Medical and Surgical Materials and Devices
- Independent Metallurgical Engineering Consultants of California (member)

## Project Experience

The following provides a brief list of Dr. James' project experience within several industries.

### *Medical Devices*

Dr. James has conducted hundreds of medical device failure analysis investigations. He has also assisted dozens of device manufacturers assess and validate device fatigue and corrosion performance of their implants and surgical tools. Selected examples are as follows:

- *Cardiovascular implants*: Has conducted failure analysis investigations of dozens of stents, filters, and coronary/peripheral devices. Also has directed several fatigue, corrosion, and/or fretting studies of cardiovascular implants for various medical device manufacturers.
- *Pacemakers/ ICDs*: Has conducted several pacemaker/ ICD failure analysis investigations. Dr. James has also helped pacemaker manufacturers with lead material selection, as well as fatigue and corrosion testing and validation.
- *Orthopedic implants*: Dr. James has conducted failure analysis investigations on dozens of orthopedic implants, including hip and knee prostheses, pedicle screws, bone plates, nails, and various other joint prostheses. He has also evaluated metallurgical, embrittlement, fatigue, coating, and corrosion issues to help manufacturers solve problems or validate device performance.
- *Heart Valves*: Has investigated several heart valve failures, and has extensive experience conducting and reviewing fatigue testing programs to help validate heart valve fatigue performance.
- *Catheters*: Has helped manufacturers design and develop catheters, as well as validate fatigue performance and investigate failures.
- *Surgical tools*: Dr. James has conducted several failure analysis investigations of surgical tools that have fractured or failed during service. He has also helped manufacturers conduct surgical tool fracture, fatigue, corrosion, and embrittlement studies.
- *Needles*: Has conducted failure analyses to determine the cause of needle breaks, as well as examined the effect of manufacturing processes on needle sharpness.
- *Neuro-implants*: Has conducted failure analysis investigations of neuro-vascular implants, as well as helped manufacturers validate neuro-vascular device fatigue performance.
- *Diabetes/insulin monitoring devices*: Has conducted failure analyses of insulin monitoring devices, as well as assisted manufacturers with coating and electrode development.
- *Obesity devices*: Dr. James has helped manufacturers develop and test various obesity devices.

- *Ventricular-assist devices*: Has conducted failure analysis investigations, fatigue performance validation, and material selection of ventricular-assist devices.
- *Corrosion testing*: Experience with potentiodynamic, open-current leaching, galvanic, and fretting testing to assess expected implant corrosion performance.

***Pipelines***

Dr. James has conducted dozens of failure analysis investigations of liquid and gas transmission pipelines and components. Dr. James has also helped assess the fitness for service and flaw tolerance of pipelines and associated components. The following list a few examples of his pipeline work.

- *Hydrotest failure analyses*: Dr. James has conducted failure analysis investigations to determine the cause of gas pipelines that ruptured during hydrotesting.
- *Sierra-Nevada Pipeline Leak*: Analyzed a pipeline leak in the Sierra-Nevada mountains that occurred due to damage from improper installation that occurred some 50-years prior to the leak. The local damage resulted in increased stresses that initiated slow-growing "near-neutral" stress-corrosion cracking.
- *LEFM-fatigue analysis*: Assessed the risk of fatigue-crack growth, leakage, and rupture in pipelines with seam-weld defects of varying depths and lengths using linear-elastic fracture mechanics. This work provided the basis for the client to establish a methodology for seam-weld defect assessment.
- *Estuary pipeline rupture*: Investigated the cause of a pipeline rupture that occurred within an estuary. Evaluated the cause and extent of corrosion that led to the rupture.
- *High pH SCC rupture*: Evaluated the cause of a gasoline pipeline rupture that occurred in a high-population area in Arizona. The cause of the rupture was high-pH stress-corrosion cracking (SCC). Dr. James recommended hydrotesting of adjacent pipeline areas, which revealed other SCC locations that were close to rupture.
- *Nevada 3$^{rd}$ party damage*: Conducted a failure analysis investigation of a gasoline pipeline that leaked in the desert outside of Las Vegas. This pipeline had suffered a gouge from third-party digging. A fatigue crack initiated from the gouge and eventually grew through wall to cause a leak.
- *Bellingham Washington pipeline*: Helped investigate the cause of a ruptured gasoline pipeline rupture that tragically killed three youths. Dr. James participated in investigations at the NTSB and Exponent laboratories. The pipeline failed several years after it had been severely damaged by an excavator.
- *Seam weld defect- Sacramento*: Investigated the cause of a gasoline pipeline leak that occurred along an electric-resistance weld (ERW) seam near Sacramento, CA. The leak was caused by fatigue crack growth that initiated and grew from the seam weld defect.
- *Seam weld defect – Texas*: Investigated the cause of a gasoline pipeline rupture that occurred in Texas. Metallurgical examination indicated the rupture occurred at an improperly welded ERW seam. A fatigue crack initiated and grew in the weld seam until it reached sufficient length to cause the rupture.
- *Australian Gas Pipeline SCC risk assessment*: Participated in a study to assess the risk of rupture in an Australian natural gas pipeline that exhibited significant stress corrosion

cracking (SCC). This analysis included using the results of in-line inspection coupled with fracture mechanics to help determine the risk of rupture.
- *Attachment vibration-induced fatigue*: Participated in a root-cause failure analysis investigation to help determine why several pump-station attachment piping fractured in a newly commissioned gas pipeline. The analysis confirmed that significant choked-flow conditions resulted in harmonic vibration-induced fatigue in attachment piping.

***Food/Chemical Processing***

Dr. James has conducted several failure analysis investigations of various food and chemical processing industry components. A representative list is shown below.

- *Process piping weld specifications*: Helped a food-processing plant revise their weld specification, testing, and validation procedures to eliminate leaks and stress-corrosion cracking of their 316L jacketed piping.
- *Food processing piping failures*: Examined the cause of leaks, fractures, and ruptures of piping and associated equipment in food processing plants. These failures have been caused by poor welding, vibration-induced fatigue, and stress-corrosion cracking.
- *Ammonia refrigeration piping failures*: Examined and determined the cause of failures in ammonia refrigeration units for ice cream and fruit processing plants. These failures have been caused by insufficient supports, vibration, and poor welds.
- *Chemical processing valve*: Determined the cause of failure of a large gate valve at a chemical processing plant. A combination of insufficient bolt torque and vibration resulted in insufficient bolt clamping force, which resulted in fatigue failure.
- *Piping creep*: Inspection of piping at a chemical processing plant revealed local bulging of adjacent piping. The cause of the failure was creep-rupture from excessive temperatures, and that the higher than desired temperatures occurred because of deposits that restricted cooling.
- *Valve bolt failures*: Bolts at a gasoline processing facility fractured causing a large loss. Analysis indicated that the bolts fractured due to stress-corrosion cracking. Material and environmental changes were recommended to eliminate the problem.
- *Tee failure*: A tee at an oil refinery ruptured resulting in release of product and environmental damage. Metallurgical analysis indicated that the tee failed due to a creep-rupture mechanism, caused by excessive temperature.
- *Ethanol storage tank weld*: An ethanol storage tank fractured at a weld, resulting in significant loss of product and damages. Analysis indicated that the tank fractured from stress-corrosion cracking at the weld heat-affected zone.
- *Gasoline storage tank failure analysis and integrity assessment*: Analyzed the cause of a gasoline tank failure, and conducted a fracture mechanics-based fitness for service analysis for floor-to-shell repair welds.

***Structural***

Besides piping and other infrastructure analyses, Dr. James has conducted metallurgical failure analysis investigations on many structural components, including several scaffolding and crane failures. Listed below is a sampling of Dr. James' metallurgical analyses of engineering structures.

- *Olympic stadium bolt failure*: Examined the cause of bolt failures that occurred during construction of the Salt Lake City Olympic stadium.
- *Swing scaffolding*: A scaffolding supporting workers on the side of a building in Sacramento fractured, resulting in significant injuries. Metallurgical analysis, including fractography, metallography, fracture toughness, and tensile testing indicated the cause of the failure was overload.
- *Paint Scaffolding*: A hoist connection of a swing scaffolding fractured in San Francisco, resulting in significant injuries to one of the workers. Failure analysis indicated the hoist connection suffered bending-induced fatigue crack initiation and growth due to scaffold misuse.
- *Bay Bridge scaffolding*: Portions of an aluminum scaffolding used for painting the San Francisco/ Oakland Bay Bridge fractured, resulting in a worker's death. Metallurgical analysis, including fractography, metallography, and mechanical property testing, in combination with weld and structural analysis was used to determine the cause of the failure.
- *Las Vegas sign welds*: Analyzed welds that fractured in a high-rise sign during a windstorm to determine whether proper welding procedures were followed.
- *Cranes*: Dr. James has conducted several crane failures. These analyses have included root-cause assessment of wire rope, axle, rail, lug, and attachment cracking and fractures.

***Fire Protection***

Dr. James has extensive experience conducting failure analysis investigations of fire protection components. These analyses include determining the cause of many unintended sprinkler activations, as well as analysis of sprinkler piping leaks and ruptures. Selected examples of Dr. James' fire protection analyses are listed below:

- *Fire sprinkler*: Dr. James has conducted many failure analyses of fire protection sprinklers that either activated in the absence of a fire or did not activate as designed. These have included many fusible-link solder as well as glass-bulb sprinkler designs.
- *Sprinkler pipe weld-o-let leaks*: Examined the cause of sprinkler pipe weld-o-let leaks in a large government building. Assessed the leaks and the likelihood that any additional could occur after hydrotesting.
- *Sprinkler Pipe*: Dr. James has conducted several analyses of fire-protection sprinkler piping that ruptured or leaked. Causes of the failures have been ranged pitting (and possible microbial-influenced corrosion), grooving corrosion, improper roll-grooving, and freezing.
- *Corrugated stainless steel piping*: Investigated the cause of leakage in a corrugated welded stainless steel sprinkler piping. Fractographic and metallographic examination indicated sensitization and stress corrosion cracking.

- *Fitting fractures*: Dr. James had examined several fire sprinkler-system fitting fractures to determine the cause of failure.

***Aerospace and Motor Vehicle***

Dr. James has conducted several aerospace and motor vehicle failure analysis investigations. These investigations typically involve metallurgical and mechanical analyses to examine the cause of a component failure, or to assess the integrity or expected lifetime of a specific component.

- *Cut copper conductors*: Helped predict the remaining life of stranded copper conductors that had been cut during the fabrication of a satellite using both stress-life and fatigue-crack growth methodologies.
- *Ultrasonic weld fatigue*: Conducted analysis and testing to predict the fatigue performance of ultrasonically welded components in satellite applications.
- *Single-engine airplane propeller shaft*: Conducted a root-cause failure investigation of a propeller shaft that fractured in service. The subject shaft fractured due to unidirectional torsional fatigue.
- *Steering knuckle investigation*: A rash of steering knuckle failures was observed in specific sport utility vehicle. Dr. James conducted a metallurgical investigation into the cause of the failures and presented the results to NTSA on behalf of the client.
- *Engine Mount*: Determined whether a broken engine mount could have contributed to a vehicle crash. Analysis confirmed the knuckle fractured by overload, and therefore was broken during the crash, rather than causing it.
- *Spot weld analyses*: Dr. James has participated in several analyses to examine fractured spot welds following vehicle accidents. These analyses assess spot weld size and failure mode.
- *Steering system failure analysis*: Dr. James has investigated several steering system failures, including projection weld fractures and bellows cracking.
- *Motorcycle gas tank ejection*: Examined fasteners associated with the gas tank ejection following a motor cycle accident. Conducted testing to determine the amount of thread engagement necessary to recreate the accident bolt features as well as to retain the tank in an accident.
- *Chopper weld failure analysis*: Conducted a failure analysis investigation of broken welds in a custom chopper to assess failure mode and any welding issues.
- *Wheel-off*: Dr. James has conducted several investigations of wheel assemblies that became detached from the vehicle while driving. These studies have included fractographic examination of the bolts, loosening studies, torque versus pre-load calculations, examination of the effect of painted hubs, and Goodman-based fatigue calculations of fatigue life as a function of bolt torque and pre-load.
- *Leaf spring failure analysis*: Dr. James' Ph.D. thesis involved embrittlement, fracture, and fatigue of leaf-spring steel, and he has done several failure analysis investigations of leaf springs that fractured in service.

- *Brake cylinder*: Conducted an investigation of a fractured brake cylinder involved in a meter maid traffic accident. The investigation determined that the brake cylinder indeed fractured, resulting in the accident. Improper assembly, just prior to the accident, cracked the cylinder leaving it susceptible to failure.

***Sporting Goods***

Dr. James has conducted failure and life assessment analyses for both industrial and legal clients. Examples of these investigations are listed below:

- *Bicycle fork analyses*: Dr. James has conducted several examinations that have involved determining the cause of bicycle fork failures. He has also worked directly with manufacturers to examine potential metallurgical issues involving bicycle forks.
- *Seat-post bolts*: Conducted multiple failure investigations of broken seat-post bolts.
- *Bicycle weld analysis*: Assisted a bicycle manufacturer with the evaluation of novel welding materials and methods with metallurgical and mechanical testing.
- *In-line skate bolt fatigue analysis*: conducted fatigue testing and analysis for an in-line skate manufacturer. Based on results, recommended bolt grade, size, and torque levels to client.

***Electronics***

Dr. James has conducted failure analysis investigations and life testing for industrial and legal electronics clients. Representative analyses are listed below:

- *Ultrasonic welded ignition module*: Conducted a failure analysis investigation of a diesel engine ignition module that had an ultrasonically-welded lead fracture that reportedly resulted in engine stall and an accident. Although severe post-fracture damage was observed, the lead fracture was determined to have been caused by thermal fatigue.
- *Capacitor fatigue*: Participated in an analysis to determine the cause of capacitor fractures. Fractographic analysis combined with finite element modeling indicated that the capacitors fractured in reverse-bending fatigue due to harmonic oscillation during service.
- *Cables and strain reliefs*: Dr. James has conducted several strain-relief failure analysis investigations for both electronics and medical device manufacturers. He has also conducted several fatigue life analyses, including testing, to assess and predict cable strain-relief fatigue performance.

# Appendix C

# Drawings provided by PG&E

# Tower Department
# Sequence For Erecting Tower 61/268

On March 19th 2015 the foundations were poured.

On April, 6th, 7th & 8th crews built the G-95 tower.

- First application was standing the 17.5' leg extensions into position and semi-bolting the individual legs to the foundation stub angles. Each leg extension was supported during this application by means of a medium size forklift (SkyTrac). All 4 legs were un-supported once bolts were installed.
- Next the lacing ( diagonal members) were affixed beginning with installations between A&B leg, D&C legs, B&C legs and last was D&A legs. The results of installing these panels would tie all legs together resulting in equal support of all 4 tower legs. Leg extensions & foundation stub bolts would be securely tighten.
- Another 15' extension was added to the newly installed 17.5' extension. This application consisted of utilizing a crane to support the members during the installation. Leg-A & leg-B along with the lacing were built on the ground and moved into position with the crane and held while bolts were installed. Once all members were secured the crews affixed ¾ inch rope to each of the 2 tower legs to support the weight of the legs/panel in the proper position and tied-off the ropes to the back of a nonessential vehicle.
- This same application was used for leg-C & leg-D and rope support applied. Next the lacing for leg-B & leg-C and leg-A & leg-D were positioned and supported by a crane until all leg members and lacings we secured and bolts tightened.
- Crews next moved into position to receive the tower body which was built on the ground and moved into position with the crane, at which time the crews positioned the supported tower body for receiving and applying bolts and tightening.
- The last step in erecting the tower is the installation of the tower cage with arm members affixed utilizing the crane, the crews positioned the supported tower cage for receiving and applying bolts and tightening.
- The last steps are freeing the crane, removing any remaining rope supports, double checking bolts and nuts and pinging the threads (method of deforming the threads to prevent nuts from backing-off.

Tower Type: G-95.

Tower Weight: 24,484 lbs.

Tower Height: 115.5 feet, ground level.

# Line Department

## Sequence for Conductor Transfer on Tower 61/268

**On September 12th 2015 the *Metcalf-Moss Landing # 1* 230 Kv conductors were transferred from the existing (old 61/268) G 95-DE tower on to newly installed G 95-DE tower 61/268.**

- Due to the higher positions of the existing conductors in relationship to tower 268, the bottom phase conductor had to be transferred first.
- Crews gradually released tension from old structure 268 until the bottom phase was in an acceptable level for the conductor transfer on to newly installed tower 61/268 lower arm.
- Once the conductor was captured and caught-off on the bottom arm by means of a conductor grip, hoist and sagging clock the tension remained between 5000 lbs. and 5600 lbs.
- The same sequence was followed for both the middle arm and the top arm. Near sag tension for transferring was to minimize any additional vertical loading on tower 61/267, and to retain as close as possible the conductor separations between the 230 kv and 115 kv crossing between towers 267 & 266.
- Once all three conductors were in position the crew began sagging the conductors starting from top, next the middle then the bottom. Sagging clock read 5800 lbs. at 90 degrees (F). Crew made final the dead-end assemblies.

**The above mentioned work procedures were specific to tower 61/268 in the span between 61/268 and 61/267.**

- The bundle was next in the process; crews began from top, then middle, then bottom with final sag of 1200 lbs. at 60 degrees (F) for each sub-conductor (bundled).

**On October 10th 2015 the *Metcalf-Moss Landing # 2* 230 Kv conductors were transferred from the existing shoofly TSP structure to tower 61/268, located on the opposite side of the recently installed # 1 circuit.**

- The shoofly TSP was located in the back span of tower 61/268. A conductor trailer was set-up 300 feet to the West of tower 61/268.
- A pulling line was threaded through a traveler which was attached with a bridle sling at the end of the arm. Another traveler was affixed at the top phase position on the TSP, the pulling line was threaded through the traveler and pulled to the ground.

- There was roughly 22 feet in height difference between the G 95-DE (112.5') structure and the TSP (90'). The top conductor on the TSP was caught off with a hoist, sling and conductor grip, the D/E compression fitting was cut-off and prepared for splicing.
- The conductor from the reel dolly was pulled-in relaxed until it reached the point on the TSP where the line workers could capture the conductor into another hoist/grip, at which point they completed their full splice application.
- A hoist, conductor tensioning meter and grip were attached to the rigging point on the D/E steel crossarm in preparation for final sagging and dead-ending.
- Prior to the moving of the conductor a "hold-down" traveler and line was positioned on the conductor and located between both supporting structures in support of reducing up-lift while the conductor was under tension.
- Crew used their line truck boom winch with a grip attached to the conductor for pulling, as tension increased the hold-down line was used to keep the conductor more in alignment with the position of the conductor on the TSP.
- When the hoist and grip attached to the TSP became slightly relaxed all pulling was stopped and all rigging detached from the conductor, with exception of the hold-down device and line, one of the crew members was located at tower 61/267 to monitor the insulators and inform the crew lead of any concerns should the insulator move to far in either direction.
- As the conductor was slowly allowed to rise by reducing the downward pull applied by the hold-down traveler and in combination with adjusting the tension applied by the line truck while moving the load line.
- Tensions remained at or below existing tensions at all times based on the insulator positioning at tower 61/267.
- With the conductor now in its intended position the crew applied their rigging and monitored their load cell until the tension was at 5800 lbs. at 90 degrees (F) and completed all work on the top phase.

**The above mentioned work procedures were specific to tower 61/268 in the span between 61/268 and 61/267.**

- The bundle was next in the process; crews began from top, then middle, then bottom with final sag of 1200 lbs. at 60 degrees (F) for each sub-conductor (bundled).

The main line conductors were 954 ACSS, 54/7, 54 outer aluminum strands and 7 steel strands.

The bundle conductors were 1113 AAC, 61 aluminum strands.